THE HONGKONG POLYTECHNIC UNIVERSITY

Department of Land Surveying & Geo-Informatics

USE OF MERIS DATA TO DETECT THE IMPACT OF FLOOD INUNDATION ON LAND COVER CHANGES IN THE LAKE CHAD BASIN.

By

IBRAHIM ASMA TURADU

A thesis submitted in partial fulfillment of the
requirements for the degree of
Doctor of Philosophy

JUNE 2008

CERTIFICATE OF ORIGINALITY

I hereby declare that this thesis is my own work and that, to the best of my knowledge and belief, it reproduces no material previously published or written nor material that has been accepted for the award of any other degree or diploma except where due acknowledgement has been made in the text.

_____ (Signed)

ASMA T. IBRAHIM (Name of student)

ABSTRACT

Lake Chad Basin is a vital source of water to human, livestock and wildlife communities. Over the last forty years, the region has experienced a series of devastating droughts and the lake has shrunk to less than a tenth of its former size leading to environmental degradation and food insecurity. Consequently, stake holders have adopted the strategy of cultivating flood recessed lands as a livelihood resource, to cope with the variability of the lake. One of the defining characteristics of the lake is the seasonal inundation that occurs every year. The inundation of the lake is an important economic event because it provides irrigation water, moisture retentive soils for recessional farming and a breeding environment for fish. A major negative impact is the harvest uncertainties experienced on seasonally inundated land and lake floor whereby unpredictable flooding can cause loss of crops and the destruction of infrastructure thus necessitating the need for data collection and monitoring to provide early warning systems. Consistent and accurate data acquisition using conventional methods has proved to be a major difficulty because of the remoteness of the region. As such, there is no current inventory of cultivated or cultivable land and little emphasis is directed to the small scale recessional farming activities that occur in and around the lake. Remote sensing as a tool offers a lot of scope for environmental assessments and has been used successfully in studies, to monitor changes in the lake environment using various satellite platforms

In this study, the potential of MERIS images for broad regional studies of Lake Chad was evaluated by investigating multi temporal patterns of change which could be used to identify farmlands in the lake basin. The MERIS data were validated with ASTER while the suitability of ASTER data for validating MERIS data was ascertained by visual comparison with high resolution IKONOS images and fieldwork. Spectral Mixture Analysis was performed on MERIS data. Three endmember fractions, soil, vegetation and water were generated. Post classification threshold change detection analysis was performed using the endmembers as indicators of land cover changes to assess temporal changes over the lake basin. To establish a preliminary basis for an early warning system, the relationship between altimetric lake level data and areal extent of surface inundation were examined. This was done by estimation of the spatial distribution and areal extent of annual flooding of the lake, from MERIS water fraction abundance. The areal extents

were then related to lake height level data derived from (i) TOPEX POSEIDON altimeter data and (ii) HYDROM generated lake level data. Results showed that temporal change patterns could be detected using MERIS thus making it suitable for inventorying and monitoring resources on the lake basin. However, due to the coarse spatial resolution of MERIS, farmlands smaller than the nominal pixel resolution of MERIS were not detected when analyzing the change patterns. The relationship between altimeter and areal extent of surface inundation showed that external factors such as the farming practices and the physical characteristics of the lake influence the surface inundation and therefore modify this relationship.

Acknowledgement

Alhamdu Lillahi Rabbil Aalaameen. Wassalatu wassalaamu ala ashrafil mursaleen. Sayyidina Maulana Mohammad, wa ala alihi wa asha bihi wa salleem. Praises to Allah for bringing me this far.

My thanks to my supervisor Prof Nichol and the HOD Prof Ding. My thanks to all the people in Hong Kong who made life wonderful and bearable for me. My love and gratitude to my immediate and extended family (especially my kids Ikhlas, Seif and Musty ,my sisters Fatima B.B. and Amina B.B and Nana) back in Nigeria and my present family (the Marafas and Ahmed), here in Hong Kong. Thanks to friends like Mairo, Halima, Peter, Anne, Charles (Wong) Adam Yau, AJ Lau, Fok, Chiara, Riccardo, Wendy Ma May Choi, Sarker, Sveta and Queeny. God Bless you all.

Special thanks to Garba Hassan (LCBC), Dr. Adamu Idris Tanko (BUK) and Bila Mohammed (LCBC) for your enormous help.

Thanks and best wishes to anyone who deserved a mention and whom I have forgotten to include.

TABLE OF CONTENTS

List of Figures

Appendix

LIST OF TABLES

List of Acronyms

Organizations

AGRHYMET	Agricultural Hydrological and Meteorological centre
CNES	Centre National d'Etudes Spatiales
ECMWF	European Centre for Medium range Weather Forecasting
ESA	European Space Agency
IRD	Institut de Recherche pour le Developpement
LCBC	Lake Chad Basin Commission
NASA	National Aeronautics and Space Administration
ORSTOM	Office pour la Recherche Scientifique et Technique d'Outre Mer
SODELAC	Societe de Developpement du Lac
UNDTCD	United Nations Department of Technical Co-operation for Development
UNEP	United Nations Environmental Program
USGS	United States Geological Survey

Satellites and radiometers

ASTER	Advanced Spaceborne Thermal Emmision and Reflection Radiometer
ENVISAT	Environmental Satellite
GEOSAT	Geodetic Satellite
JASON	Joint Altimetry Satellite Oceanography Network
LANDSAT	Land Satellite
MERIS	Medium Resolution Imaging Spectrometer
MODIS	Moderate Resolution Imaging Spectrometer Resolution Radiometer
NRA	NASA Radar Altimeter
SPOT	Satellite pour l'Observation de la Terre
TOPEX/POSEIDON	Topographic Experiment/POSEIDON
TMR	TOPEX Microwave Radiometer
METEOSAT	Meteorological Satellite
NOAH AVHRR	National Oceanic and Atmospheric Administration's Advanced Very High

Remote Sensing terminology

TIR	Thermal Infra Red
FR	Full Resolution
GDR	Geophysical Data Records
GRE	Ground Resolution Element
KT	Kauth Thomas Transformation
NPV	Non Photosynthetic Vegetation
LSU	Linear Spectral Unmixing
MLC	Maximum Likelihood Classification
MNF	Minimum Noise Fraction Transformation
NIR	Near Infra Red
PPI	Pixel Purity Index
ROI	Region of Interest
RR	Reduced Resolution
SMA	Spectral Mixture Analysis
SMAC	Simplified Method for Atmospheric Correction
SWH	Significant Wave Height
SWIR	Short Wave Infra Red
FOV	Field of View

Remote Sensing and other software

ENVI	Environment for Visualizing Images
BEAM	**B**asic **E**RS and ENVISAT **A**TSR and **M**ERIS toolbox
HYDROM	Hydrometeorological software

Others

AVISO	Archiving Validation and Interpretaion of Satellite Oceanography data
FEWS	Famine Early Warning Systems
ITCZ	Inter Tropical Convergence Zone
UTM	Universal Transverse Mercator

CHAPTER ONE

1.0 THE LAKE CHAD BASIN

1.1 INTRODUCTION: SCOPE AND BACKGROUND TO THE STUDY

Lake Chad is one of the largest freshwater lakes in Africa. It provides a vital source of water to human, livestock and wildlife communities (Odada *et.al*, 2003). Over the last four decades, the region has experienced a series of devastating droughts which led to the shrinkage of the lake and the loss of its biodiversity, as well as negative impacts on communities whose livelihoods depend on economic activities such as fishing farming and livestock rearing that the lake provides.

In this chapter, the background and scope of the thesis is discussed. A description of the geography and physical characteristics of Lake Chad, together with problems encountered are discussed. The aims and objectives of the thesis are underlined.

1.2 PHYSICAL CHARACTERISTICS OF THE LAKE CHAD DRAINAGE BASIN

The Lake Chad Basin can be described on three spatial scales – geographical (UNEP, 2004), conventional (Odada *et.al*, 2003) and lacustrine (Carmouze and Lemoalle, 1983).

1.2.1 The geographical basin

The geographical basin is located between lat 6° and 24°N, and longitude 7° and 24°E and covers 2,434,000 km^2 or 8% of the surface area of the African continent (UNEP, 2004). It is bounded by the Air and the Tibetsi Mountains to the north (Algeria) and the Ennendi and the Jebel Marra (Sudan) in the east and the northern slopes of the Jos Plateau (Nigeria) in the west (Figures 1.1 and 1.2). It was formed by extensional tectonic forces during the Cretaceous Period (UNEP, 2004) into a regional hydrological sink known as the Chad Artesian Basin which consisted of the Lake Chad and the Chari-Logone river system.

The southwestern part of the basin is made of three aquifers of which two are of regional importance within the Lake Chad (Olivry, 1996). These are referred to as the upper, middle and lower aquifers and are shared by the four countries bordering the Lake Chad (Niger, Chad, Cameroon and Nigeria). The upper aquifer is a Quaternary phreatic aquifer made up of fine-grained sediments approximately 30 m thick, and is

hydrologically connected to Lake Chad (Isiorho & Matisoff 1990). The middle aquifer is a Pliocene aquifer found at depths of between 150 and 400 m, and comprises approximately 200 m of clay-rich sediment (Kindler *et al.*, 1990). It is well exploited in Nigeria and the extreme north of Cameroon where many boreholes constructed in the 1960s constitute permanent drains of this aquifer (Odada *et.al*, 2003). The lower aquifer is cretaceous lying at depths of approximately 600 metres.

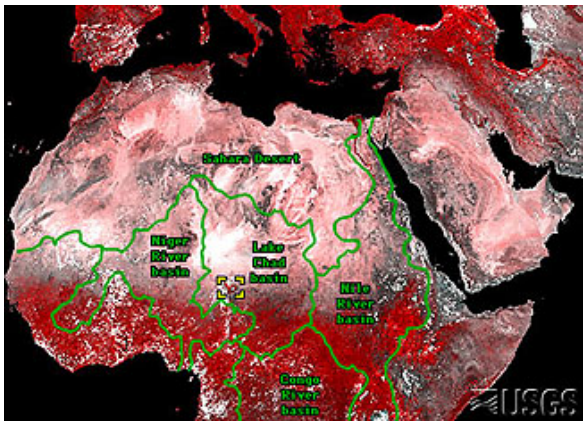

Figure 1.1: Location of Lake Chad in Africa from NOAA AVHRR.
(Source: EarthShots USGS, 2003)

1.2.2 The conventional basin

The conventional Lake Chad Basin is shared by five countries Cameroon, Nigeria, Chad, Niger and Central African Republic. The basin extends over 967,000km^2 and is home to about 20 million people (UNEP, 2004). The landscape within the conventional basin is very diverse. There are three types of lakes; Piedmont lakes in Cameroon and Chad, interdunal lakes in Chad and Nigeria and hydrographic lakes such as the Lake Chad. About 15 landforms have been identified (Odada *et.al*., 2003), including active and relict deltas, sand barriers of the present and past lake shorelines; sand dune and other Aeolian landscapes; flatlands derived from quarternary lagoons; pediments from eroded massifs, fossil valleys and wadis; and incised stream and river beds.

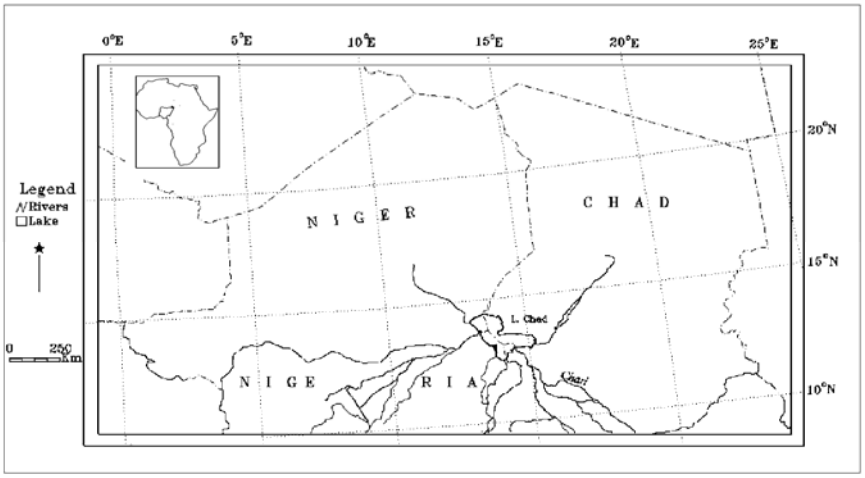

Figure1.2: The Geographical Chad Basin. (modified from: UNEP, 2004)

1.2.3 The lacustrine basin

The lake lies at an altitude of about 283m above mean sea level (UNEP 2004) on the border of the Sahara between latitudes 12ºN and 14º30′N and longitudes 13ºE and 15º30′E. It is hydrologically closed and occupies less than 1% of the geographical drainage basin (Coe and Foley, 2001). The lake is shallow with average depths varying between 1.5 and 5 m (UNDTCD, 1993; Odada *et.al,* 2003). This makes its overall surface area very sensitive to changes in level caused by fluctuations in water inflows and wind movements.

Lake Chad is characterized by a mixture of dune island archipelagos comprising 23% of the surface, reed beds 39% and open water comprising 38% of the surface (Odada *et. al,* 2003). In the northern part of the lake basin, the lake is bounded by a continuous dune chain whose altitude is always above 284 m (Carmouze and Lemoalle, 1983). From the northeastern side of the lake and along the east and southeast, (from Daboua to Koloudia, figure 1.3), the lake is bounded by sandy dune islands. Along the southwestern end of the lake extending southwards (from Baga Kawa to Koloudia), the lake is bounded by a low flat plain. The lake is divided into a south and a north basin by a line from Baga Kawa on the western side of the lake to Baga Sola on the eastern side of the lake, due to the narrowing of the coastal periphery. The northern basin forms an elongated peninsula that is about 10,325 km^2 in area and its position is slightly north of the geographical centre of the basin. It has the lowest regions in terms of altitude, with a mean level of 275.5 m. The southern basin which broadens out into

a bowl shape is about 10,975 km^2 in area (Carmouze and Lemoalle, 1983). The mean altitude of the southern basin regions is approximately 278.5 m.

The dunes in the north and east which constitute the bottom of the lake, are oriented in a Southeast – Northwest direction. The dunes are on average 3 to 6 km in length and 7 to 9 m in height. The heights as well as the altitudes of the crests decrease from the shoreline towards the inner part of the lake. Therefore areas of the lake bottom furthest away from the northern and eastern limits of the lake are much less influenced by the dune system. The coastal dunes of the south are on average 5 to 10 km in length and 10 to 15 m high. The dune relief of the southern basin diminishes more rapidly than it does in the northern basin, as the lake interior is approached.

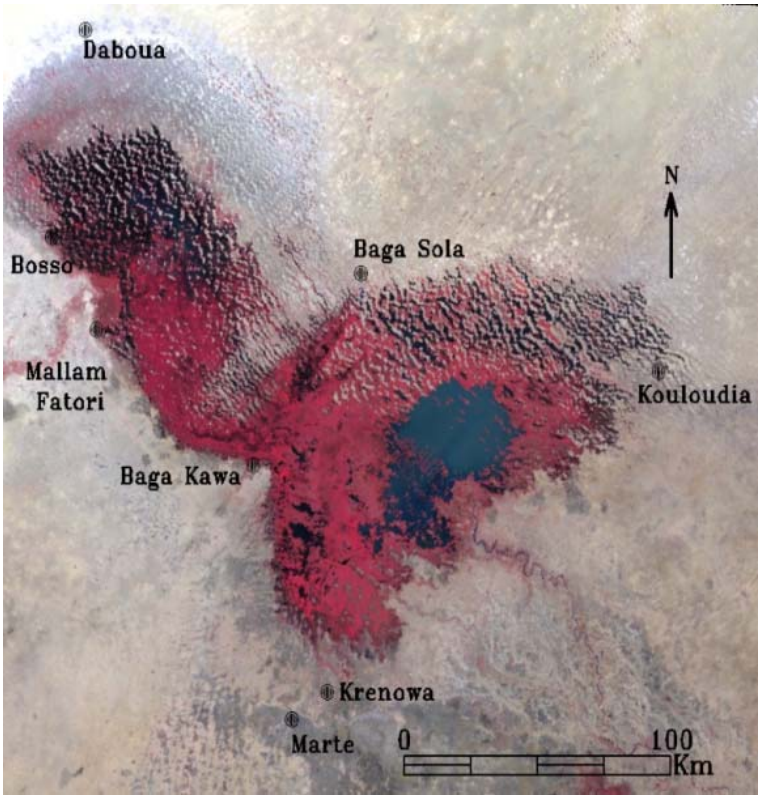

Fig.1.3: Topography of Lake Chad (MERIS 25th February 2004. RGB 12, 7, 5)

1.2.4 Hydrology and salinity of Lake Chad

The Chari-Logone river system which rises on the southern margin of the basin is the major contributes over 95% of the total lake inflow. Other rivers that directly enter the lake are the El Beid, the Yedseram and Ngadda and the Komadougou Yobe rivers. The first three rivers together with the Chari Logone feed the southern part of the lake. The Komadougou Yobe River enters Lake Chad from the Northern part of the Lake.

Lake Chad is considered a fresh water lake and the lake water has low levels of salinity and chemical analyses of the lake have shown that the lake water is of the bicarbonate type (Roche, 1980 in Isiorho *et.al*., 1996). When the Chad water level was normal (at around 281.9 metres asl) the salinity varied between 40-50 mg/l in the Chari River; 60-120 mg/l in the open waters of the southern basin and 250-400 mg/l in the open waters of the northern basin. The overall mean solute concentration for the whole lake was estimated at 320 mg/l by Roche (1980 in Isiorho *et.al*.,1996), 120 mg/l by Carmouze (1983) and at 188 mg/l by Isiorhor and Matissof (1990). (Isiorho et. al, 1996) noted that the chemical composition of the lake had not changed significantly over the past 25 years before their research and the proportions of the different chemical ions had remained constant despite the fluctuations in lake level. They attributed the discrepancy in the three different values of the mean solute concentration obtained above (by Carmouze, 1983, Roche 1980 and isiorho and Matissof, 1990) to the different methodologies used by the authors to estimate the values. The solute budgets from both Roche (1980 in Isiorho *et.al*., 1996) and Carmouze (1983) were estimated using independent water or solute balance approaches, while the recharge volume for Isiorho and Matissoff (1990) was calculated from seepage meter measurements.

Carmouze and Lemoalle, (1983), observed a very good correlation between lake level and total dissolved solutes, notably TDS decrease with decrease in lake volume and vice versa as opposed to the normal salinity - lake level relationships. On the other hand, both pH and salinity become higher with increasing distance from the Chari delta. The pH levels in the Chari are between 7 and 8, and subsequently in the southern lake basin it does not exceed 8. On the other hand, it can reach a pH of 9 in the northern basin. This is likely to make the soil infertile for agricultural purposes. Thus it is likely that the northern lake basin is used solely for fishing and pasture.

The lake water is always turbid because winds always contribute to the mixing of the shallow waters. Therefore the transparency is always low and it fluctuates according to water level. Water is clearest in the southern open waters in December to January, and most opaque in August.

1.3 CLIMATE AND CHANGE: EFFECTS ON LAKE CHAD

Rainfall is the most important factor controlling the hydrology and climate of the region. In turn, the rainfall regime is governed by the seasonal movements the Inter Tropical Convergence Zone (ITCZ) which is a zone of moist unstable air caused by the

convergence of the trade winds in the vicinity of the equator (Pietroniro et.al, 1990). Over the whole Chad Basin the annual rainfall decreases from south to the north. The rainfall varies from between 1500 mm annually in the southern parts of the region to less than 100 mm in the northern parts of the Chad Republic. Around the lake itself, average annual rainfall is of the order of 450 – 200 mm (Beauvilain, 1996). The rainy season begins in May – June and ends in October with a maximum rainfall in August. About 90% of the rain falls between June and September. The average annual air temperature is about 28ºC (Carmouze and Lemoalle 1983). During the hot season, the average monthly temperatures vary from 29° C to 32° C. In the Harmattan season, the temperature may range from between 22ºC and 24ºC, from December to February with a minimum of 21ºC to 23ºC in January. Humidity measurements across the lake show that humidity is at a maximum at night and a minimum at around midday. The seasonal maximum ranges from 72% to 81% in August and the minimum ranges from 23% to 31% from February to March. High temperatures, insolation, wind frequency and intensity and low humidity contribute to high evaporation that often equals to, or exceeds water influx (UNEP, 2004). Annual estimates of evaporation range from 2.1 to 2.2 m while evapo-transpiration rates reach up to 2300 mm per year (Carmouze and Lemoalle 1983, Isiorho and Matissof, 1990; Isiorho *et.al,* 1996).

1.3.1 Climate and human modification of Lake Chad

One of the factors thought to account for the drastic changes observed in the lake is climate. Changes in the climate due to global warming are usually cited as a major catalyst to changes in the Lake Chad basin. More recently, El Nino has been used to explain the persistence of the dry conditions in the African Sahel (AGRHYMET, 2003b). The climate of West Africa is thought to be greatly influenced by the movement of the ITCZ. The strongly seasonal rainfall in Africa has varied from year to year and decade to decade, with persistent rainfall anomalies (Nicholson *et.al.,* 2005). There has also been a pattern of continued aridity since the late 1960s. In the Sahel, rainfall was mainly above average between 1927 and 1936 and below average in the 1910s. Some recovery occurred during the 1990s, with rainfall in some years being near or just above the long-term mean of 471 mm.

Another factor responsible for changes in the basin is human modification of the lake environment. While rainfall over the Chad drainage basin decreased greatly in the decades following the 1960s, water demand and diversion increased due to the

construction of dams for mainly irrigated cultivation in the hydrologically active sector of the Basin. During the 1960s discharge losses due to irrigation were almost nonexistent. However from 1983, while precipitation became lower, water withdrawn for irrigation continued to increase volume. Between 1982 and 1984 the total run-off of the Chari River was at an all time low (Evans et.al 2003). The Maga Dam Project for fisheries and rice irrigation in the Waza Logone flood plains of Cameroon reduced the stream flow of the Chari-Logone River by almost 1000km^2 in an average year (Evans *et.al*, 2003). This led to serious ecological degradation of the flood plain, a decline in wildlife and biodiversity, the collapse of the fishing industry and a drastic reduction in grazing capacity.

Upstream of the Komadugu Yobe River, in Nigeria, 20 reservoir dams were constructed on the Hadejia River system. These dams controlled 80% of the total runoff of the Hadejia River. This negatively affected the hydrology of the Komadugu Yobe which was the only inflowing river into the lake from the northern basin and whose contribution to the lake was reduced to 1%. Moreover, the dam and irrigation projects were planned without any environmental impact studies on the effects on the environment or the people living downstream (L.C.B.C., 1998).

The countries within the Lake Chad basin are among the poorest in the world. Inhabitants of the lake region are affected by widespread poverty, chronic food insecurity, climate change, cyclical droughts and heavy reliance on agriculture and animal husbandry (Badolo *et.al*, 2003 AGRHYMET, 2003a). Most people are engaged in fishing, farming and livestock grazing as a means of livelihood with the lake as a focus of that livelihood (World Bank, 2002). The contraction of the lake became a source of resource conflicts, and disagreements and clashes between fishermen from neighboring countries over national boundaries (Isiorho *et.al*, 1996) as they followed the shrinking shoreline. The contraction of the lake also led redundant fishermen to switch to farming the lake bed as a livelihood adaptation strategy to cope with the nature of lake level fluctuations.

1.3.2 Lake Chad variability

Lake Chad has also had a history of regressions and transgressions since the Holocene (Servant & Servant 1983; Thiemeyer 2000, Gumnior and Thiemeyer, 2003). Drake and Bristow, (2006) identified numerous shorelines at different elevations indicating

different periods of lake fluctuations. Three hydrological periods have been defined as characteristic of the trends in the fluctuating water levels of Lake Chad (UNEP, 2004).

- The period of 'Greater Chad' prior to 1960. Lake Chad was the sixth largest lake in the world by areal extent with an open water area of 25 000 km^2 or more.
- The period of 'Normal Chad' between 1967 and 1973. The north and south lacustrine basins occupied 10000km^2 and 11000km^2 of water respectively (Carmouze and Lemoalle, 1983).
- The 'allometric' or 'Lesser Chad' period which occurred after 1973 (Holz *et.al*, 1984 in UNEP, 2004). This was the period when the water disappeared completely from the northern basin.

The first images of Lake Chad from space were obtained in 1963 (Fig 1.4a [Coe and Foley, 2001]). In the mid-1960s the lake reached record levels for the 20^{th} century. With the sudden onset of the Sahelian drought in the 1970s lake levels began to fall. By 1973, a marked lowering of the lake occurred as a result of a smaller discharge into the lake, ($17.3 \times 10^9 m^3$ in 1972 -73 as against $40 \times 10^9 m^3$ annual average in previous years). The small floods of 1972- 1973 resulted in the emergence of shallow zones in the lake and the breakup of the basin into the northern and southern pools. Additionally vegetation in the northern basin began to disappear while dunes and dry land emerged on the dry lake bed (Figure 1.4b). The water level decreased from an average level of 280.1 meters above sea level to 278.4 metres above sea level. By 1997, (Figure 1.4c), Marsh and dry land replaced most of the open water. By 2001, the lake had been reduced to $1/20^{th}$ of its former size to about 1,500km^2 (Figure 1.4d), changing its character to a swampy delta at the mouth of the River Chari. Thus the lake was significantly decreased to 10% of its former size (Lemoalle 1991, USGS 2001). During the wet season, the lake is inundated and the north basin only holds temporary water. Speculations of the lake levels rising again and the recovery of rainy season in the Sahel were entertained due to the wet year of 1999 especially when the northern basin began to experience some flooding (Diouf *et.al*, 2000 in UNEP, 2004). However the lake still remains in its Lesser Chad state as the wet years are only intermittent and a sustained upward trend has not been observed (L'Hôte *et al*, 2002).

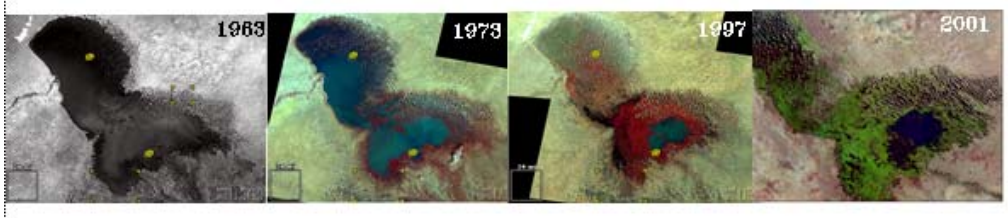

Figure 1.4: Metamorphosis of Lake Chad from Lake to Swamp between1963 and 2001(Source: Earthshots 2001).

1.4 SUB REGIONS OF THE LAKE BASIN AND AGRICULTURAL ACTIVITIES IN THE REGIONS

Carmouze and Lemoalle (1983) divided the lake into 11 sub regions based on topography, landform and vegetation type (figure 1.5). At the extreme northern end of the lake is a region of reed islands which are divided into the Northern Reed Islands (1) and North Eastern Reed Islands (2). They occupy an area of about 3600 km^2. To the east of the Reed Islands is a zone of dune Islands which are located along the former lake shoreline on the northern and eastern side of the lake. This area is the North Eastern Archipelago (3). It is about 25 km wide, contains about 500 flat islands and occupies an area of about 2400 km^2. To the southwest of the basin is the Northern Open Water (4). The size of the area is about 4200 km^2 and its depth increases from an average of 2 m in the south to 6.5 m in the north. The Northern Open Water is bordered to the southeast by a region of numerous sandy islands with shallow interdunal depths. This region is called the Grand Barrier (5N) and it extends into the southern basin (5S), and interferes with water transfers between the two basins.

To the southeast and east are the South Eastern Archipelago (6) and Eastern Archipelago (7) covering an area of 3200km^2. Some of the interdune depressions of the Southeastern and Eastern Archipelagoes are used as polder farmlands. To the east and north of the Chari delta is a large open area of water which is divided into the South Eastern Open Waters (8) and the Southern Open Waters (9). The South Eastern Open Water is the permanent pool of water at the mouth of the Chari delta. It is now about 1642 km^2. The regions around the open zone of water are higher and contribute to the establishment of macrophytes. The Southern Reed Islands (10) are an area of relatively flat land along the southwestern shoreline of the lake basin, occupied by reed vegetation. The area is about 1500 km^2. The lakeshore along the Southern Reed Islands is intensively cultivated and form part of the area of recessional farmlands named by

this author as the Southwestern Lakeshore Farmlands. To the east of the Southeastern Open Waters, is a swampy zone called the Southeastern Reed Islands (11) which is an area about 1700 km^2 in size.

Table 1: Original names of regions in Lake Chad given in Carmouze and Lemoalle's nomenclature and the new names adopted for the regions:

Region	Name	Renamed as	Region	Original Name	Renamed as
1	Northern Reed Island		6	South Eastern Archipelago	Southeastern Dune Islands
2	Northeastern Reed Islands		7	Eastern Archipelago	Eastern Dune Islands
3	North Eastern Archipelago	Northeastern Dune Islands	8	South Eastern Open Waters	Open Water Region
4	Northern Open Waters	Northern Open Swamps	9	Southern Open Waters	Southern Open Swamps
5N	Grand Barrier	Northern Grand Barrier	10	Southern Reed Islands	
5S	Grand Barrier	Southern Grand Barrier	11	South Eastern Reed Islands	

Prior to 1973, Carmouze and Lemoalle (1983)'s regions of Northern Open Water and the Southern Open Water was one continuous open body of water extending across the southern and northern lake basin. Both the Northern and Southern Open Waters were replaced by swamp vegetation and only residual pools exist in the Southern Open Water region. Thus the Northern Open Water region and the Southern Open Water region are renamed as the 'Northern Open Swamps' and the 'Southern Open Swamps' by this author. All the other regions have been renamed except regions 1, 2, 10 and 11. Two other regions were identified by this author. These regions were the Polder Farmlands which are the cultivated interdune depressions located in the Southeastern and Eastern Archipelagoes and the Southwestern Lakeshore Farmlands (figure 1.6) which are located in the Southern Reed Islands. Table 1 shows names of the regions by Carmouze and Lemoalle's nomenclature and the new names given to the regions. The most important regions for this project are the Southeastern Dune Islands in which the Polder Farmlands are located and the Southern Reed Islands in which the Southwestern Lakeshore Farmlands are located.

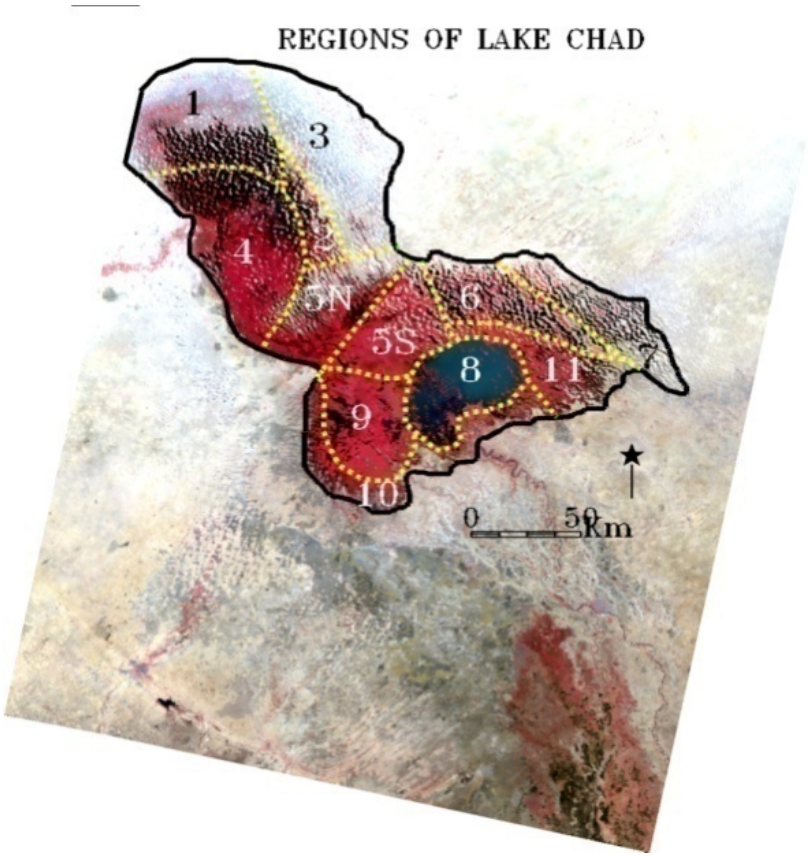

Fig. 1.5: Regions of Lake Chad outlined by Carmouze and Lemoalle.

1.4.1 Agricultural activities and risk zones

Despite the reduction in river volume discharge of the Chari River, seasonal flooding occurs in these sub regions of lake every year between October and December. The flooding season starts from mid October and reaches a peak in November when 50% of the Chari River is discharged into the lake. The period of the lowest discharge is between June and early October. When the waters recede, the still moist lake bed is cultivated. This kind of agricultural practice is called recessional farming. Recessional farming is practiced on land inside or outside the lake that is subject to flooding and in which crops utilize residual moisture left from flood retreat. The area of farmlands on the western side of the lake estimated by the researcher from LANDSAT and ASTER images was approximately 952.4 km^2

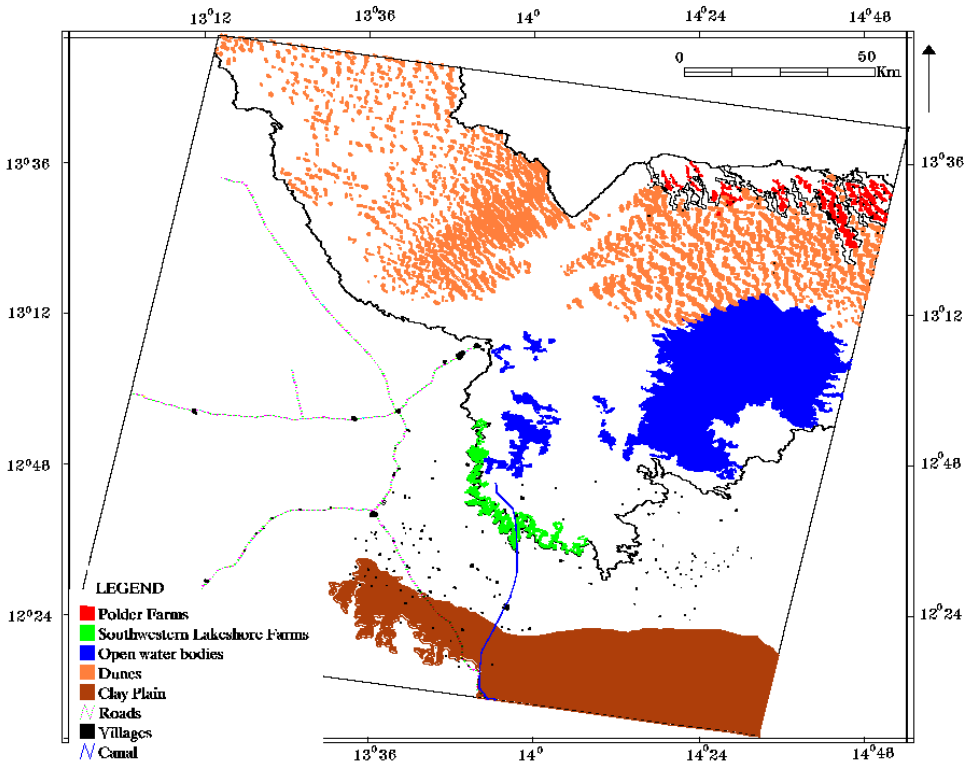

Fig. 1.6: Location of Polder Farmlands and Southwestern Lakeshore Farmlands (source: Drawn from LANDSAT RGB May 2003**).**

Due to the annual variation in flood fluctuation, there is always an uncertainty as to whether the annual floods will cause damages with a risk of livelihood loss for villagers. Because of this uncertainty, these areas are regarded as constitute risk zones. These risk zones are areas of cultivable land that are prone to flood inundation with a high risk of crop loss to the farmers.

Dune islands are cultivated at the edges where the dunes form an interface with the lake water. These dunes are used as settlements when the villagers move eastwards into the lake to follow the contracting lake and take advantage of the exposed lake floor (Sarch and Birkett, 2000).

The recessional farming calendar is variable. It starts around the end of February (Sarch and Birkett, 2000). However in the Southwestern Lakeshore Farmlands, planting begins as early as December (researcher's field observations). Figure 1.7 is the recessional farming calendar for the major crops in the Southwestern Lakeshore Farmlands. The calendar was constructed by the author from interviews with farmers in December 2003. The cycle of planting and harvesting takes a period of nine months

starting in December with the first cropping cycle. The third cropping cycle occurs in June and harvesting occurs in September.

Polder Farmlands are interdune depressions across which dams are built to cut off the flow of lake water into them. The water in the enclosed area eventually evaporates and exposes the lake floor. Crops are planted on the exposed floor of the depression and the water needs of the plant are supplied through residual moisture and seepage to the surface. This happens when the ground water table is sufficiently high to cause the capillary movement of the water. If the water table is deeper, irrigation is practiced with the use of pumps to draw water into the depressions. There are two types of polders, the traditional polders and improved polders (FEWS, 1997). The traditional polders use sand barriers as dams to keep the water out of the depressions or use residual moisture when the lake water recedes each season. The improved polders are

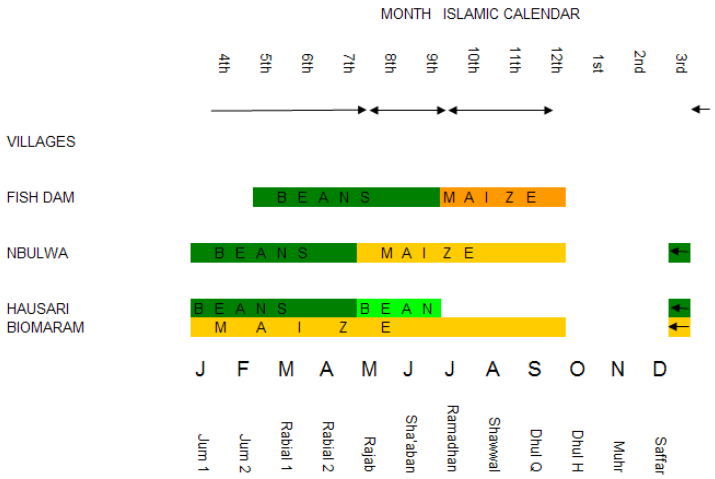

Figure 1.7: Recessional farming calendar for the major crops grown in the Southwestern Lakeshore Famlands of the Lake Chad

constructed with concrete dams so the lake water is permanently kept from reentering the depressions, although in years of exceptionally heavy rains, these polders are also inundated (Dieleman and Ridder, 1963). Improved polder farms minimize the risk of inundation and therefore three cropping cycles are possible on the improved polders farms. On the other hand, traditional polders are vulnerable to flood inundation and therefore only one crop a year is produced. The main crops are rice, wheat and corn. Wheat is sown after the rainy season, between November and December and harvested between March and April. Corn is sown and harvested in July and a third crop is

sometimes sown in the rainy season, which is either corn or millet. The area of Polder Farmlands in the southeastern part of the Lake Chad was estimated by the researcher from MERIS images at approximately 179 km^2.

1.5 PROBLEM DEFINTION, OBJECTIVES AND METHODS

The most significant features of the Lake Chad have been the persistent decline in rainfall over the whole of the basin in the last 30 years, the contraction of the lake, lowering groundwater table levels, declines in perennial vegetation and increases in vulnerability to soil erosion (World Bank, 2002).

Close to 20 million people rely on lake-based economic activities and this figure is expected to increase to 35 million by the year 2020 (World Bank, 2002). People living near and around the lake have developed strategies for taking advantage of the opportunities provided by it especially in the areas where recessional agriculture is practiced. The receding lake left behind an estimated 0.5 million ha of cultivable land, but it is estimated that only 10% of the lake's cultivable areas are now being used (FEWS 1997). These farming activities constitute a very important contribution to the food production in the area and the region has been regarded as a food basket. However, variability in seasonal inundation levels of the lake causes the loss of un-harvested crops and the destruction of infrastructure. In dry years, there is reduced fishing and farming and in wet years settlements and farmlands are flooded (Coe and Birkett, 2004)

The institutional framework policies for the management of the lake basin are still inadequate. Regional and sub regional managerial institutions exist with the sole purpose of coordinating and promoting regional cooperation in the use of the lake's resources amongst the stakeholder countries. However, these institutions have not been effective in achieving their set objectives. This is because there is a lack of coordination and a lack of an integrated approach to the management of the lake's resources at the regional and sub regional levels.

Poor decisions are implemented through insufficient knowledge of the lake's resources and lack of methods for monitoring them. For example Nicholson *et.al.,* (2005) noted the lack of homogeneous series of rain gauge data because gauge networks changed significantly over time. There are few facilities for early warning systems for forecasting flood disasters. Some available data series date back to the 1960s and

1970s (Odada *et.al*, 2003). For example, the most comprehensive maps of the Lake Chad Basin at scale 1:50000, were produced in 1976 and they have never been updated. Some Lake Chad basin organizations established in member countries such as Nigeria made substantial contributions in the area of data collection up to the late 1980s. However lack of political will and funding resulted in the collapse of the previous monitoring networks (Odada.*et.al*, 2003).

The use of remote sensing has opened many avenues for monitoring the environment from space. This is particularly convenient for a region like Lake Chad which not only suffers from institutional mismanagement but also from inaccessibility due to lack of good road and water transportation networks and the nature of the terrain which is very sandy in some areas and clayey in others so that movement is virtually impossible in the rainy season. Therefore obtaining ground based data becomes impractical (Coe and Birkett, 2004).

In general, little emphasis has been directed at the impact of interannual fluctuations of the lake on small scale recessional farming activities that occur around the lake. Given the region's contribution to food security, which is being threatened, this project was conceived with the aim of using a multi temporal approach to evaluate the potential of MERIS optical data as a means of establishing a database for Lake Chad farmland resources, and the use of radar altimeter data to relate areal extent of water to lake level height as an early warning system for the uncertainties associated with seasonal flood inundations.

Although Lake Chad is drying out at an increasing pace, proposals to replenish the lake by rechanneling water from River Obangui in the Congo have been discussed (World Bank, 2002), with some initial funding provided by some of the stakeholder countries. If the project succeeds then there will be an even greater need for establishing an inventory database of natural resources as well as the implementation of early warning systems to cater for unforeseeable changes in the lake ecosystem.

1.5.1 Aims and objectives

The aim of the research is to use a multi sensor, multi temporal approach to evaluate the potential of ENVISAT MERIS optical data

a) as a means of establishing a database for Lake Chad farmland resources.

b) as a means to investigate the relationship between the variation in surface water level and lake areal extent using TOPEX/POSEIDON radar altimeter data and the MERIS optical data.

The objectives of the project are to:

- Evaluate the overall potential of MERIS data for broad regional studies.
- Investigate patterns of change which can indicate croplands in the known areas of polder farmlands of the Southeastern Dune Islands, and recessional farmlands of the Southwestern lakeshore using change detection methods.
- Identify such patterns (which indicate the cropland) over the whole lake basin.
- Relate the spatial distribution and areal extent of the annual inundation of the lake to water level data derived from radar altimeter readings.

The above objectives mentioned above were pursued using the following research methodologies:

Literature on the background, current situation, problems and research in the area of remote sensing in Lake Chad as well as literature on ENVISAT MERIS, TOPEX POSEIDON radar altimeter, Spectral Mixture Analysis and Change Detection was reviewed. Validation of MERIS data for regional studies using the higher spatial resolution imagery of ASTER data was done through Maximum Likelihood Classification and Point Pixel Sampling. Spectral Mixture Analysis (SMA) was performed on MERIS data. Accuracy assessments were carried out on spectrally unmixed MERIS data through comparison of endmember fraction proportions with class area statistics of Maximum Likelihood Classified ASTER data. Post classification Change Detection using threshold binary masking was performed on MERIS for the purpose of examining seasonal change patterns for identifying cropland in the lake basin as distinct from permanent (natural) vegetation which does not change. The areal extent of water and vegetation in interdune depressions, Polder Farmlands and the Southwestern Lakeshore Farmlands was estimated from MERIS LSU images and related to radar altimeter data of Lake Chad water levels between 2003 and 2004.

1.5.2 Thesis outline

In chapter one, the background and scope of the thesis are discussed through an introduction of Lake Chad its background and the current situation. The problems encountered in the Lake Chad, how remote sensing can help in mitigating them are also discussed. The aims and objectives of the thesis and thesis structure are outlined.

In chapter two, research done in the Lake Chad Basin and current literature on Spectral Mixture Analysis, Change Detection is presented. The MERIS and ASTER instruments as well as the TOPEX POSEIDON satellite and radar altimetry are reviewed. Work done on Lake Chad using radar altimetry is also discussed.

In Chapter 3, the procedures and results of validating MERIS data with ASTER through Maximum Likelihood Classification and Point Pixel Sampling are presented. The procedures used for the Spectral Mixture Analysis of MERIS and the accuracy assessments of the SMA classified MERIS using ASTER are also presented. Chapter 4 describes the threshold binary masking technique used in change detection over the lake basin together with the results, discussions and conclusions of the change detected in the farmland areas and patterns of change noticed over the whole lake basin. In Chapter 5, the procedure followed to relate the TOPEX/POSEIDON altimeter data with the areal extent of the lake is first presented. Then the application of the relationship between altimeter data with the areal extent of the lake to MERIS data is presented together with discussion and conclusion of the results obtained. Chapter 6 presents conclusions and recommendations of the study. Figure 1.8 shows the flow chart of the thesis structure.

The data and software used for the study included five optical MERIS images acquired in October and December 2003; February, March and May 2004 and three optical ASTER images data acquired in February, 2004. Auxiliary optical data used were ASTER December 18th 2002; IKONOS acquired in May 2000; Landsat 7 ETM + acquired in May 2003. The Landsat was obtained courtesy of the Lake Chad Basin Commission (LCBC). The software used are BEAM (by Brockmann Consult); ENVI 4.1 (by ITT) and ER MAPPER (now part of Leica Geosystems).

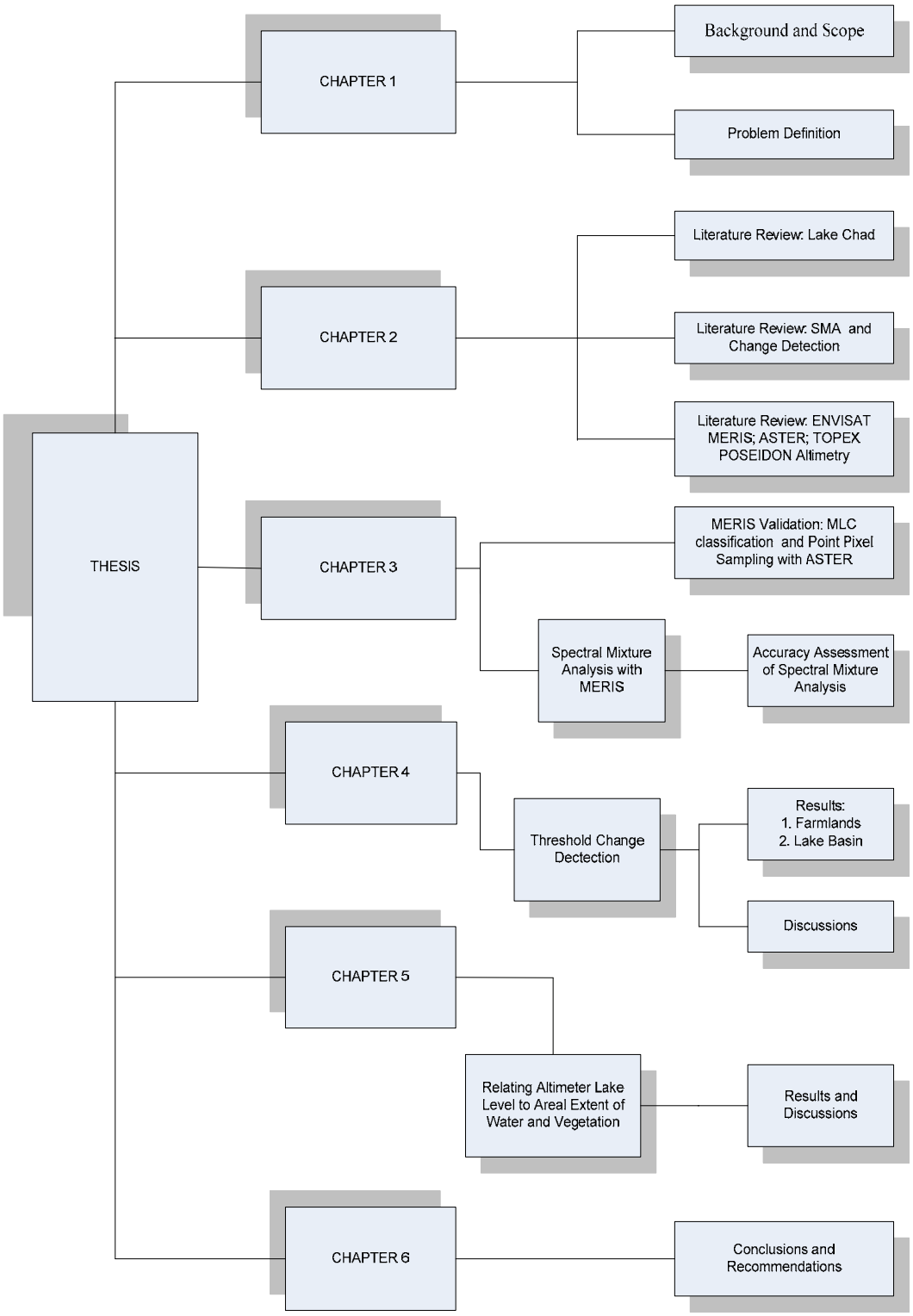

Fig. 1.8:Flow chart of thesis structure

CHAPTER TWO

LITERATURE REVIEW

2.1 INTRODUCTION

The first section of this chapter describes studies undertaken in the Lake Chad basin using remote sensing. The second section of the chapter discusses some basic concepts of the remote sensing techniques used in this project and a review of work done using these techniques. The third section gives an overview and comparison of the ENVISAT MERIS and ASTER optical instruments. The fourth section gives a short overview of radar altimetry and the TOPEX/POSEIDON instrument and the application of radar altimetry over Lake Chad.

2.2 REMOTE SENSING AND NON REMOTE SENSING RESEARCH WORK ON LAKE CHAD

The first comprehensive studies were on Lake Chad published by Tilho in 1910. His work included studies on variations in lake level (Carmouze and Lemoalle, 1983). After Tilho, a half century elapsed before research in Lake Chad resumed (Carmouze and Lemoalle, 1983). Meteorological, hydrological and hydro-biological studies were the backbone of the research done by ORSTOM at Bol.

Some of the earliest remote sensing studies were conducted by Lemoalle (1978). Using LANDSAT, Lemoalle (1978) mapped the bathymetric curve of the lake and distinguished between soil and water in the Chad basin. He was also one of the first to note important fluctuations of Lake Chad in the second half of the 20^{th} century which were captured on LANDSAT data. In Nigeria, the conception of the South Chad Irrigation Scheme, led to land feasibility studies using aerial photography (Evans, 1974; Wickens 1974; Guganeshrajah 1974). Schneider *et.al.,* (1985) monitored the lake boundaries, vegetation growth and surface temperature patterns using LANDAT and NOAA AVHRR data.

Rosema and Fiselier, (1990) used three thermal inertia images from METEOSAT data of 1978, 1983 and 1985 to illustrate changes in the flooding of the Chari/Logone/ Chad system. The very coarse spatial resolution (at 5 km) of the thermal band of METEOSAT meant that the study was very generalized and detailed analyses on changes occurring in specific regions of the lake could not be made. On the other

hand, using a combination of medium resolution LANDSAT and SPOT, and METEOSAT data, Africa and Lemoalle (1996) tracked changes in the surface area of the lake from 1973 to 1995 and found that the flow of water to the north of the basin was a function of the amount of discharge from the Chari River. This finding was important because it established the threshold for the volume of river discharge volume required to cause flooding over the whole lake basin. Discharges of less than $15km^2$ meant that no flow of water reached the northern basin, while an inflow of greater than $28km^3$ into the lake flooded the whole basin. Leblanc et.al; (2003; 2006), also used METEOSAT data to delineate areas with high thermal inertia (open and covered water) from regions with low thermal inertia (dry land) and combined MODIS, LANDSAT and AVHRR images with hydro-geological data to identify and map key surface indicators of recharge and discharge areas of the Lake Chad basin. This ground water modeling revealed that the impact of lake shrinkage on the water table was strong, but limited in space to a relatively small area around the lake.

Change detection on the clay plains adjacent to the lake was performed by Franke Scharfe (2000, 2001) and Franke Scharfe and Skorupinski (2000) who used aerial photographs and SPOT images to map changes in agricultural land use in the southwestern region of the Chad Basin between 1957 and 1990. It was found that 80% of agricultural land south of the lake basin had been replaced by settlement areas. Deflation hollows were also found in recently harvested or densely settled areas in the southwestern region. This was an indication that some areas of the Lake Chad basin were threatened by desertification. The findings showed evidence of anthropogenic pressure applied on the resources of Lake Chad.

Birkett (2000) compared time series TOPEX/POSEIDON radar altimetry with imagery from NOAA AVHRR to examine flooding patterns of the lake. She discovered a positive correlation between the seasonal inundation of the lake and lake level measured from satellite radar altimetry. Sarch and Birkett (2000) compared the relationship between time series lake level fluctuation derived from radar altimeter and livelihood decisions and responses of farming communities to the lake level fluctuations during flood inundation and recession. They categorized 20 years of flooding events (1975 to 1995) on the settlements around the lake shores (together with the farmers' coping strategies to the flooding) into 4 classes (depending on the intensity of flooding). A graph illustrating the categorization is given in figure 2.1. The flood status of the study area over 20 years is shown on the Y axis as class 0 (no

inundation); class 1 (fringes of study area inundated); class 2 (inundated or mostly inundated); class 3 (completely submerged).

From the graph, there were only four years in twenty when flood water did not impact on the settlements. Sarch and Birkett (2000) found that farmers' decisions and responses to the lake fluctuations coincided with the altimeter lake level measurements. They proposed that altimetry could offer a flood forecast and warning system to enhance the ability of farmers to take preventive measures against loss during flooding events.

The above discussion has shown that the ecology and hydrology of the Lake Chad have been studied quite extensively using different remote sensing techniques. In summary, remote sensing studies of Lake Chad used data that either have very broad bandwidths i.e. low spectral resolution,(LANDSAT, SPOT, 1, 2 and 3) or poor spatial resolution (NOAA AVHRR METEOSAT). Where relatively high spatial resolution data like SPOT 4 were used, the areas studied were not risk zones (Firki, clay plains,) although the studies have highlighted increasing pressure on the Lake Chad resources which in turn affect the whole lake basin. Only the works of Sarch and Birkett (2000) dealt with flooding events and their socioeconomic effects on the farmers living in the risk zone regions of the Lake. Moreover Birkett (2000) related time series altimeter lake height data to areal extent of basin inundation. However as NOAA AVHRR data with 1.1 km resolution was used to examine the areal extent of basin inundation, the

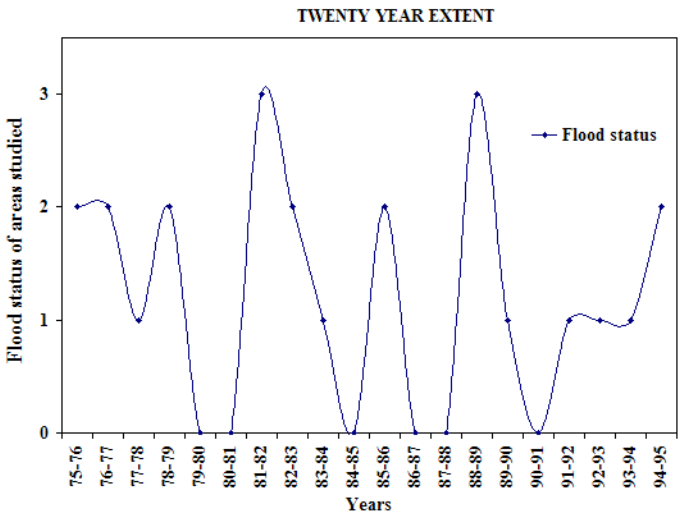

Fig.2.1 Variations in the inundation of the southwestern shore of Lake Chad (Source: Drawn by author from tabulated data)

conclusions drawn from the study can only be generalized over the whole lake area and are not specific to any certain region. Also identifying land uses such as agricultural lands for a lake database requires higher spatial resolution data. The limitation of high spatial resolution data is that the swath widths are small and therefore data acquisition for a basin like Lake Chad can be expensive. The MERIS medium resolution optical data may be able to provide the solution to both small swath widths, low spectral and spatial resolutions. With a spatial resolution of 300m, the area that is resolved by a MERIS pixel is 11 times smaller than the ground area resolved by a NOAA AVHRR pixel. With a 298 by 298 km swath size, the whole basin is covered in a single image. Therefore MERIS may be able to prove a suitable data to use for building an inventory of the Lake Chad resources.

2.3 PRINCIPLES OF LINEAR MIXTURE MODELLING

Traditionally, multispectral data classification has used hard classifiers in which pixels are assigned to one of several classes. Until recently, due to the low spectral resolution of satellite sensors, multispectral image processing has focused on spatial domain based techniques where land covers or patterns are often of major interest. The presence of large heterogeneous pixels or even smaller pixels containing several land cover types has presented problems with hard classification methods because pixels do not clearly fall within the available classes (Mather, 2004). Thus linear spectral unmixing became a viable option for classifying multispectral data.

Radiation reflected from a heterogeneous field of view on the ground can be considered as a mixture of a number of spectrally pure materials (Van der Meer, 1999) because land cover types are often composed of a variety of materials and the distinction between them especially from space is not clear thus resulting in mixed pixels. Mixed pixels have been recognized as a problem affecting the effective use of remotely sensed data in Land Use and Land Cover (LULC) classification and change detection (Cracknell, 1998; Fisher, 1997).

Linear Spectral Unmixing (LSU) is the technique used to estimate the fractions of the land cover elements called endmembers of spectrally pure materials. The technique is based on the assumption that measured spectra are linear mixtures of the scene constituents i.e. the source of the spectra from a pixel is more than one spectrally distinct component (Bannari *et.al.,* 2006). Each pixel is a physical mixture of several

components weighted by surface abundance, and the spectrum of the mixture is a linear combination of the individual endmember reflectance spectra. The mathematical model of LSU can be expressed as follows (Adams *et.al.,* 1986; Boardman, 1994):

$$R_b = \sum_{i=1}^{m} f_i r_{bi} + e_b \text{ and } \sum_{i=1}^{m} f_i = 1.0; \quad (1)$$

Where R_b is reflectance of a pixel in band *b*; f_i is the fractional abundance *i*; *m* is the total number of bands. r_{bi} is the reflectance in band b of endmember *i*; e_b is the residual error or noise in band *b* which is the difference between the observed pixel reflectance and the model computed reflectance of the pixel.

The LSU model, strictly speaking is always true model on a pixel by pixel basis. Thus if there are *n* land cover types present in the area that is covered by a single pixel, and if each photon reflected from the pixel area interacts with only one of these land cover or endmember types, then the integral signal received at the sensor in a given band (R_b) will be the linear sum of the n individual interactions (Mather, 2004). The constraint imposed on the model is that only fractional abundances between 0 and 1.0 are found in the data. For a constrained unmixture solution, f_i becomes subject to the following restrictions:

$$\sum_{i=1}^{m} f_1 = 1 \text{ and } 0 \leq f_1 \leq 1 \quad (2)$$

The model is also limited in the assumption that a single pixel (e.g "grass") endmember can accurately represent grass in every pixel in the scene. There are also variations in the spectral illumination throughout the scene or in different view and illuminating angles, or in multiple reflections which may occur for example in trees and even in grasses (Mather, 2004). The RMS error is used to assess the fit of the model. The RMS is computed using

$$RMS = \sqrt{\frac{\left(\sum_{i=1}^{m} e_i^2\right)}{m}} \quad (3)$$

The RMS error is calculated for all the image pixels. The larger the RMS error, the worse is the fit of the model. Therefore the error image can be used to assess whether the endmembers are properly selected and whether the number of endmembers selected is sufficient (Lu *et.al.,* 2003). The Linear Spectral Unmixing result is expressed as the percentage coverage of each defined ground cover material or endmember in each pixel.

The unmixing processing generally involves three steps (Huete, 2004).The first step is the assessment of the dimensionality or number of unique reflecting materials making up the land cover. This is accomplished by reducing the data using the Minimum Noise Fraction (MNF) transformation. This is a two step principal component analysis, in which during the first step, noise is decorrelated to unit variance and there is no band to band correlation (Van der Meer, 1999). The second principal component transformation results in a data set in which the components are ranked in terms of noise equivalent radiance. The inherent spectral dimensionality of the data set can be found by examining the eigenvalues and associated MNF images. Some of the MNF images are associated with large eigenvalues and coherent (MNF) eigenvalues images while the remainder of the MNF bands has near unity eigenvalues and images dominated by noise. Thus the MNF eigenvalues and images yield the absolute number of endmembers required to model the image spectral response.

The second step is the identification of the physical nature of the endmembers within a pixel. This is done using the Pixel Purity Index to determine the locations of the endmember pixels. The PPI is based on the approach developed by Smith *et.al.*, (1985), which regards spectra as points in an *n*-dimensional space where *n* is the number of bands. The body (referred to as a simplex) which spans the data points in a 2 dimensional space is a triangle having *n+1* facets. The purest endmembers are found at the locations in this space where the sides of the triangle intersect. This principle is extended to higher dimensions in a similar way. The PPI compares the pixels in a scene with the best fitting simplex and records the number of times a pixel is found at the extreme facets of the simplex. When this is shown as an image of cumulative count values, the locations of the spectrally pure endmember pixels in data space can be known.

Endmembers are also determined from various reference spectra acquired from laboratory or field reflectance measurements; from the image itself, (Quarmby *et.al.*, 1992, in Lu *et.al.*, 2003), or from a combination of image and reference endmember

selection methods, including a spectral alignment of the image endmembers to the reference endmember spectra and a calibration relating the image endmembers to the reference endmembers (Roberts *et.al.*, 1998 in Lu *et.al.*, 2003).

The last step in the unmixing procedure is the determination of the amounts of each endmember component in each pixel. The number of endmember fractions that can be used in SMA is limited by the number of bands contained in the images, and cannot be more than the number of bands. This is a limitation except for hyperspectral sensors. Normally between 2 and 5 endmember fractions are used (Scholte *et.al.*, 2006).

2.3.1 Applications of Spectral Mixture Modelling

SMA has been widely applied. Some examples are: LULC and change detection (Roberts *et.al.*, 1998; Govaerts and Verstraete, 1999; Souza and Barreto, 2000; Townshend, *et.al.*, 2000), vegetation mapping, (Oki et.al, 2002; Dennison and Roberts, 2003; Braswell *et.al.*, 2003; Lu *et.al.*, 2003 Glenn *et.al.*, 2005), vegetation change detection (Adams *et.al.*, 1995; Carlson and Azofeifa, 1999; Hostert, *et.al.*, 2003) cover estimation in arid environments, (Sohn and McCoy, 1997; Grandell *et.al.*, 1998; Drake *et.al.*, 1998; McGwire, *et.al.*, 2000; Pontius *et.al.*, 2005) and non arid (Gilabert *et.al.*, 2000) environments, and vegetation stress (Radeloff *et.al.*, 1999). It was also applied to wetlands and flood plain habitat mapping (Novo and Shimabukuro, 1997; Rosso, *et.al.*, 2005; Mundt *et.al.*, 2005; Sonnetag *et.al.*, 2007; Wang *et.al.*, 2007; Vanderbilt *et.al.*, 2007); measuring water turbidity (Kameyama *et al*., 2001), for crop and farmland estimations (Bannari *et.al.*, 2006; Lobel and Asner 2006) and mapping soils (Chabrillat, *et.al.*, 2002; Robichaud et. al, 2007).

Mapping of urban impervious surfaces has been performed using SMA (Ridd 1995; Hung and Ridd, 2002; Phinn *et al*., 2002; Small, 2002; Wu and Murray 2003; Wu, 2004; Rashed et.al 2003; Wang and Zhang, 2004; Song, 2005; Powell *et.al.*, 2007; Tang *et.al.*, 2007; Pu *et.al.*, 2008) urban vegetation abundance mapping (Small, 2001 Nichol and Wong, 2007); and mapping land degradation (Metternicht and Fermont, 1998).

Verhoeye and de Wulf (2002) in a study of the Logone flood plain which is a part of the Lake Chad Basin, introduced a new approach to S.M.A in which spatial autocorrelation within an image is maximized. The need to maximize the spatial autocorrelation in the image arose because the results of fuzzy techniques like S.M.A

describe class composition without providing any indication as to how the classes are spatially distributed within the pixel. Furthermore, Verhoeye and de Wulf (2002) reported that with this technique, fine spatial resolution data is not needed. The drawback with Verhoeye and de Wulf's method was that land cover maps at 500, 200, and 100 m resolution which were derived from synthetic data had accuracies close to 89%, while the accuracy of land cover maps derived from real data dropped to 78% therefore the methodology needed to be improved (Verhoeye and de Wulf, 2002).

Although there have been many studies using remote sensing in the lake Chad Basin, only the study by Verhoeye and de Wulf (2002) have applied SMA to lake Chad. They mapped a section of the Lake Chad Basin by applying SMA to SPOT VEGETATION data as noted above. As this study uses ENVISAT MERIS data at 300 m resolution to detect changes in flood inundation dynamics and also to identify farmlands, SMA was used because many farmlands and land cover units are smaller than this.

2.4 CHANGE DETECTION TECHNIQUES

Change detection is the process of identifying differences in the state of an object or phenomenon by observing it at different times (Lu *et.al.,* 2004). Many techniques for change detection have been developed in the past twenty years as a result of improvements in sensor spatial and spectral resolutions. The earliest techniques include image differencing, principal component analysis, and post classification comparison. In recent years new techniques such as spectral mixture analysis, artificial neural network analysis and the integration of GIS and remote sensing have been included. Lu *et.al.,* (2004) categorized change detection into seven major techniques which include algebraic (e.g. Image differencing), transformation (e.g. PCA), classification (e.g. Post classification comparison), advanced models (e.g. Spectral Mixture Analysis), GIS approaches, visual analysis and other approaches.

Jensen, (1996) outlined seven parameters which are considered when acquiring image data for change detection. These parameters are the same interval of temporal resolution in all images, same spatial resolution, IFOV, look angle, spectral resolution, radiometric resolution, atmospheric, moisture and plant phenological conditions.

In this project, the SMA technique is combined with threshold binary masking of multi-temporal MERIS data to examine patterns of change over time that could be

characteristic of cultivated farmland areas. In this way, areas determined as farmlands which exhibit seasonal changes can be identified distinctly from other (natural) vegetation and recorded. Then SMA classified and binary masked multi temporal MERIS and ASTER data are quantified to determine cultivated areas as well as the areal extent of surface inundation. The areal extents are then related to the TOPEX/POSEIDON altimeter data, in order to evaluate the predictive capability of altimetry. The following discussion briefly describes the nature of the techniques employed for the project and their applications in other studies.

2.4.1 Change Detection using SMA and Threshold Binary Masking.

Change detection using Spectral Mixture Analysis is an advanced form of post classification change detection and is the most often used approach for detection of land cover change. The advantage of using SMA in change detection is that when the image reflectance values are converted to physically based parameters, i.e. endmembers, they are easier to use for information extraction than spectral signatures (Lu *et.al.,* 2004). Rogan *et.al.,* (2002) compared multi-temporal Kauth Thomas (KT) and multi-temporal SMA methods for vegetation change detection using TM images in southern California. They found that the SMA technique outperformed the KT approach because the KT coefficients were fixed and could not be iteratively selected in the same fashion as SMA reference endmembers. For example, the introduction of non photosynthetic vegetation (NPV) as an endmember increased the robustness of vegetation change studies (i.e., detecting vegetation decrease caused by fire). Thus this flexibility associated with SMA provides an advantage over the KT approach.

In binary masking, a threshold is applied to two different date images using an algebraic function to produce a binary mask that highlights changed pixels at a certain threshold level. This method selects suitable thresholds to identify the change and non-change areas and develops accurate classification results. Binary mask change detection has been used for LULC change (Luque, 2000) and vegetation changes, (MacLeod and Congalton, 1998; Petit, *et.al.,* 2001).

2.5 THE ENVISAT MERIS AND ASTER INSTRUMENTS

In this project, ENVISAT MERIS data is validated using ASTER data. A description and comparison of the sensors is made in the following paragraphs.

2.5.1 The ENVISAT MERIS instrument

ENVISAT (ENVIronmental SATellite) is an advanced polar orbiting earth observation satellite. It has ten onboard instruments and among them is the Medium Resolution Imaging Spectrometer (MERIS), first launched in March 2002. The primary goal of MERIS was to monitor the aquatic environment only (Rast *et.al.*, 1999; Verstraete, *et.al.*, 1999). This goal was later expanded to environmental monitoring.

MERIS is a 'push broom' instrument with five optical cameras, which scan in the across-track direction. Each camera has a 14µ field-of-view (FOV). This provides an overlap of around 10 pixels between the modules so that at nadir, the MERIS's FOV is 68.5µ and from a mean platform altitude of 800 km, a swath width of 1150km can be covered (ESA 2006). The pixel size at nadir is 260m across track by 300m along track. The design of the instrument allows the data resolution to be reduced to 1040m by 1200m by combining together onboard, four adjacent pixels across track and four consecutive lines along track (Rast *et.al.*, 1999). MERIS completes a global coverage in three days with a repeat coverage of 35 days.

The MERIS instrument has dual spatial resolution: a reduced spatial resolution (RR) which is 1200m at nadir and a full spatial resolution (FR) which is 300m at nadir (Merheim-Kealy et.al, 1999). The FR ground resolution element (GRE) is invariant at 300m along track, but increases across track from 260m at nadir to 420m at the swath edge. The combination of the spatial coverage with both medium and coarse spatial resolution data facilitates monitoring of the terrestrial environment on a regional, continental and global scale.

As MERIS is both an ocean and a land sensor, its radiometric performance is critical (Rast *et.al.*, 1999, Curran and Steel, 2005) because it has to encompass a large dynamic range to cover weak signals from the ocean as well as signals from bright targets such as clouds and land surfaces, throughout its spectral range.

Table 2.1 MERIS instrument spectral channel bands

	BAND		
Number	Centre (nm)	Width (nm)	Environmental Variables of Interest
1	412.5	10	Yellow substance (gelbstoff), turbidity
2	442.5	10	Chlorophyll absorption
3	490	10	Chlorophyll, other pigments
4	510	10	Turbidity, suspended sediment, red tides
5	560	10	Chlorophyll reference, suspended sediment
6	620	10	Suspended sediments*
7	665	10	Chlorophyll absorption*
8	681.25	7.5	Chlorophyll fluorescence*
9	708.75	10	Atmospheric correction*
10	753.75	7.5	Oxygen absorption reference*
11	760.625	3.75	Oxygen absorption R- branch
12	778.75	15	Aerosols, vegetation
13	865	20	Aerosols correction over ocean
14	885	10	Water vapor absorption reference
15	900	10	Water vapor absorption, vegetation

* Indicates bands for calculating the red edge position.

Therefore the radiometric capabilities of MERIS were designed to be superior to that of a sensor designed for typical land applications. MERIS has 12 bit signal digitization (Curran and Steel, 2005). The radiometric error of MERIS is less than 2% of the detected signal between 400nm and 900nm and less than 5% of the detected signal between 900nm and 1050nm (Rast *et.al.,* 1999). The fine radiometric resolution and high radiometric accuracy has allowed MERIS data to be suitable for ocean remote sensing. For example, MERIS was able to differentiate between 30 classes of chlorophyll concentration over open ocean (van der Meer *et.al.,* 2001). It also allows it to be superior for the estimation of land biophysical data and particularly for the spectral unmixing of image pixels where pure and distinct endmember signatures must be identified. MERIS records visible and NIR radiation in 15 narrow programmable bands (390- 1040nm) therefore it has the capacity to change its band position, width and gain throughout its lifetime. Table 2.1 lists the default MERIS spectral channel bands.

The usefulness of ENVISAT MERIS data is proven by its application to a wide range of projects. Both MERIS RR mode and FR mode have been successfully used in vegetation studies such as assessing forest fire damage (Huang and Sigert 2004; Gonzalez-Alonso *et.al.,* 2007). Goeverts, *et.al.,* (1999) explored the possibility of designing a vegetation index that could be applied in the specific context of the ENVISAT instrument. Clevers *et.al.,* (2002,) showed that the MERIS standard band settings at 665nm,705 nm, 753.75 and 775nm could be used for deriving a red edge index which provides useful information on the physiological status of plants. Clevers *et.al.,* (2007) also noted that the MERIS band 9 at about 708 nm provided additional information, which could be an important innovative feature of the MERIS sensor for vegetation studies.

Dash and Curran (2004) designed a vegetation index for MERIS (MERIS Terrestrial Vegetation Index) which was more sensitive to change in chlorophyll content than the Red Edge Index, and evaluated its potential together with that of the MERIS Global Vegetation Index (Dash et.al, 2007) for land cover mapping. The key feature was to determine if the vegetation indices could be used to map land cover as accurately as a set of individual MERIS bands. Their findings indicated that the two vegetation indices provided a higher degree of inter class separability than data acquired in many of the individual spectral wavebands. Berberoglu, *et.al.,* (2007) quantified net primary productivity (NPP) of conifer forests in Turkey using full resolution MERIS and found the ENVISAT MERIS data was useful for quantifying NPP on a regional scale and also detecting land use and land cover mosaics within a topographically complex terrain of the Mediterranean environment. Clevers *et.al.,* (2007) used MERIS for land cover mapping in the Netherlands as part of ENVISAT validation exercise. They concluded that MERIS was a relevant sensor for land applications as it had greater potential to differentiate major land cover types due to its high radiometric accuracy.

One of the drawbacks of the MERIS data was the redundant information in its spectral bands. Seiler and Csaplovics, (2004), found correlation coefficients in the range of 0.8 and 0.9 for bands 1 – 5; 6 – 10 and 12 – 15 of MERIS data and noted the potential for information overlap within a group of correlated bands. This therefore becomes a major disadvantage for land applications because it becomes more difficult to discriminate between sub classes within a major land cover type. Additionally MERIS data lack shortwave infrared spectral bands (SWIR) which could have offered

additional information that can improve the discrimination of vegetation cover types. For example Sato and Tateishi (2004) showed that SWIR was particularly important for discriminating barren or sparsely vegetated areas. Another drawback was that for the land cover mapping of highly fragmented landscapes e.g. the Netherlands, the MERIS pixels at 300m were very often mixed consisting of various land cover types even for the aggregated classes used for the study (Clevers *et.al.,* 2007). Clevers et.al therefore recommended sub-pixel analysis for land cover mapping with MERIS.

2.5.2 The ASTER Instrument

The ASTER sensor consists of three separate instrument subsystems. Each subsystem operates in a different spectral region. The characteristics of the ASTER instrument include high spatial and radiometric resolution, 15 channel broad spectral coverage from 0.53～11.65μm (visible- through thermal-infrared), and stereo capability for the same path. The three separate subsystems are VNIR, SWIR and TIR (table 2.2). The VNIR subsystem has a spatial resolution of 15m, and consists of two respective backward and forward looking telescopes. This enables the production of pairs of stereo images with a 0.6 base-to-height ratio. The SWIR subsystem has a spatial resolution of 30m and operates in six bands in the shortwave infrared portions of spectrum. The TIR subsystem has a spatial resolution of 90m and five bands in the thermal infrared spectral range for deriving land surface temperature and land surface emissivity. ASTER images have swath widths of 60 km. ASTER has a sun synchronous orbit and is flown at a mean altitude of 705km crossing the equator at 10:30 AM daily.

2.5.3 RELATIONSHIP BETWEEN MERIS AND ASTER SPATIAL AND SPECTRAL RESOLUTIONS

MERIS provides large swath coverage of the whole lake basin but has relatively coarse spatial resolution. However, the sensor has very high radiometric resolution which discriminates of subtle changes in radiance. It also has enough temporal resolution for seasonal change detection and for frequent repeat coverage. In contrast ASTER provides finer spatial resolution for discriminating detailed information on land cover. The sensors overlap spectrally in the wavelength regions between 510 nm and 865 nm (table 2.3). With 15 channels and narrower bandwidths, in the VNIR range, the spectral resolution of the MERIS is finer than ASTER. However the

spectral range of the ASTER sensor is better than MERIS because it includes SWIR and TIR spectral channels.

Table 2.2 Characteristics of the ASTER instruments

Characteristics	VNIR µm	SWIR µm	TIR s µm
Spectral range	1: 0.52 - 0.60	4: 1.600 - 1.7	10: 8.125 - 8.475
	2: 0.63 - 0.69	5: 2.145 - 2.185	11: 8.475 - 8.825
		6: 2.185 - 2.225	12: 8.925 - 9.275
	3: 0.76 - 0.86	7: 2.235 - 2.285	13: 10.25 - 10.95
		8: 2.295 - 2.365	14: 10.95 - 11.65
		9: 2.360 - 2.430	
Ground resolution	15m	30m	90m
Temporal resolution	monthly	monthly	monthly
Swath width	60 km	60 km	60 km
Quantization	8 bit	8 bit	12 bit

Table 2.3: ASTER and MERIS VNIR Overlapping Spectral Bands

ASTER Bands	ASTER Band Width (µm)	MERIS Band Equivalents to ASTER	MERIS Band Centres (nm)
Band 1	0.52 – 0.60	Band 4; Band 5	510; 560;
Band 2	0.63 – 0.69	Band 7; Band 8	665; 681.25
Band 3n	0.76 – 0.86	Band 11; Band 12; Band 13	760.625; 778.75; 865.0

2.6 RADAR ALTIMETRY

Altimeters emit signals at high frequencies (over 1,700 pulses per second) to the earth, and receive a return echo or wave form from the surface. (AVISO, 2006). The time required for a pulse to travel from the satellite antenna to the earth's surface and back to the satellite receiver together with the knowledge of the satellite orbit is used to calculate the range. The range is the spot height measurement made by the altimeter and is the distance from the satellite to the surface of the Earth. The range is calculated as the speed of the electromagnetic waves multiplied by half the total time

from the satellite to the earth's surface in question and is derived within the instrument's foot print diameter.

The altimetric height *H* of a non ocean surface is determined by the difference of the satellite orbit (*Alt*) and the altimeter range R_{corr} measurement, with a final correction for earth tide T_E effects.

$$H = (Alt - R_{corr}) + T_E \qquad (1)$$

where *H* is with respect to a mathematical reference ellipsoid. This surface height is a mean height over the altimeter footprint. The effective footprint diameter depends on the nature of the surface, but is typically 3 to 5 km over ocean surfaces (Daly, 2001), a few kilometers over lakes and potentially a few hundred meters over more specular river or wetland surfaces (Birkett, 2000). Surface heights are recorded at set intervals along the satellite ground track and as each satellite is in a repeat orbit (to ±1 km), time series of variations in the relative surface level can be constructed. Since altimeters were designed for ocean and ice applications, echoes cannot be retrieved over highly undulating land surfaces, or surfaces of a complex nature. In these cases erroneous results are obtained. For example the presence of multiple small pools or many small pools at differing elevations, may bias the overall average height value leading to erroneous results. On the other hand, since the altimeters are nadir viewing and very sensitive to water within a foot print, the presence of dunes or floating vegetation (such as is found in the Lake Chad basin), is not a major hindrance except at the times of extreme water level minimum (Birkett, 2000).

The amplitude of the echo describes the backscatter coefficient σ which is proportional to the power returned to the instrument. The backscatter coefficient is used to identify the presence of surface water (Birkett, 1994; 1995; 2000). Over inland waters its value is dependent on the percentage of water within the footprint and the roughness of the surface due to winds. At the 13.6 GHz operating frequency of TP radar, a backscatter coefficient of less than 5 decibels is indicative of lakes and inland seas and a backscatter coefficient of greater than 20 decibels is indicative of rivers and wetlands. Within the 5 to 20 decibel range, there are no clear divisions to identify the transition between continuous wetland and numerous open pools, muddy banks and saturated soils.

2.6.1 Accuracy of Altimetry Data

To achieve a high accuracy in surface height measurements, both range and orbit heights are carefully estimated (Brown *et.al.,* 2005). Errors in orbital precision used to pose the greatest problem to using satellite altimetry to measure stage in rivers or lakes (Rees, 2001). Orbital errors for some satellites (for example the GEOSAT) were estimated at about 50 cm (Koblinsky *et.al.,* 1993). The TOPEX/POSEIDON orbital precision has been improved to a 3-4 cm rms (Le Traon *et.al.,* 1995 in Birkett 1995) This precise orbit determination is based on satellite laser ranging, GPS or Doppler tracking of the spacecraft and is independently performed from the range measurements (Brown *et.al.,* 2005). The small orbital error of TP has made radar altimetry over inland water surfaces a routine procedure in sites where a lock on the land surface can be maintained.

Range heights are corrected for both instrumental and geophysical effects. The overall accuracy of the range depends on the range precision and the instrumental and geophysical range corrections which is a measure of the internal consistency or repeatability. The corrections depend on surface conditions of the lake. The type of surface determines the shape complexity and intensity of the radar backscatter of the returned echoes. Large surface undulations result in wider footprints and consequently a wider range in return period. The changes in surface height can be caused by variable wind speeds leading to stormy lake conditions. For example wind speeds of 20 ms^{-1} and a large fetch of 600km can induce a Significant Wave Height 7.3m (Sly, 1978 in Birkett, 1994). In situations like this, the radar backscatter coefficient over lakes is broad and ocean like at about 8dB. Where the lake is surrounded by some terrain or growing vegetation the lake is buffered from the effects of the wind and low wind conditions are experienced. The radar backscatter coefficient becomes narrow peaked and can be in excess of 40 dB especially over smooth specular lakes. For Lake Chad, the radar backscatter coefficient is around 20 dB in the region of open water (Birkett, 2000). An electromagnetic bias (embias) correction is applied to the Geophysical Data Records (GDR) to correct for the instrumental errors. Birkett (1995) noted an embias correction of ~2-4 cm at a 1-Hz SWH for calm lakes and an embias correction of ~10 – 15 cm at a 1-Hz SWH for stormy conditions across a lake.

The geophysical corrections are corrections applied due to water vapor in the troposphere. The magnitude of the tropospheric range correction depends on local

climate and precipitation patterns. The spatial variability of the wet correction across lakes ranges between 0 for small lakes and 7 cm rms for large lakes and seas. The tropospheric correction data is obtained from the European Centre for Medium-Range Weather Forecasting (ECMWF) and also from instantaneous measurements derived onboard TOPEX using the TOPEX microwave radiometer (TMR). The uncertainty in the TMR correction is 1.2 cm rms, while the uncertainty in the ECMWF correction is in the order of 3 cm rms (Birkett, 1995). This is coincident in size with the T/P orbit error of ~3-4 cm rms, therefore errors due to water vapor may not be resolved adequately. Furthermore, the ECMWF model can show higher humidities than the TMR correction especially in regions with high humidities. This leads to a bias which is variable for each lake. On the other hand, according to Birkett, (1995), for some lakes e.g. Lake Chad, the EMCWF corrections are comparable to TMR, thus either correction can be applied in the absence of the other. The TMR corrections were used for the majority of repeat cycles for the Lake Chad data.

Altimeter data are usually validated by comparison with ground based gauge measurements. Koblinsky *et.al.*, (1993) using GEOSAT wave form data, found a rms error of 0.7m between ground and altimeter estimates of water surface level along the Amazon river. They concluded that uncertainties of ground measurements and the radial component of the orbit estimated at 50cm were major contributors to the error. Ayana (2007) found a correlation coefficient of 0.97 between gauge data and T/P data for Lake Tana in East Africa. A comparison of T/P and JASON results with gauge data for the Great Lakes showed an accuracy of ~3-5 cm rms (Cretaux and Birkett, 2006), although this accuracy was reduced for smaller lakes. Coe and Birkett, (2004) also validated T/P altimetric water height variations for Lake Chad by comparing daily gauge data with altimeter data. A rms value of 21cm was considered to be an approximation because the gauge and satellite sites were not in the same location and differences in spatial location between altimeter and gauge sites can result in height and timing variations. This is one of the problems encountered in the Lake Chad basin where gauge data is sporadic because of operational difficulties (Coe and Birkett, 2004). At locations where the sites are more closely aligned, accuracies of > 3cm rms have been shown to be obtainable. Validation exercises for other lakes revealed typical accuracies of the satellite altimeter measurements (e.g. 5cm rms for Lake Issykkul and 10 cm rms for Lake Chardaryar in central Asia). Birkett, (1995) concluded that altimetric accuracy of Central Asian lakes and reservoirs was not

homogeneous but was dependent on the quantity and quality of the satellite altimetric data available for each lake or reservoir.

2.6.2 The TOPEX/POSEIDON Satellite.

The TOPographic Experiment /POSEIDON (TP) satellite was first launched in October 1992 as a joint venture between the US and French governments. The NASA Radar Altimeter, (NRA) instrument aboard the satellite is owned by NASA while the POSEIDON instrument is owned by the Centre National d'Etudes Spatiales (CNES). The NRA is a dual-frequency active microwave sensor at nadir which operates in Ku band (13.6 GHz frequency, 2.3-cm wavelength), and C-band (5.4 GHz frequency, 5.8-cm wavelength). It was primarily designed to measure range, wave height and wind speed and amount of atmospheric precipitation. It has a10-day repeat cycle, in which the oceans and continental surfaces from 66° latitude North to 66° latitude south, are observed along its track. Each cycle consists of 254 passes, which is half an orbit around the earth and contains approximately 56 minutes of data (MacMillan *et.al.,* 2006). The temporal resolution of the satellite is governed by the repeat orbit of the satellite. The TP equatorial ground track spacing is about 300 km and its swath width only amounts to a few kilometers. Its dual frequencies make simultaneous measurements over a time interval of 0.1s, corresponding to a 700-m along track distance (Papa *et.al.,* 2003). The measurements are used for ionospheric correction (Rosmorduc *et.al.,* 2006).

To date, the best retrieved height accuracies deduced from the TOPEX/POSEIDON mission have been observed to be 3-4 cm RMS for the largest lakes (for example lake Ontario Birkett, 2000), while the accuracy of T/P elevation time series for rivers, wetlands and floodplains can range from ~10cm to tens of centimetres.

2.6.3 Radar Altimetry over Lake Chad.

Initially, TOPEX POSEIDON satellite's primary objective was to measure sea surface heights, and derived climatic phenomena. However, the TP altimetry studies over inland lakes and rivers were shown to be successfully applied. Lake Chad is one of the inland lakes which have been extensively monitored by the TOPEX POSEIDON radar altimeter. Birkett (1995) produced the first altimetric time series of level variations for Lake Chad using data (September 1992 to May 1994) from the TOPEX POSEIDON mission. Coe and Birkett (2004) used a combination of gauge and radar altimetry data, to estimate inflowing river discharge, and predict the

downstream discharge and lake level. The prediction of the wet season water height in the lake and marshes was considered important because the seasonal maximum level determines the success of the farming and fishing season for the people on the southern shore of the basin.

In a synergistic study of the relationship between mean radar backscatter coefficient, surface water height and inundation extent within the lake basin, Birkett (2000) discovered that the values of the radar backscatter ranged from between 5 and 44 decibels. The seasonal variation of the σ° averaged over the zone of interest was found to correlate quite well with the expected water level and inundation extent. Seasonal and interannual variability associated with the surface water level was also observed from the TP altimeter. It was noted that within the lake basin, a period of 7 to 8 months elapses between periods of minimum and maximum water levels. Birkett also noted a rate of change in water level of approximately 1 cm per day, amounting to approximately 15 cm to 35 cm per year. The peak levels for the lake appeared to be mid November in the area of open water and late December for the southwestern regions of the lake.

She was able to detect with an accuracy of greater than 10cm RMSE, seasonal water level variations of the order of 0.5 – 6m. She also discovered that there was a rise in the minimum level of the water of 15 – 35 cm per annum within the lake basin. The image analysis revealed a permanent lake area of open water of 1,385km^2 with an additional flood area of up to 3600km^2.

2.7 SUMMARY

The ecology of the Lake Chad has been studied using different remote sensing techniques and newer and evolving satellites. However, the studies used satellite data with either broad bandwidths or poor spatial resolution. There are no studies which have dealt with flooding events and their effects on agricultural activities in the risk zone regions of the Lake. Even studies undertaken by Birkett which were relevant to this project used altimetry data together with coarse spatial resolution AVHRR images and the conclusions drawn from the study on the synergistic remote sensing of Lake Chad, can only be generalized over the whole lake area and are not specific to individual regions.

In terms of mapping techniques there have been only a few researches on the Lake Chad using subpixel spectral unmixing. Within what is available in the literature to

date, only Verhoeye and De Wulf (2002) applied SMA to test a new algorithm and map the Logone flood plain of the Lake Chad Basin. So far there have been only two studies carried out using ENVISAT data in Africa and none on Lake Chad, although the LCBC is plans to acquire ENVISAT data for monitoring lake level fluctuations (Jones, et.al, 2006).

Thus as building a useful database requires higher spatial resolution data the MERIS medium resolution optical data can provide the solution to swath size, and the high radiometric ability to discriminate subtle changes in energy levels, can compensate for the relatively low spatial resolution of 300m.

This is the justification to use MERIS data and combine spectral mixture analysis with multi temporal change detection to detect flood inundation dynamics in order to identify farmlands within Lake Chad basin.

CHAPTER THREE

VALIDATING MEDIUM SPATIAL RESOLUTION MERIS DATA WITH HIGH RESOLUTION ASTER DATA FOR THE STUDY OF LAKE CHAD BASIN.

3.1 INTRODUCTION

Due to the difficulty of obtaining ground truth over large areas for validating MERIS image classification, 15 m resolution ASTER data were used. The ASTER data were classified using Maximum Likelihood Classification. In order to verify the ASTER data, IKONOS images with 4 m resolution were obtained for visual analysis and observations were conducted and LULC identified. A description of the LULC from fieldwork is given in appendix A1. Consequently ASTER data were used to validate results obtained from the MERIS LSU classification and also to check the analysis of the relationship between net changes in areal extent of water and vegetation found in MERIS data and time series variations in lake level using TOPEX/POSEIDON altimeter data (described in chapter 5). A comparison between MERIS and ASTER sensors was done in chapter 2. Figure 3.1 illustrates the procedure followed in the validation process.

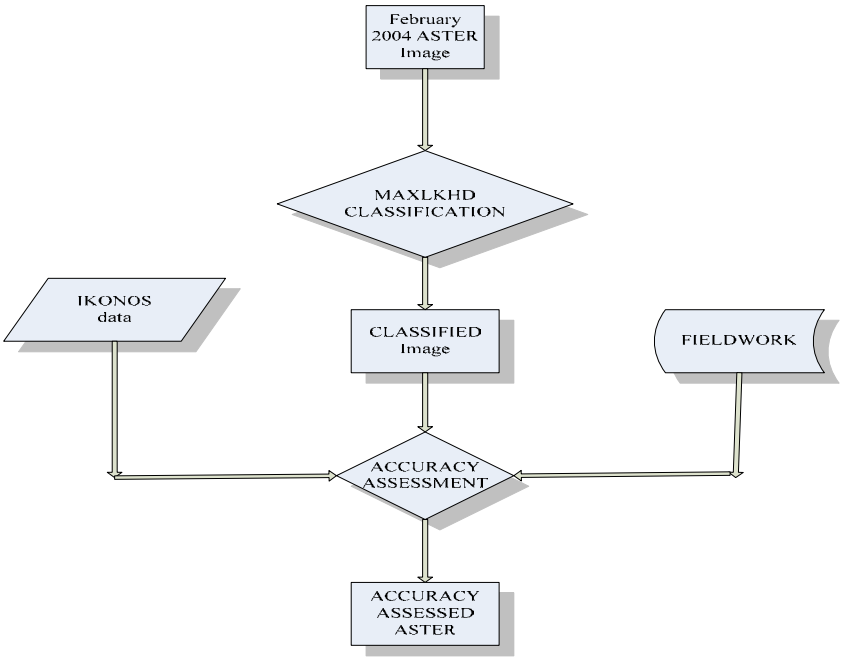

Fig. 3.1: Flow chart of procedure involved in the validation process

3.2 ASTER DATA USED FOR THE ACCURACY ASSESSMENT OF MERIS

Three ASTER images of a single date and 1 MERIS image were used. The centre latitude and longitude of the three ASTER images were 13.4°N 13.9°E; 12.9°N 13.8°E and 12.3°N 13.7°E. All three were acquired on February 7th 2004 at approximately 9:43 AM. The centre latitude and longitude of MERIS is 13.4°N, 14.2°E. The MERIS image was acquired on February 25th 2004 at approximately 8:57 AM. All data were geo referenced to a UTM map projection and WGS84 datum. Each ASTER image shows an area 60 km by 60 km of the southwestern part of the Lake Chad basin while the MERIS image at 298 km by 298 km shows the whole basin. Therefore all the ASTER image scenes can be located on the MERIS image.

The scenes on MERIS corresponding to the ASTER images were subset into three separate files. Figure 3.2 illustrates the location of the image scenes of the lake bounded by the rectangle. A description of IKONOS data used to verify ASTER data is given in appendix A2. The three 60 by 60 km ASTER images are referred to as datasets 1, 2 and 3. The region covered in ASTER dataset 1 shows part of the region known as the Grand Barrier. This is a ridge that divides the lake into northern and southern basins (UNDTCD, 1993). The scene in the February ASTER dataset 2 image consists of the southwestern portion of Lake Chad where the Southwestern Lakeshore Farmlands are located. The area is flat and lies between 281m and 284m above sea level and gently slopes northwards towards the lake. It is characterized by lacustrine sediments with three dominant land cover types (see figures A1.1 and A1.2 and plates A1.1 to A1.6 in appendix A1.1).

The third ASTER image is the area immediately to the south of the lake. The image shows the black clay plains sandwiched between sandy soils and sandy clay loam soils. Figures 3.2 to 3.4 show the outline of the study area, and the boundaries of the datasets on ASTER and MERIS images.

The supervised Maximum Likelihood classification procedures performed on ASTER and MERIS are described in Appendix A3.1 and A3.2. The accuracy assessment and validation of ML classified MERIS was done by comparison with ML classified ASTER data through point pixel sampling. The procedure is described in Appendix A3.5.

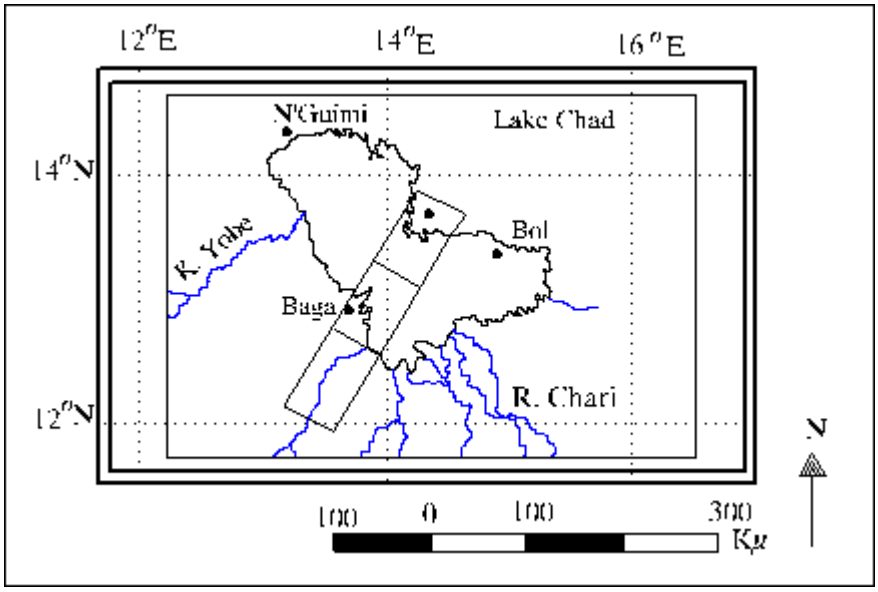

Fig 3.2: Rectangle bounds ground scene of the three ASTER images (Modified from: S. Cross UNDTCD/LCBC 1993)

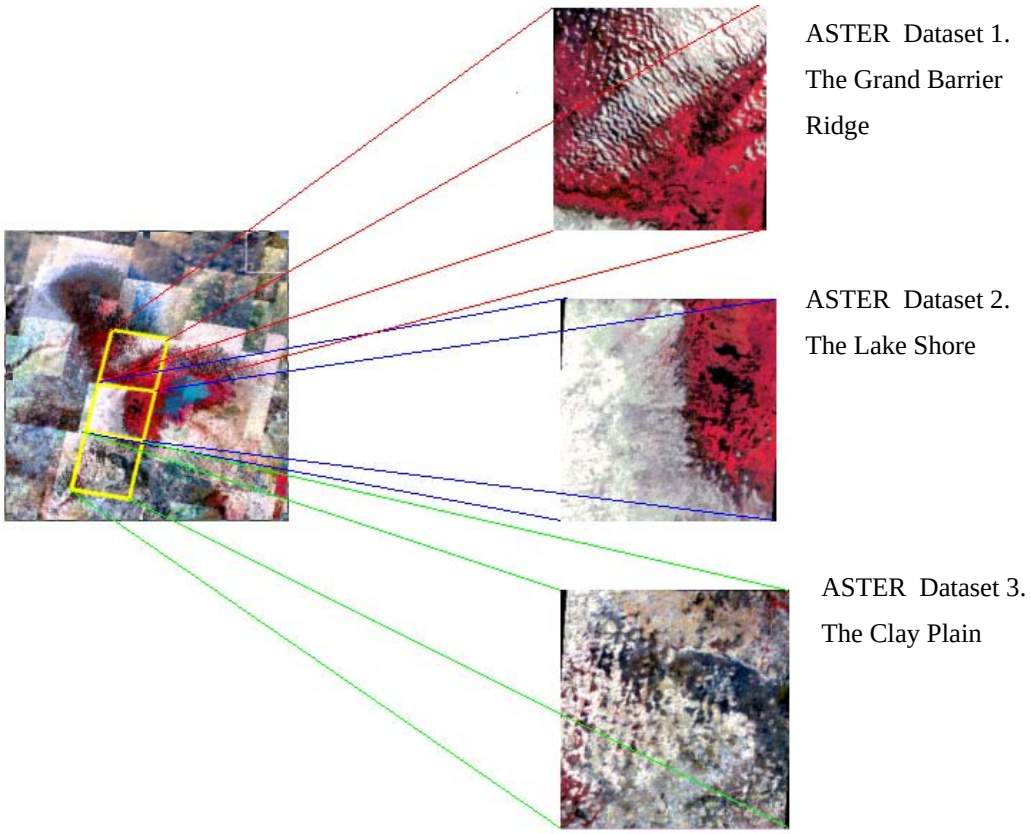

Fig 3.3: Location of ASTER RGB datasets in the Lake Chad.

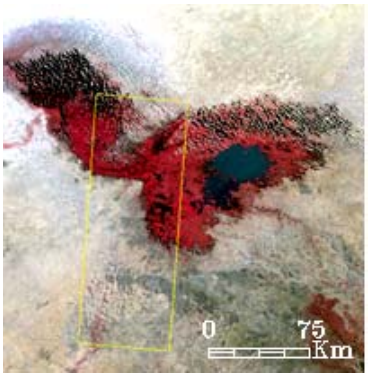

Fig 3.4: MERIS image (RGB 12,7,5; February 25th 2004)

3.2.1 Results

Accuracy assessment was carried out on classified ASTER with ROIs generated from the ASTER image on the basis of identified land use/land cover from IKONOS image and field observations. The Kappa Coefficients obtained for ASTER datasets 1, 2 and 3 respectively were 0.95, 0.94 and 0.92 respectively (table 3.1. See appendix A3 for confusion matrix tables). The accuracy assessments indicate a very good agreement between ASTER and field data and suggest that ASTER data is a reliable substitute for ground data when validating MERIS.

Tables 3.2, 3.3, 3.4 show the accuracy assessment of the point pixel sampling using the Confusion Matrix while table 3.5 shows the overall accuracy and Kappa coefficients between data pairs.

Table 3.1: The Overall Accuracy and Kappa Coefficient of the ASTER datasets.

	Overall Accuracy (%)	Kappa Coefficient
ASTER Dataset 1	96.44%	0.9505
ASTER Dataset 2	95.12%	0.939
ASTER Dataset 3	94.125%	0.9183

Table 3.2: Pixel point sample accuracy assessment tables: Grand Barrier.

		ASTER DATA							
		Swamp	Sand	Clay	SCL	Water	Crop	V S S	Total
M E R I S D A T A	Swamp	791	2	8	2	34	31	8	876
	Sand	0	151	0	0	1	0	3	155
	Clay	4	1	39	19	0	0	4	67
	SCL	0	18	0	92	0	0	5	115
	Water	13	0	1	1	285	0	0	300
	Crop	15	12	6	8	4	103	29	181
	VS S	3	24	0	2	0	1	116	146
	Total	826	208	54	137	324	135	156	1840

(SCL = Sandy Clay Loam; VSS = Vegetated Sandy Soil).

Table 3.3: Pixel point sample accuracy assessment tables Lake Shore.

MERIS DATA \ ASTER DATA	Swamp	Sand	Clay	SCL	Water	Crop	VSS	Total
Swamp	789	0	5	0	58	13	0	855
Sand	1	24	0	5	0	0	23	53
Clay	1	0	230	5	1	12	23	68
SCL	0	5	4	139	0	9	29	186
Water	6	0	2	0	205	0	0	213
Crop	19	1	38	21	8	137	14	238
VSS	0	2	0	3	0	3	60	68
Total	816	32	135	224	262	174	135	1922

(SCL = Sandy Clay Loam; VSS = Vegetated Sandy Soil)

Table 3.4: Pixel point sample accuracy assessment tables Clay Plains

MERIS \ ASTER DATA	Clay	SCL	Water	Crop	VSS	Total
Clay	549	21	15	15	9	609
SCL	44	561	2	1	64	672
Water	1	1	1	0	1	4
Crop	1	12	0	32	7	52
V SS	7	34	0	6	426	473
Total	602	629	18	54	507	1810

(SCL = Sandy Clay Loam; VSS = Vegetated Sandy Soil)

Table 3.5: Overall Accuracy and Kappa Coefficients for MERIS datasets.

	Overall Accuracy (%)	Kappa Coefficient
Pixel Point Sampling 1	85.7%;	0.804
Pixel Point Sampling 2	82.41%	0.765
Point Pixel Sampling 3	86.71%	0.806

3.2.2 Discussion: ASTER datasets and MERIS subset data classification accuracy

The individual Kappa Coefficients for the pixel point sampling on MERIS (table 3.5) show a strong agreement with all three ASTER subsets. Because of the predominance of swamp vegetation in datasets 1 and 2 and the predominance of the clay plains in dataset 3, the landscape was not fragmented thus giving higher accuracy. On the other hand, the spatial resolution of the MERIS has meant that many mixed pixels have been ultimately assigned to the predominant class. This gave the impression of greater homogeneity of the land cover types. This was quite apparent in the discrepancy between ASTER dataset 2 and MERIS dataset 2. There was still a lot of inundation on

the southwestern shore of the lake in February (Figure 3.5). However, because the dates of the image acquisitions were 7th February and 25th February for ASTER and MERIS respectively, some of the water had evaporated between 7th and 25th February, thus allowing more vegetation to be seen on the MERIS than on the ASTER. The mixed MERIS pixels represent a combination of water and vegetation on the farmlands and a combination of soil and vegetation on the upland area adjacent to the farmlands (figure 3.5). Because the water reflectance was dominant on the farmlands (figure 3.5 MERIS blue circles), the large MERIS pixels were assigned to the water class. On the adjacent upland area the vegetation reflectance was more dominant in the pixels than the soil reflectance (figure 3.5 MERIS white circles) and so the pixels were assigned to the vegetation class (see figures A3.1 and 3.2 ASTER and MERIS datasets 2 middle images in Appendix A3.2). Likewise soil land cover was misclassified. The soil land cover was already quite heterogeneous on ASTER dataset 2. However in certain areas where the soil was purely sandy, land cover was homogeneous, (the extreme right side of ASTER figure 3.5) which gradually increased in clay content as the edge of the lake is approached. Towards the bottom centre of ASTER image, the soil appeared sandy but with specks of red, indicating the presence of upland vegetation. Most of these details were not present in the MERIS image (figure 3.5), because overall, sandy regions are interspersed between loam and sand clay loam areas and therefore due to the spatial resolution of MERIS, the overall appearance on MERIS was of clay soil. This also contributed to misclassification of the ASTER pixels where vegetated sandy soil were assigned to other soil classes (Table 3.3)

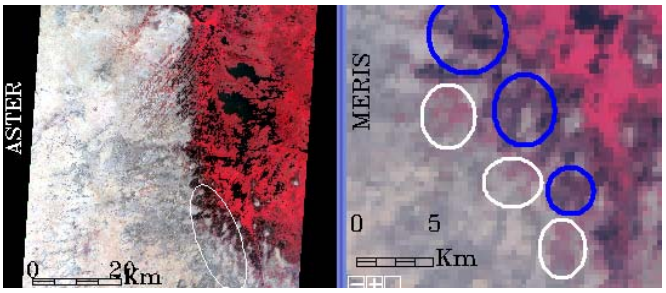

Fig. 3.5: ASTER and MERIS February images showing areas of misclassification due to mixed pixels.

3.2.3 Conclusion

The aim of this section was to determine whether the analysis using MERIS could be validated using ASTER thus confirming that the MERIS sensor could be used for regional studies. An observed agreement ranging from 82% to 87% between the datasets was determined, and Kappa ranging from 0.77 to 0.8 was derived. In view of the large differences in resolution, this is high and this was attributed to the high degree of homogeneity of the landscape. Classification discrepancies resulting from MERIS mixed pixels were found around the shoreline of the lake where the farmlands of interest were located. These areas are the ones liable to misclassification and these are some of the areas that are important for the project. MERIS has fine radiometric resolution and high radiometric accuracy. These properties offer an opportunity for the spectral unmixing of imagery and the estimation of biophysical variables (Curran and Steele, 2005). Therefore any further classifications should employ soft classification methods such as spectral mixture analysis.

3.3 SPECTRAL MIXTURE ANALYSIS OF MERIS DATA.

Soil, vegetation and water are the features that make up the dominant land cover types on the MERIS images. Cultural features like villages are indistinct and there were no impervious surfaces like tarred roads in the area. Thus the LSU method is easily applicable to this study area as the endmembers are spectrally distinct.

This chapter discusses the Linear Spectral Unmixing processes used to extract the end member fractions of vegetation, soil and water from optical MERIS data of Lake Chad and also the validation of the accuracy assessment of the classification using ASTER data. The flow chart of the LSU process followed is given in figure 3.6

3.3.1 Methodology

All data were geo referenced to a UTM zone 33 map projection and WGS84 datum. Each MERIS image shows an area that is 298 km by 298 km covering the whole Lake Chad basin. Each image was imported into the BEAM (Basic ERS and ENVISAT ATSR and MERIS toolbox) software. The images were rotated to true north and then atmospherically corrected using the SMAC Processor, an integral tool in the software. The SMAC processor implements the Simplified Method for Atmospheric Correction as described by Rahman and Dedieu (1994).

Minimum Noise Fraction transformation (MNF) was performed to de-correlate and separate noise from the data. All bands with eigenvalues less than 2 were regarded as noisy bands and discarded. Bands 13, 14, 15 were discarded for October and December 2003; March and May 2004 images. Bands 12 to 15 were discarded for February 2004. Figure 3.7 shows the eigenvalues plot for October 2003.

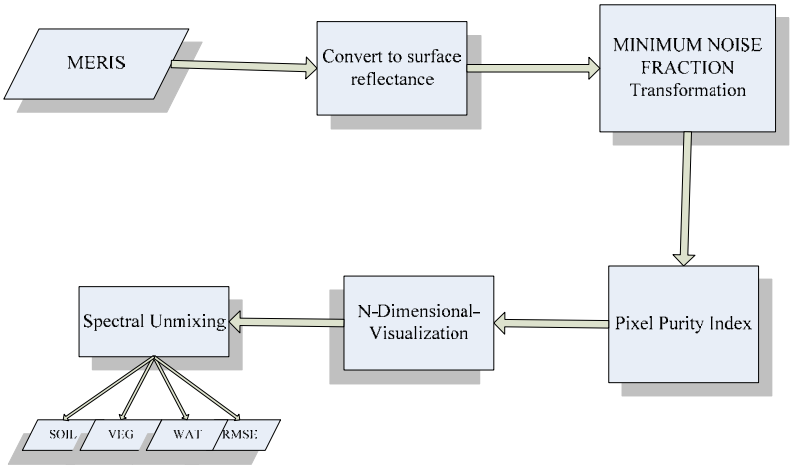

Fig. 3.6: Flow chart of LSU processing.

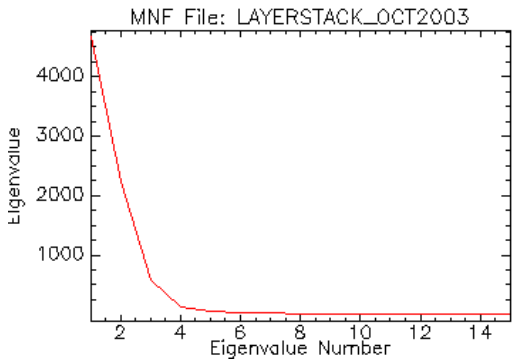

Fig. 3.7: October 2003 plot of eigenvalues

Pixel Purity Index iterations were performed on the retained MNF bands. The number of iterations for each image was 5000 and the threshold or tolerance factor of 3 noise standard deviation was applied. PPI graphs and image maps were generated (figure 3.8). The pixel values on the PPI image indicate the relative degree of purity of the pixel. The higher the value of a pixel, the purer it is.

In order to extract pure pixels, regions of interest were identified from the PPI maps and visualized in an *n*- Dimensional scatter plot. This was done by generating a

statistics file for each PPI image. A histogram curve of the number of pixels identified as pure (Y axis) and the number of times the pixel was identified as pure (X axis) was plotted from the statistics file and a threshold was selected from the value nearest to the break in slope. All pixels equal to or over the threshold value were displayed as regions of interest on the PPI image. Table 3.6 lists the thresholds for the five MERIS data

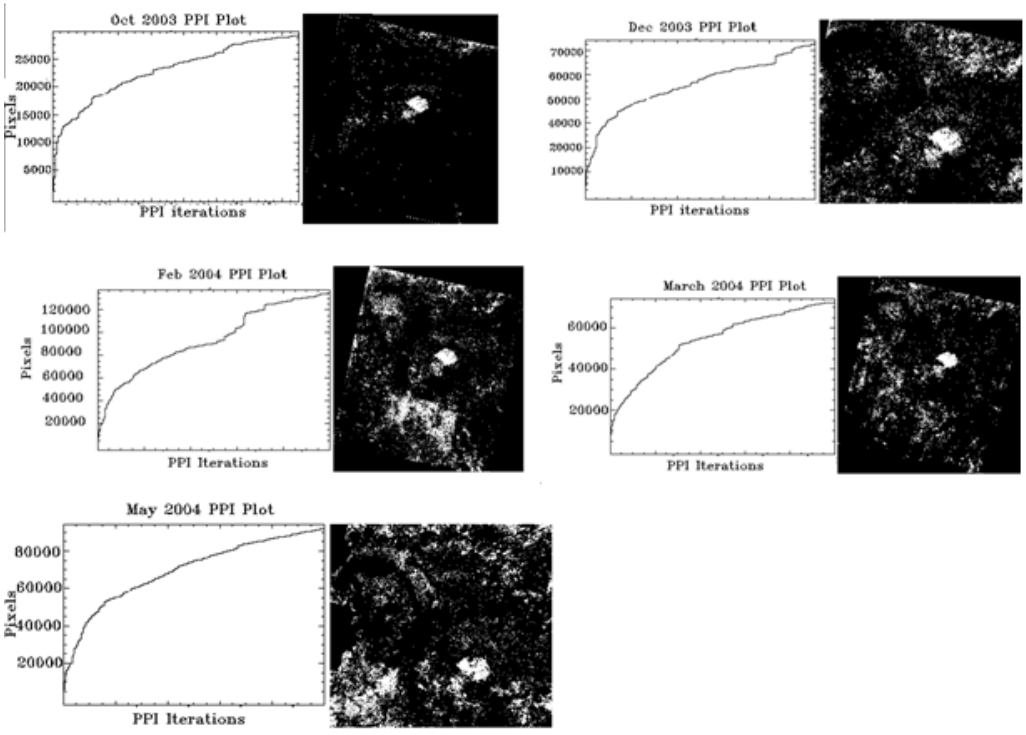

Fig. 3.8: Pixel Purity Index maps and plots: MERIS October 2003 to May 2004.

Table 3.6 Threshold values for determining the purest pixels: October to May MERIS data.

MONTH	THRESHOLD(Number of Pure Pixels)
OCTOBER	217
DECEMBER	448
FEBRUARY	315
MARCH	396
MAY	287

The locations of pure pixels of vegetation, soil and water were identified on the original and MNF transformed MERIS images using the n-Dimensional Visualizer. A 2d scatter plot of pixel cloud simplexes were displayed from the MNF transformed images. The simplexes showed the positions of the pure pixels to be at the vertices of the simplexes (red patches, figure 3.9). Endmember spectral plots were generated

(figure 3.10). Pixels were projected through the axes of the different bands and endmembers were defined by isolating pixels which formed clusters and remained together throughout the projections.

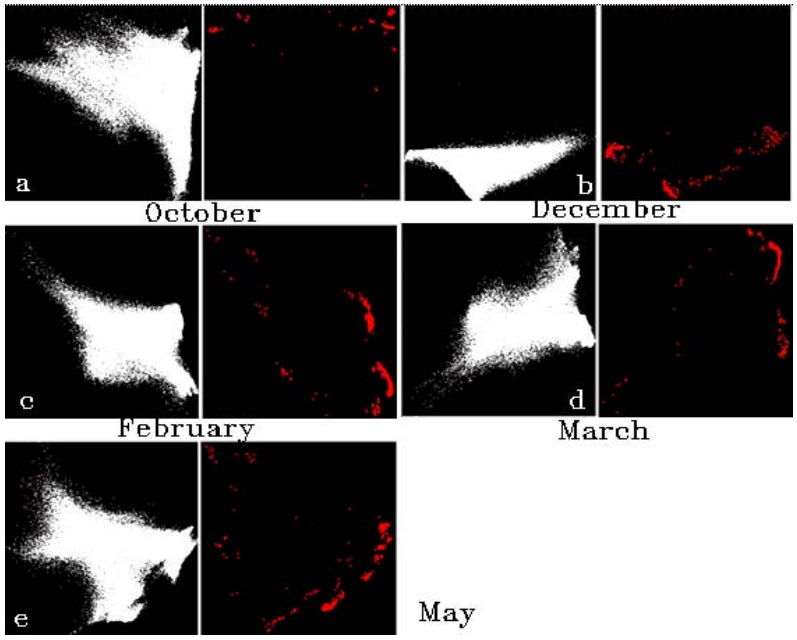

Fig. 3.9 Image simplexes with location of extreme pixels (colored red)

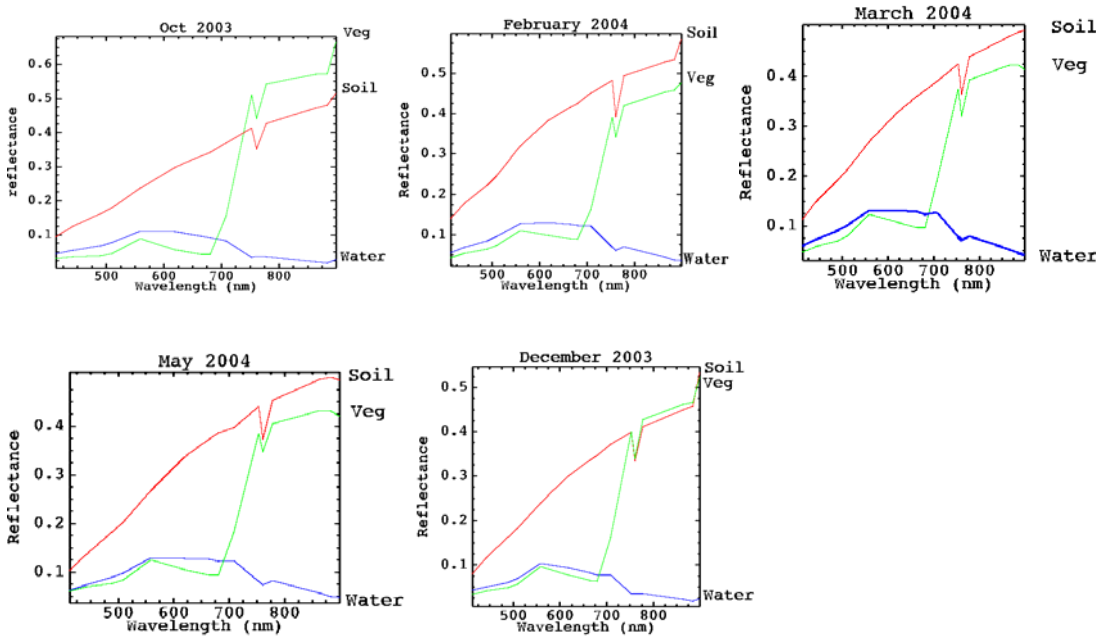

Fig. 3.10: Endmember spectra of vegetation soil and water

A constrained linear spectral un-mixing classification was performed using the derived end members of vegetation, water and soil. A constraining weight of 10 was applied to all the images and was found to be sufficient to make the pixel end members sum to 1.

3.3.2 Results

Four bands were generated from the LSU classification for each dataset (figures 3.11 to 3.15). Three of the bands were for the three endmembers i.e. vegetation, water, soil. The fourth band was an error (RMSE) image band. The error band is a noise image band used to assess the fit of the LSU model. The larger the RMS error, the worse is the fit of the model (Lu *et.al,* 2003). Small (2003) applied SMA on IKONOS imagery to quantify and compare reflectance properties in urban areas. The resulting RMS error was less than 3% which was considered by Small as sufficiently low to make the classification accurate.

The RMS error obtained from the Linear Mixture Analysis of MERIS was found to be less than 0.033 for 99% of the classified pixels. That is less than 3% classification error in 99% of the pixels in all the fraction abundance images examined. The RMSE is shown in table 3.7.

Table 3.7 RMSE of images

Data	October	December	February	March	May
Percentage of pixels	99%	99%	99%	99%	99%
RMSE	≤0.0325	≤0.0318	≤0.023	≤0.025	≤0.035

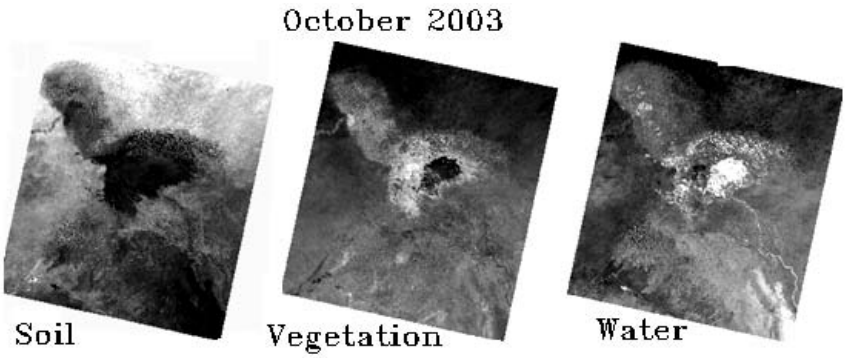

Fig. 3.11: October 2003 showing soil, vegetation and water LSU bands

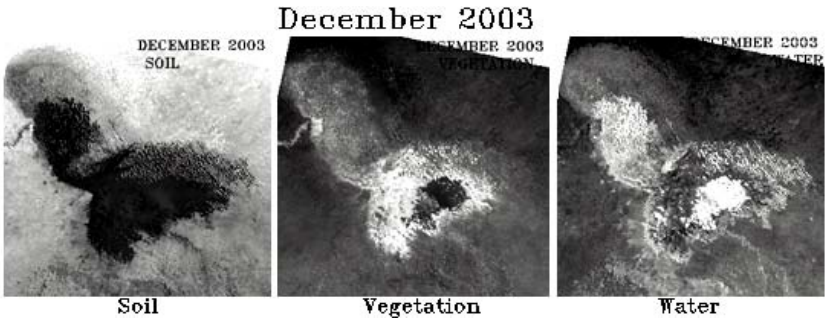

Fig. 3.12: December 2003 showing soil, vegetation and water LSU bands

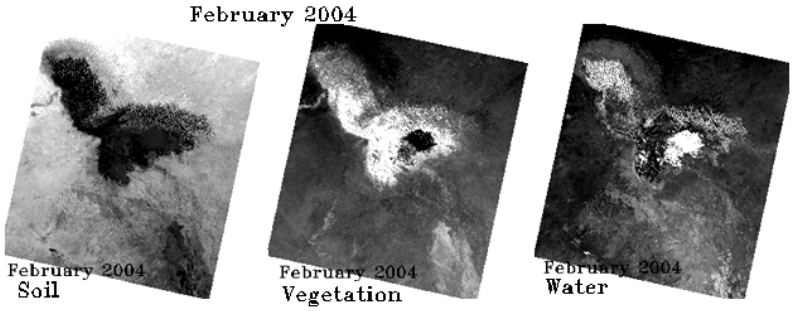

Fig. 3.13: February 2004 showing soil, vegetation and water LSU bands

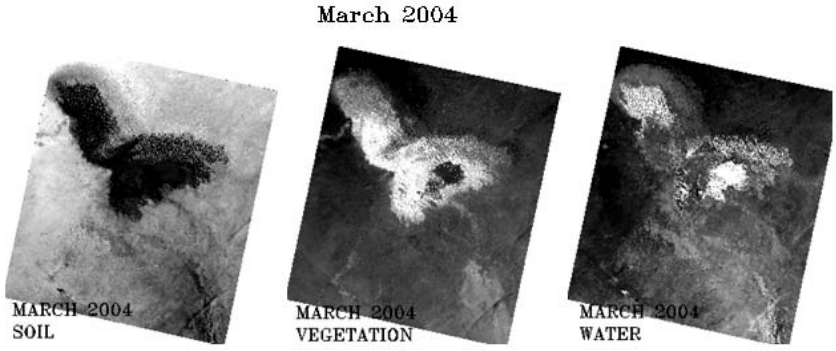

Fig. 3.14: March 2004 showing soil, vegetation and water LSU bands

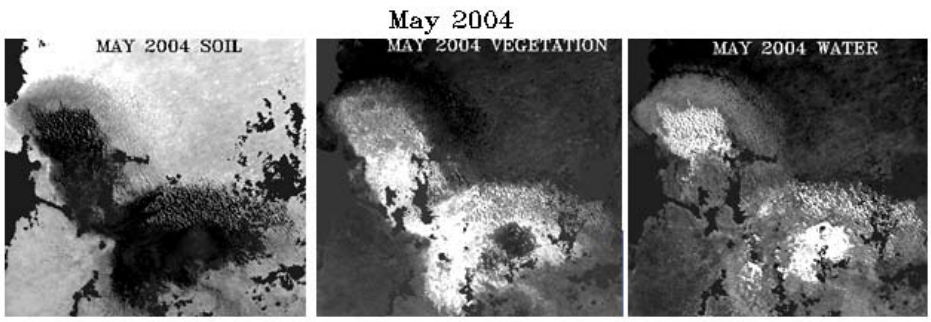

Fig. 3.15: May 2004 showing soil, vegetation and water LSU bands

3.4 ACCURACY ASSESSMENT OF MERIS LSU CLASSIFICATION

According to Small (2003), a low RMS error is necessary but not sufficient condition for accurate estimation of actual areal abundances of specific endmembers. In other words, a small error does not guarantee that the endmember abundances will agree with field validation measurements. In general insufficient attention is paid to verifying the accuracy of the LSU model before claiming its validity (Nichol and Wong, 2007), and only a small number of studies have attempted to assess the accuracy of derived endmember fractions. In practice, it is difficult to find sufficient reference data that can directly be compared against the continuously varying surface of endmember fractions generated over large areas (Rashed *et.al.,* 2003). It is also difficult to obtain sufficiently accurate image registration to compare the fractions with a single pixel with more detailed reference data. Discrete areas within a pixel must be located on the reference image in order to test the endmember proportions, and the standard RMS error of coregistration of less than +/- half a pixel appears to be inadequate (Nichol and Wong, 2007).

Rashed *et.al.,* (2003) compared the overall results of LSU from Landsat with the overall estimates derived from higher resolution air photos, in terms of the accumulated fraction totals of each endmember over the study area. This method suffers from gross generalization, which the authors acknowledge.

The present MERIS LSU classifications were validated by comparing the total area of soil, vegetation and soil classes in MLC ASTER and the total area of soil, vegetation and water fractions calculated from MERIS LSU.

ASTER RGB of the Grand Barrier was classified into three classes of soil, vegetation and water. Training ROIs for the ML classification were obtained from examining the positions of the classes in scatter plots of pixel clouds displayed in the spectral feature space in the visible (0.52 -0.60 µm as x axis) and near infrared (0.78-0.86 µm as y axis) regions of the spectrum. The range of mean radiance values from which the ROIs were obtained is shown in table 3.8

The ASTER RGB was classified using the Maximum Likelihood classifier. The area bounded by each class was obtained from the class statistics and converted into percentage area occupied by soil, vegetation and water respectively on the ASTER image. MERIS LSU was subset to the exact scene of the classified ASTER RGB. The areal extent of each soil, vegetation and water fractions were calculated. The percentage area bound by each fraction was calculated.

Table 3.8: Mean Radiance Values used to determine training ROIs

Bands	SOIL		VEGETATION		WATER	
Radiance Values	Min	Max	Min	Max	Min	Max
	$Wm^{-2}sr^{-1}$		$Wm^{-2}sr^{-1}$		$Wm^{-2}sr^{-1}$	
B1:0.52 -0.60 µm	105.39	125.43	61.02	86.96	52.48	75.16
B2: 0.63-0.69 µm	92.16	113.03	40.36	79.62	35.91	60.89
B3: 0.78-0.86 µm	86.28	99.68	76.95	99.13	30.41	59.56

The percentage values calculated from the class area of soil, vegetation and water were compared with the percentage values obtained from the endmember fraction. Figure 3.16 illustrates the MLC ASTER and MERIS LSU classifications.

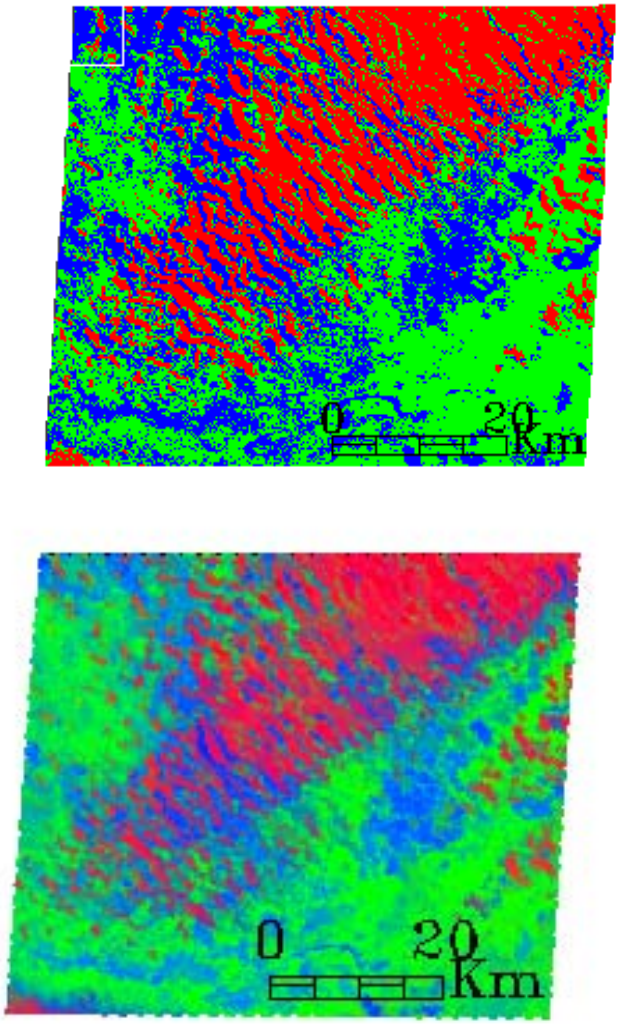

Fig. 3.16: A comparison of ML classified ASTER (top image) and LSU MERIS image (bottom image).

Table 3.9:ML ASTER Class proportion of soil, vegetation and water compared with the corresponding proportions of soil, vegetation and water fractions from MERIS LSU

	ASTER MLC		MERIS LSU	
Class/endmember	Area km^2	Percentage %	Area km^2	Percentage %
Soil (red)	769.31	23.38	801.86	23.86
Veg (green)	1668.42	50.70	1807.18	53.78
Water (blue)	852.83	25.92	751.31	22.36
	3290.56		3360.35	

There is a good agreement between the area of MLC ASTER classes and total area of the three resampled MERIS LSU endmembers, and The correlation coefficient between the areas of MLC soil, vegetation and water and corresponding areas of LSU fractions of soil, vegetation and water was 0.96 therefore the LSU classification was accepted.

CHAPTER FOUR

LAND COVER CHANGES OVER LAKE CHAD BASIN

4.1 INTRODUCTION

One objective of the study was to investigate the pattern of change which could indicate the presence of croplands in the known areas of farmlands as distinct from natural vegetation which shows less change. The other objective was to extrapolate these patterns to identify croplands over the whole lake basin.

A binary masking change detection technique was used to investigate the pattern of change. The Southwestern Lakeshore Farmlands and the Polder Farmlands were identified from field observations and the visual interpretation of texture, image tone, pattern, shape, size and site location using ASTER, LANDSAT AND IKONOS images. Differences between the two farmland regions, and the characteristics that differentiate croplands from swamp vegetation, were observed. Patterns of change between endmember fractions on the two known farmlands and how these changes indicate cropland were analyzed. Similar patterns of change which could indicate farmlands in other regions of the lake were also examined. The results of these observations and also the changes produced over the whole lake were recorded and discussed. Conclusions and recommendations were given.

4.1.1 The sub regions of the lake basin

The Southwestern Lakeshore Farmlands are located in Southern Reed Islands (Region 10) while the Polder Farms are located in the Southeastern Dune Islands (region 6). Field work observations were carried out in the Southwestern Lakeshore Farmlands only. The delineation of the sub regions of the lake and their nomenclature are adapted from those used by Carmouze and Lemoalle (1983, [see figure 1.5, page 13, chapter 1 for illustration]). Table 4.1 lists the modified names of the regions:

Table 4.1: Modified names of regions of Lake Chad delineated by Carmouze and Lemoalle.

	Modified Name		Modified Name	Sub regions
1	Northern Reed Island	6	Southeastern Dune Islands	Polder Farms
2	Northeastern Reed Islands	7	Eastern Dune Islands	
3	Northeastern Dune Islands	8	Open Water Region	
4	Northern Open Swamps	9	Southern Open Swamps	
5N	Northern Grand Barrier	10	Southern Reed Islands	Southwestern Lakeshore Farmlands.
5S	Southern Grand Barrier	11	South Eastern Reed Islands	

4.1.2 Change Detection using Threshold Binary Masking

The aim of thresholding the data was to determine if a pattern of temporal change would emerge which could indicate the presence of croplands in the known areas of farmlands as distinct from natural vegetation which shows less change. The MERIS LSU fractions of soil, vegetation and water dated October 2003, December 2003, February 2004, March 2004 and May 2004 were layerstacked into a 15 band file and imported into ERMapper software. The area of the lake was delineated into regions following the same region division employed by Carmouze and Lemoalle, (1983).

The October soil fraction band, was assigned as time T1, and paired with a December soil fraction band which was assigned as time T2 band. An algebraic query which displayed all pixels which have **increased** in fraction abundance equal to or exceeding a certain threshold between T1 and T2 was applied. Another algebraic query which displayed all pixels which have **decreased** in abundance equal to or exceeding a threshold between T1 and T2 was also applied. For each query, a binary change map was generated in which all pixels below the threshold were masked out. The algebraic functions were expressed as:

$$if\,(In - I1) \geq p\ then\ I1\ else\ null \qquad (1)$$

i.e. increase between T1 and T2

$$if\,(I1 - In) \geq p\ then\ I1\ else\ null \qquad (2)$$

i.e. decrease between T1 and T2

Where variable *In* was the input band at time T2, $I1$ was the input band at time T_1 and *p* was a percentage *p* of the original values of the endmember fractions at time T2. The threshold level *p* was applied at percentage increments of 10% starting from 10%, to 80%.

The December endmember fractions were subsequently replaced with the January February, March and May endmember fractions as time T2 while retaining the October fractions as T1. Afterwards, the October endmember fractions were replaced by the December fractions as time T1. A time series analysis was thus performed in which the endmember fraction bands of all the months (except May), were assigned as T1 and the fractions of the subsequent months were assigned as time T2.

The change detection analysis was performed at different threshold levels to investigate the following parameters of change

- Land cover changes from water to vegetation or soil from time T_1 to time T_2, suggesting a fall in water levels.
- Land cover changes from vegetation to water or soil from time T_1 to time T_2, suggesting flooding or harvesting.
- Land cover changes from soil to vegetation or water from time T_1 to time T_2, suggesting planting or flooding.

The change map pixels were converted to vector format and overlaid over the original LSU layerstacked 15 band image. The endmember fraction values for the initial time period T1 (October, December, February or March) and the final time period T2 (December February March or May) were extracted and the initial total area of endmember fraction in T1 month and the final total area of the water endmember fraction in T2 month were calculated. The difference in area between T1 and T2 was calculated to produce increase in areal extent from the results of the first algebraic expression and a decrease in areal extent from the results of the second algebraic expression. The net change was calculated by summing up the increase and decrease in areal extent. A net change in areal extent of soil, vegetation and water in each region of the lake was plotted for each month and tabulated.

All the T2 data values were queried to reveal change pixels whose resulting values were higher than or equal to a threshold *p*. The threshold *p* was set at $p = 0.1$, $p = 0.2$….. to $p = n$, where $n = 0.8$ or when no change pixels were displayed on the screen. It was discovered that because the fraction abundance values were not nominal but continuous data, applying successive thresholds had no effect in producing a pattern of change that could indicate croplands. Thus, any pixel whose fraction value satisfied the threshold criterion was displayed. Additionally, when the threshold was high (i.e. $p \geq 0.7$), very few change pixels were displayed on the screen. Successively lower thresholds increased the information content, but still some pixels remained suppressed which might provide some information. Therefore a decision was reached to use a threshold of $p = 0.05$ to display the increase and decrease in change maps because the average size of farmland plots in the Southwestern Lakeshore Farmlands estimated from IKONOS was 0.64 ha. This value approximates to 7% of the ground area which can be resolved by a MERIS pixel and as the 5% threshold level was closer to farm plot sizes in the study area, this threshold level was used.

4.2 RESULTS

4.2.1 Land cover changes on the Southwestern Lakeshore Farmlands (part of sub region 10) and the Polder Farmlands.

i) The Southwestern Lakeshore Farmlands

Initially, the presence of farmlands on the ENVISAT MERIS images could only be identified from fieldwork combined with references to higher resolution ASTER and IKONOS and LANDSAT images. Existing areas of cropland in the flood recessional areas of Lake Chad in the southwestern part of the lake were identified on ASTER VNIR 15 meter spatial resolution images acquired on December 18th 2002, February 7th 2004 and 25th April 2004 based on field observations between December 2003 and May 2004. These images only covered the Southern Reed Islands, and the Southern Open Water Swamps. High resolution IKONOS images were used to identify individual farmlands because the ASTER images could only be used to verify the positions of the farmlands based on location and differences in the reflectance values of vegetation in the areas designated as farmlands and the areas designated as swamp. The IKONOS images at 4 meter resolution revealed the geometric arrangement of the farmlands. The pattern was a gridlike arrangement of the individual farms which were both cultivated and fallow (figures 4.1b). On the ASTER images these areas of rectangular farmlands appeared as crisscrossed patches of vegetated and bare land (figures 4.1a). These geometric patterns and the reflectance value of the vegetation on the farmlands which was very high between March and May, and differed from low values of swamp vegetation, were used to identify other areas of farmland on the ASTER image. LANDSAT 7 ETM of the whole lake was also used to locate areas of other farmlands along the western coastline, not shown on the ASTER images.

The Southwestern farmlands are part of the Southern Reed Islands located along the southwestern shore of the lake (figures 4.2a to 4.2e). Between October and December, there was increase in water endmember fractions which replaced vegetation fractions on the farmlands (figures 4.3a and 4.3b). Water retreat was noticed in February, but the farmlands were still partially inundated from the December high water level and therefore some were not cultivated between October and February because the soil was still waterlogged.

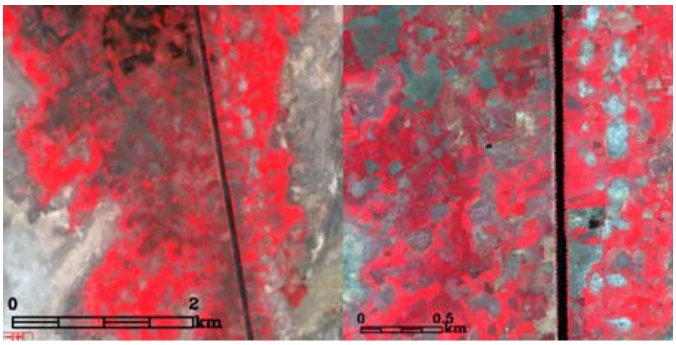

Fig. 4.1: a) ASTER VNIR image of fieldwork region (15 m resolution) and b) IKONOS VNIR image of the same scene as ASTER at 4 m spatial resolution.

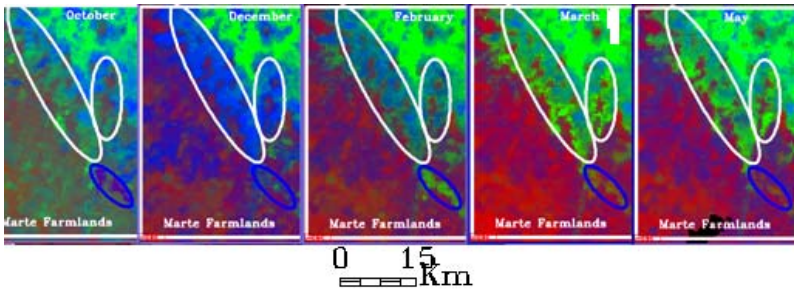

Fig. 4.2a to 4.2e: Conditions of the Southwestern Lakeshore Farmlands between October and May (color legend: red = soil; green = vegetation; blue = water).

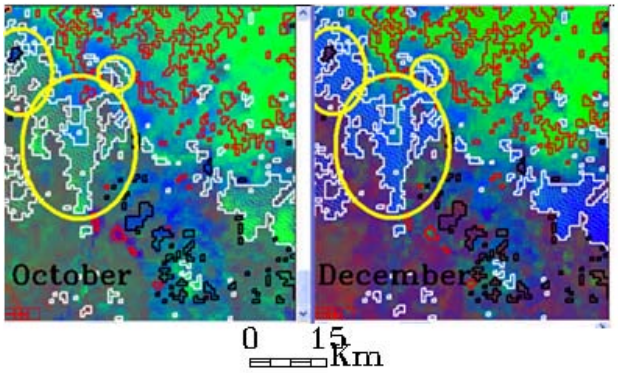

Fig. 4.3a to 4.3b: Land cover changes between October and December. (red is soil; green is vegetation; blue is water).

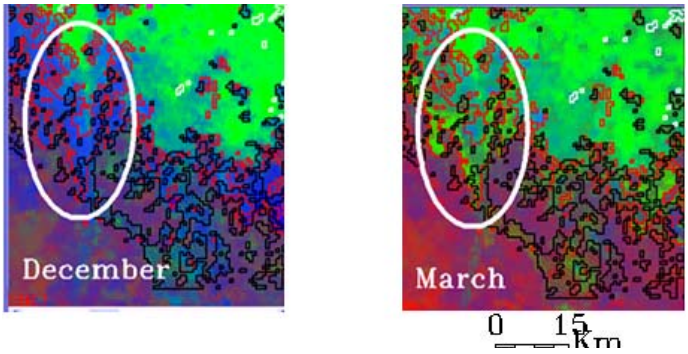

Fig. 4.4a and 4.4b: Land cover changes between December and March on the Southwestern Lakeshore Farmlands (red is soil; green is vegetation;blue is water).

Between December and March, water fractions changed to vegetation fractions as a result of the flood retreat and the start of cultivation from February (figures 4.4a and 4.4b). Soil was at a minimum in March and May because these were the periods of time when vegetation was most vigorous at the Southwestern Lakeshore Farmlands. Indeed it was seen that vegetation replaced soil in these farmlands at these times. Vegetation reached its peak in March and began to decline in May (figure 4.5). This decline in vegetation in May is partly explained by the fieldwork observation recorded in May that the bean crop on some of the farmlands, had failed as a result of insect infestations (Plates 1 and 2). On some other farms however, the crop had already been harvested, or was yet to be harvested.

Plate 1: Infected cowpea plant.

Plate 2: Larva on cowpea pod.

Table 4.2 and graph of figure 4.5 summarize the net change in area of vegetation, soil and water between the T1 and T2 on the Southwestern Lakeshore Farmlands.

Table 4.2: Increase, decrease and net change in the area of soil, vegetation and water on the Southwestern Lakeshore Farmlands between Times T1 and T2.

Southwestern Lake Shore Farmlands									
Increase in area of endmember fractions between times T1 and T2 (Km^2)				Decrease in area of endmember fractions between times T1 and T2 (Km^2)			Net change in area of endmember fractions between times T1 and T2 (Km^2)		
Oct	**Soil**	**Veg**	**Wat**	**Soil**	**Veg**	**Wat**	**Soil**	**Veg**	**Wat**
Dec	0.49	0.82	17.63	-2.17	-2.30	0.00	-1.68	-1.48	17.63
Feb	-0.20	4.78	-21.63	-2.87	-0.29	-2.83	-3.07	4.48	-24.46
Mar	3.96	10.97	0.43	-1.15	0.00	-8.84	2.81	11.0	-8.41
May	3.00	7.43	0.72	-1.23	0.00	-5.40	1.77	7.43	-4.68
Dec	**Soil**	**Veg**	**Wat**	**Soil**	**Veg**	**Wat**	**Soil**	**Veg**	**Wat**
Feb	3.14	10.83	-0.01	-0.29	0.00	-13.5	2.85	10.83	-13.5
Mar	9.90	17.49	0.00	0.00	0.00	-27. 0	9.90	17.49	-27.0
May	9.27	13.88	-1.09	0.00	0.00	-23.2	9.27	13.88	-24.3
Feb	**Soil**	**Veg**	**Wat**	**Soil**	**Veg**	**Wat**	**Soil**	**Veg**	**Wat**
Mar	6.26	7.97	0.03	0.00	-1.20	-9.96	6.26	6.77	-9.93
May	6.07	5.08	0.72	0.00	-2.37	-7.43	6.07	2.71	-6.71
Mar	**Soil**	**Veg**	**Wat**	**Soil**	**Veg**	**Wat**	**Soil**	**Veg**	**Wat**
May	0.57	1.56	4.27	-0.23	-3.16	0.00	0.34	-1.61	4.27

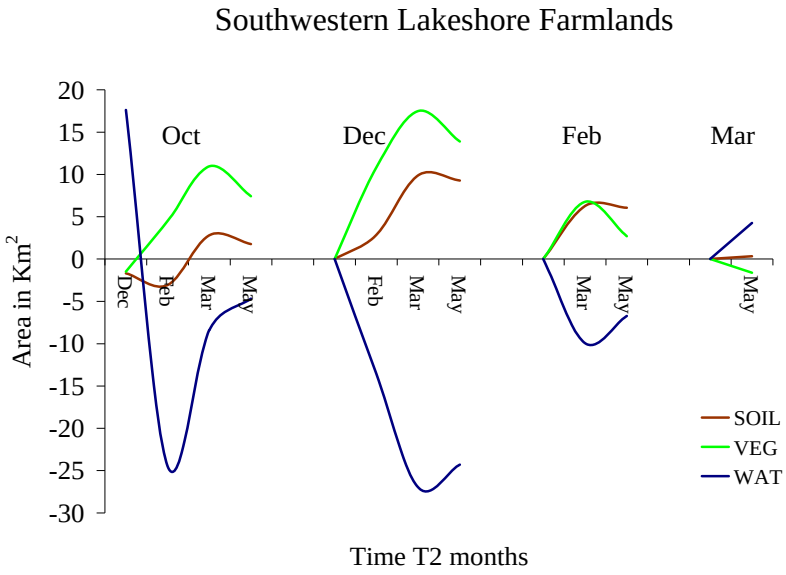

Fig. 4.5: Graph showing the trend in soil, vegetation and water land cover changes on the Southwestern lakeshore farmlands between Times T1 and T2 months.

ii) Polder Farmlands (Part of sub region 6).

The known Polder Farmlands on interdune depressions managed by the Lake Development Society (SODELAC) were identified from six high resolution ASTER scenes of the southeastern and eastern dune islands of April 25th 2000, May 27th 2000, 6th June 2000 29th January 2001, March 31st 2001, and 31st December 2001 and a LANDSAT 7 ETM + image of on 25th May 2003.

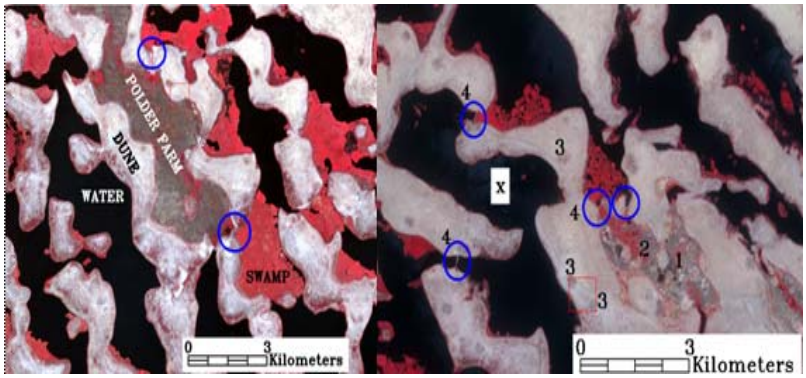

Fig. 4.6: ASTER RGB of a) Government and b) privately owned Polder Farmlands. 1 = drained depressions; 2 = disturbed striated vegetation; 3 = settlements; 4 = dams (in blue circles).

Unknown farmlands on the interdune depressions were identified visually from a combination of their hue, size, shape and pattern and associated features. Thus drained interdune depressions with water logged soil comprised a mixture of striated vegetation and disturbed striated soil, the presence of villages and also presence of dams or dykes obstructing the flow of water into the interdune depressions. These dams were identifiable on high resolution ASTER and LANDSAT 7 ETM images (figures 4.6a and 4.6b). Also on the ASTER scenes, it was possible to see the gridlike arrangement of farm plots inside some of the interdune polders.

The Polder Farmlands are located in the Southeastern and Eastern Dune islands. Figure 4.7 shows some polder farms including those that are government assisted in white and those that are privately owned in black (FEWS, 1997 and Personal communication with LCBC staff).

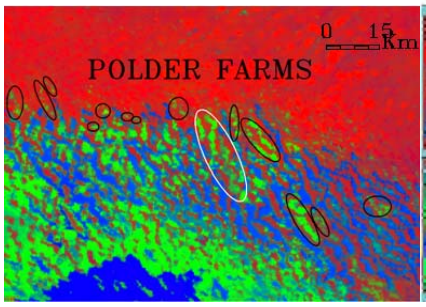

Fig. 4.7: Location of some of the Polder Farmlands in the Southeastern and Eastern Dune Islands (red is soil; green is vegetation; blue is water). White circles are modern polders and black circles are traditional polders

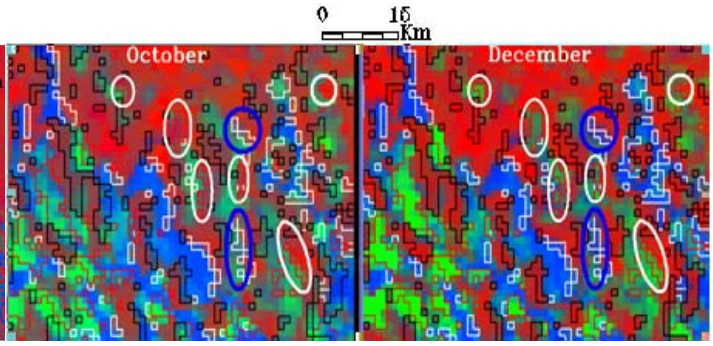

Fig. 4.8: Changes in soil, vegetation and water fractions between October and December in the Polder Farmlands of the southeastern Dune Islands (red is soil; green is vegetation; blue is water). .

Between October and December on some of the Polder Farmlands, the peripheral areas, i.e. the interface between the farmlands and the dunes changed from soil endmembers in October to vegetation in December (white ellipses figure 4.8a and 4.8b). This is because wheat crop was growing there since the main crops grown are wheat and corn and wheat is sown following the summer rains and is harvested between March and April (Dieleman and Ridder, 1963). Also according to WWF (2003), wheat is the main crop grown in the polder areas of the Lake Chad and the time period on the cropping calendar for wheat is from January to May. Thus it is reasonable to assume that the wheat was sown in November since vegetation replaced soil between October and December. Other polder farmlands were vegetated in October but became waterlogged in December (blue ellipses figure 4.8a and 4.8b). Some of these farms that were waterlogged in December were traditional polder farmlands (figure 4.9a and b) as the government assisted polder farms have permanent dikes which stop the re-entry of water into the farms from inundated depressions and therefore did not appear to be waterlogged.

Overall though, there was a net decrease in the area of vegetation and water and a net increase in the area of soil between October and December (graphically illustrated in figure 4.16), and this net increase in the soil is because some of the farmlands were not under cultivation between October and December.

In February, the area of vegetation rose to a maximum, while the area of water continued to decline and reached a minimum in March (figures 4.10 and 4.11). This was due to maturation of the crops at this time of the year as harvesting time is between March and April as noted earlier.

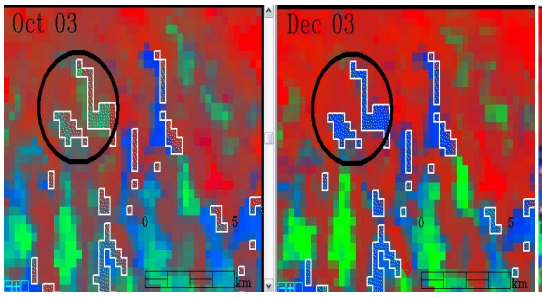

Fig. 4.9 a and b: Change from, vegetation fractions to water fractions in the Polder Farms between October and December

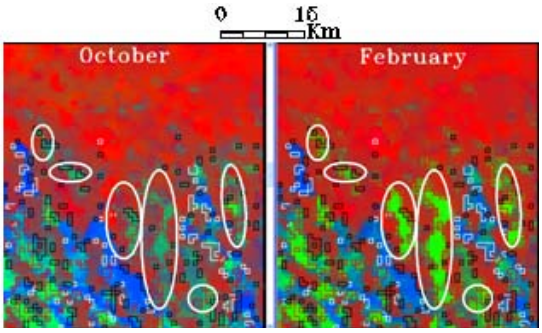

Fig. 4.10a and b: Increase in vegetation in the Polder Farmlands between October and February.

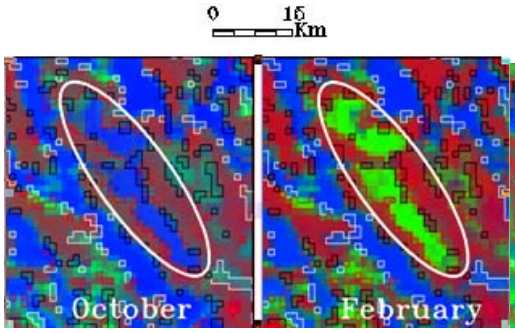

Fig. 4.11: Change from inundated farmlands to vegetated farmlands between October and February.

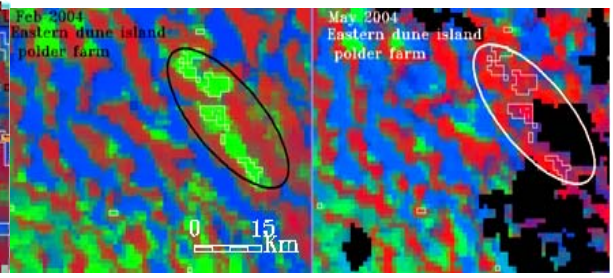

Fig 4.12: Change from vegetation fractions to soil fractions between February and May.

The area of vegetation then declined from a maximum extent in February to a minimum extent in May while the area of soil reached a maximum in March in part due to crop harvests (figure 4.12). March was also found to be the month in which evaporation and evapo-transpiration were highest. Therefore the area of water continued to decline between February, March and May (figure 4.13). Some of the small farms lost all vegetation in March. These were thought to be the traditional polders with one harvest per annum. By May, many farmlands had reverted back to soil and some had become waterlogged again.

There was not much conversion to soil on the government assisted polder farms (ellipses on left side in figure 4.14a and b). This is probably because as three crop cycles can be harvested in the government assisted farmlands, then another crop would have been planted. On non government assisted farmlands, some of the farmlands became partially inundated in May in some areas and in other areas, bare land (ellipses on right side, figure 4.14b). These changes are indicative of the peculiar nature of polder farmlands which could help in identifying them as cultivated areas. This is because under normal circumstances, only the adjacent dune surfaces would experience vegetation loss, whereas the interdune depressions being at a lower

elevation, are always vegetated due to residual moisture in the interdune depression in these areas or due to underground water capillarity seeping into the dune depressions where the water table is not below a depth of between 30 – 50 cm from the surface.

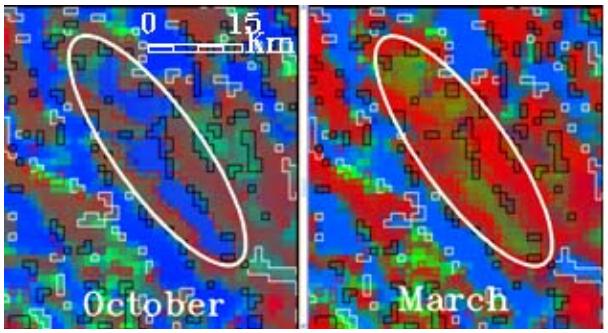

Fig. 4.13: Change from inundated farmlands to sparsely vegetated farms between October and March.

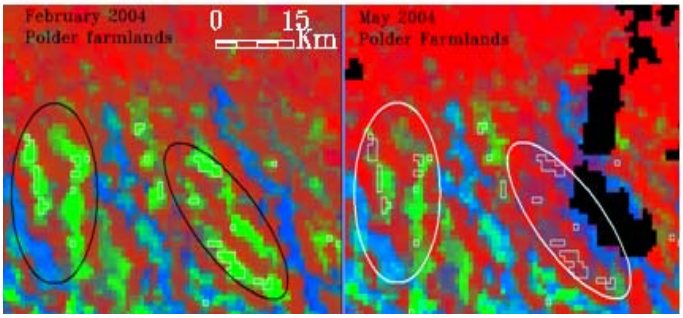

Fig. 4.14: Reduction in vegetation fractions between in government assisted farms (a) and change from vegetation fractions to waterlogged soil between February and May on traditional polder farms (b).

Therefore where interdune depressions become bare of vegetation, especially around the normal harvest period, this must be due to cultivation. It was noticed that some pixels with a mixed combination of vegetation and water fractions on farms in December, changed to soil fraction in February which indicated that not all the farmlands had been cultivated (figure 4.15). This was due to rise in salinity in the soils because seepage and evaporation of water leaves salt residues on the soil surface. Salt residues on soil were noticed on some dune island farms during field work. A rise in salinity of the soil can be considered as another reason to qualify the polder farms as risk zones.

Table 4.3 and figure 4.16 summarize the net change in area of vegetation, soil and water between the T1 and T2 on the Polder Farmlands.

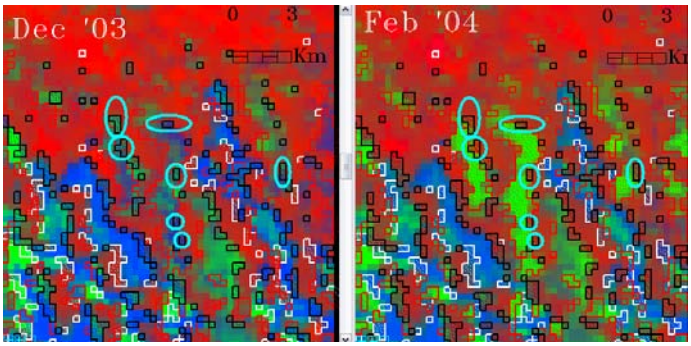

Fig. 4.15: Changes from vegetation and water fractions to soil fractions on polder farms between December and February.

A phenomenon of increase in water fractions between March and May was noticed in the southern lake basin on the MERIS LSU images. An explanation was proffered by (Dieleman and Ridder, (1963), which had to do with the level of the ground water. If precipitation exceeds the average 300mm per annum, prolonged inundation of large areas usually occurred due to a rise in the water table. The water table fluctuates between 0.25 and 1.0 m below the surface. It is highest immediately after the rainy season in October and then it begins to fall. The rate of fall depends both on evapotranspiration and on the water level of Lake Chad. If the level is high, the amount of seepage will be relatively large and the rate at which the water table decreases will be relatively slow.

Table 4.3 Increase, decrease and net change in the area of soil, vegetation and water on the Polder Farmlands between times T1 and T2.

Polder Farmlands									
Increase in area of endmember fractions between times T1 and T2 (Km^2)				Decrease in area of endmember fractions between times T1 and T2 (Km^2)			Net change in area of endmember fractions between times T1 and T2 (Km^2)		
Oct	**Soil**	**Veg**	**Wat**	**Soil**	**Veg**	**Wat**	**Soil**	**Veg**	**Wat**
Dec	8.92	2.34	2.66	-1.07	-3.08	-4.18	7.85	-0.74	-1.52
Feb	2.98	25.2	0.35	-1.87	0.00	-16.8	1.10	25.2	-16.5
Mar	14.2	10.3	0.13	0.00	0.00	-20.1	14.2	10.3	-20.0
May	16.3	3.68	1.89	-1.23	0.00	-5.40	15.27	0.35	-10.0
Dec	**Soil**	**Veg**	**Wat**	**Soil**	**Veg**	**Wat**	**Soil**	**Veg**	**Wat**
Feb	1.89	29.6	0.42	-5.44	0.00	-13.5	-3.6	29.6	-13.1
Mar	9.54	14.9	0.34	-1.39	-0.52	-15.1	8.15	14.4	-14.8
May	12.3	3.33	2.61	0.00	-1.27	-9.04	12.3	2.06	-6.44
Feb	**Soil**	**Veg**	**Wat**	**Soil**	**Veg**	**Wat**	**Soil**	**Veg**	**Wat**
Mar	13.5	1.47	2.62	-0.27	-11.1	0.00	13.6	-9.59	2.62
May	16.9	0.90	1.41	-1.25	-24.6	-0.55	15.7	-23.7	0.86
Mar	**Soil**	**Veg**	**Wat**	**Soil**	**Veg**	**Wat**	**Soil**	**Veg**	**Wat**
May	6.44	0.99	8.43	-3.47	-9.63	0.00	2.97	-8.64	8.43

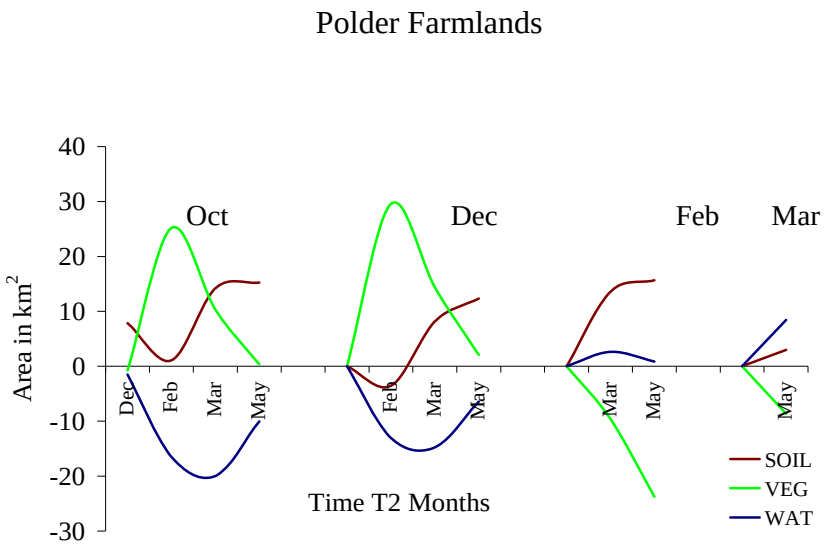

Fig. 4.16: Soil, vegetation and water change patterns on the Polder Farmlands between Times T1 and T2 months.

The fall in the water table continues at an even rate until March-April. In March, the plants start to die and this reduces evapotranspiration. As a result, the rate at which water is being taken out of the ground also decreases. Thus the fall in the level of the water table level decreases, and seepage to the surface can result. Therefore the increase in the area of water in the southern lake basin that was noticed between March and May is likely attributed to this phenomenon. Also as 2003 was a very wet year, with cumulative rainfall as of September 30th 2003 ranging from 1000mm in the southern part of Chad republic to 300 mm in the northern part of Chad Republic (AGRHYMET BULLETIN 2003a), it can be assumed that the water table was very high in the following year, (2004) and that the slight rise in the area of water observed in May could be the combined effect of high water table and high seepage rates.

4.2.2 Land cover changes in other regions of the Lake Chad basin

The section is based on the second objective of the study in which patterns of change between endmember fractions indicating cropland in the lake basin are examined. The important regions for this study lie in the southern lake basin because this is where the Chari flows into the lake and this is where flooding occurs every year. Also altimeter measurements which are used to compare the areal spread of water are acquired in this region of the lake only. Therefore changes in the southern lake basin regions are

described in detail while changes in the northern lake basin regions are summarized. Additional information is given in tables and graphs of increase, decrease and net change.

i) Northern Reed Islands (Region 1)

The Northern Reed Islands, (region 1) are usually bare and devoid of vegetation from October to May (white ellipse, figure 4.17a blue ellipse figure 4.17b). Land use activity here is mainly natron (hydrated sodium carbonate) mining for commercial purposes and there appeared to be no change in land use. The soil in this part of the basin is very saline due to the presence of the natron. The presence of water dilutes the salt concentration, even though the water in the northern basin can be four times more saline than in the southern lake basin (Carmouze and Lemoalle 1983). However since the drying up of the northern basin, the concentration of salt has increased and very little vegetation growth is found here and the environment is not suitable for farming therefore it is not likely that farmlands would be found in this region.

The Northern Reed Islands form the limit of the distance travelled by water between the southern lake basin and the northern basin (figures 4.17a and b). A large volume of water is displaced into the region and it becomes rapidly flooded by February. From the LSU image analysis, the greatest spatial increase in area of water of approximately 323 km^2 occurred between October and February (table 4.4 and figure 4.19).

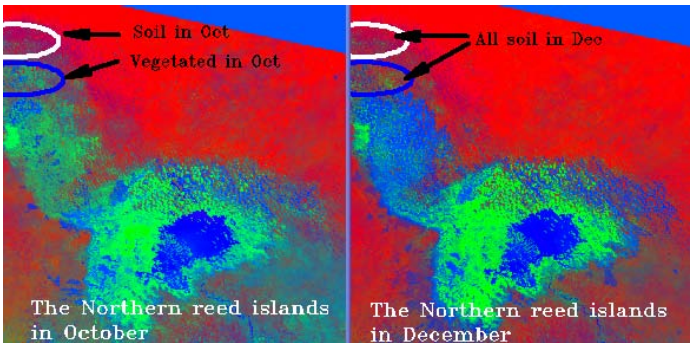

Fig. 4.17a and b: Northern (white ellipse) and southern (blue ellipse) parts of the Northern Reed Islands in October and December.

This area of water remained constant between February and May (figures 4.18 b-d), thus implying that the maximum areal extent of the flooding was reached in February. It also implied that the rate of discharge into the lake had subsided, since according to

Carmouze and Lemoalle, (1983), the amount of water that enters the lake from mid December to February is only 8 to 10% of the annual supply.

It was not possible to ascertain from the MERIS LSU images whether the dune islands in the inundated area of the northern reed Islands were inhabited or not. Examination of ASTER 15 metre spatial resolution images did not show any signs of habitation on these dune islands. This could be because the soils of area are not suitable for agriculture due to the salinity.

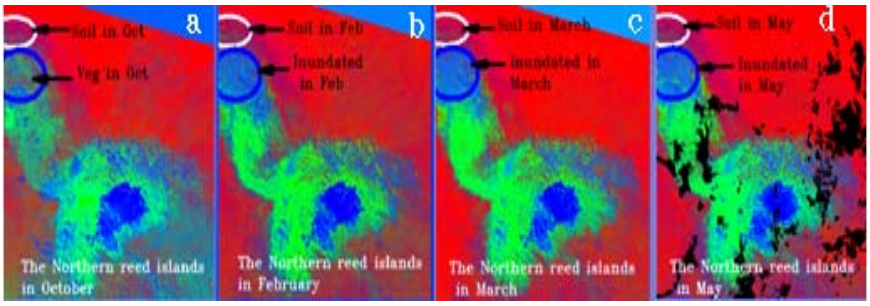

Fig. 4.18: Northern (white) and southern (blue) parts of the Northern Reed Islands between October and May. (red = soil; green = vegetation blue = water).

Table 4.4: Increase, decrease and net change in the area of soil, vegetation and water in the Northern Reed Islands between Times T1 and T2.

Northern Reed Islands									
Increase in area of endmember fractions between times T1 and T2 (Km^2)				Decrease in area of endmember fractions between times T1 and T2 (Km^2)			Net change in area of endmember fractions between times T1 and T2 (Km^2)		
Oct	**Soil**	**Veg**	**Wat**	**Soil**	**Veg**	**Wat**	**Soil**	**Veg**	**Wat**
Dec	90.1	1.92	67.3	-12.6	-24.0	-18.6	77.5	-22.1	48.7
Feb	4.5	17.6	325.7	-33.3	-3.2	-2.6	-28.8	14.4	323.1
Mar	7.5	9.3	314.6	-26.4	-3.03	-1.63	-19.0	6.23	314.0
May	6.14	42.0	292.8	-39.4	-4.7	-2.9	-33.3	37.3	289. 9
Dec	**Soil**	**Veg**	**Wat**	**Soil**	**Veg**	**Wat**	**Soil**	**Veg**	**Wat**
Feb	6.48	28.2	332.2	-60.5	-2.82	-10.4	-54.0	25.4	321.8
Mar	6.30	23.2	326.6	-60.5	-2.4	-8.3	-54.2	20.8	318.4
May	6.72	60.6	309.8	-70.2	-3.5	-13.9	-63.5	57.0	295. 9
Feb	**Soil**	**Veg**	**Wat**	**Soil**	**Veg**	**Wat**	**Soil**	**Veg**	**Wat**
Mar	31.4	1.86	34.6	-12.7	-8.7	-30.7	18. 7	-6.9	3.89
May	23.6	17.3	34.0	-18.2	-7.5	-48.0	5.39	9.83	-14.0
Mar	**Soil**	**Veg**	**Wat**	**Soil**	**Veg**	**Wat**	**Soil**	**Veg**	**Wat**
May	19. 1	15.0	26.3	-21.5	-2.6	-44.1	-2.39	12.4	-17.8

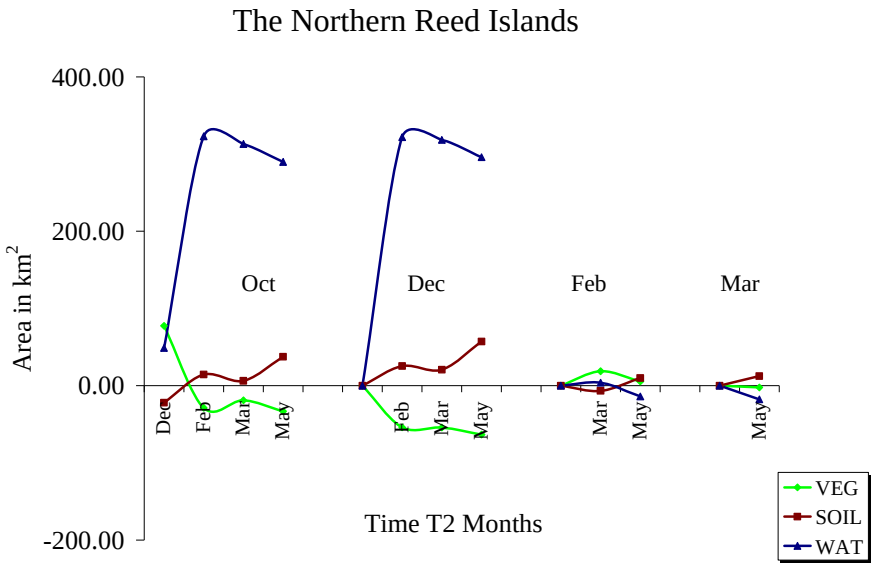

Figure 4.19: Soil, vegetation and water change patterns in the Northern Reed Islands between times T1 and T2 months.

ii) The Northeastern Reed Islands (Region 2).

The Northeastern Reed islands define the boundary of the current shoreline on the northeastern side of the lake and form the limit of water inundation in the area (first image, figure 4.20).

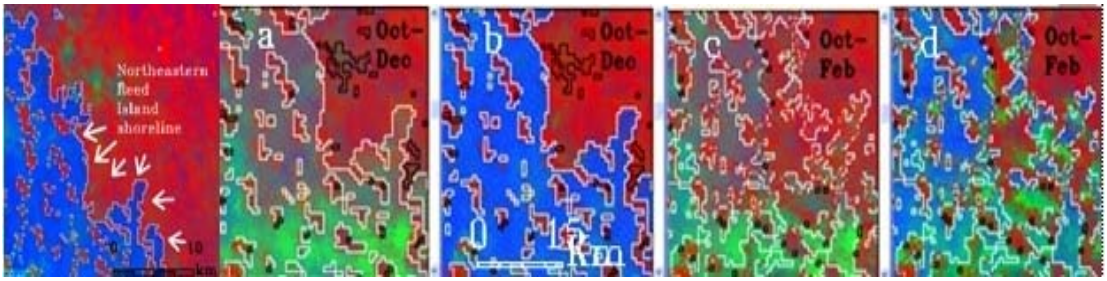

Fig 4.20: The shoreline of the Northeastern Reed Islands and changes between October, and February in the Northeastern Reed Islands (a to d).

Vegetation becomes inundated in December due to rising lake water levels, but by February, the shore line begins to dry out even though the hinterland remains inundated (figure 4.20 second to fifth image). The area is recolonized by vegetation in March and May. This phenomenon of water retreat in February and vegetation colonization in May is also seen in the Southwestern Lake Shore Farms. Therefore this suggests that the area contains farmland and some recession cultivation is practiced (see sub section 4.2.3 below). Soil also replaces water in March because March is the month with the greatest rate of evaporation at around 437.5 mm (in the region in March 2004) and a

mean maximum temperature at around 38°C (AGRHYMET, 2004). By May, inundation towards the hinterland is replaced by vegetation.

iii) The Northeastern Dune Islands (Region 3)

The Northeastern Dune Islands form an interface with the Northeastern Reed Islands. This interface is the current shoreline on the northeastern side of the lake and forms the limit of water inundation in the area. Beyond that, the area is made of dessicated dunes and interdune depressions.

Table 4.5: Increase, decrease and net change in the area of soil, vegetation and water in the Northeastern Reed Islands between times T1 and T2.

Northeastern Reed Islands									
Increase in area of endmember fractions between times T1 and T2 (Km^2)				Decrease in area of endmember fractions between times T1 and T2 (Km^2)			Net change in area of endmember fractions between times T1 and T2 (Km^2)		
Oct	**Soil**	**Veg**	**Wat**	**Soil**	**Veg**	**Wat**	**Soil**	**Veg**	**Wat**
Dec	15.0	0.15	142.5	-15. 9	-12.8	-1.3	-0.8	-12.7	141.2
Feb	3.97	16.4	148.5	-34.8	-5.5	-2.0	-30.8	10.8	146.5
Mar	24.3	38.6	100.6	-29.4	-3.4	-12.9	-5.1	35.2	87.7
May	15.2	70.0	52.1	-33.1	-3.5	-18.9	-17.96	66.5	33.2
Dec	**Soil**	**Veg**	**Wat**	**Soil**	**Veg**	**Wat**	**Soil**	**Veg**	**Wat**
Feb	13.2	33.2	67.4	-45.7	-0.1	-35.6	-59.7	33.1	-148.7
Mar	25.2	66.6	43.3	-35.8	-0.95	-69.8	-10.6	65.7	-26.4
May	21.5	95.0	28.6	-40.2	-1.4	-93.8	-18.7	93.7	-65.2
Feb	**Soil**	**Veg**	**Wat**	**Soil**	**Veg**	**Wat**	**Soil**	**Veg**	**Wat**
Mar	44.2	10.6	7.2	-7.3	-5.1	-52.2	36.9	5.5	-45.0
May	32.3	43.9	3.5	-6.1	-3.4	-92.7	26.3	40.5	-89.1
Mar	**Soil**	**Veg**	**Wat**	**Soil**	**Veg**	**Wat**	**Soil**	**Veg**	**Wat**
May	16.7	25.6	4.9	-14.2	-3.1	-52.4	2.6	22.5	-47.5

Before 1973, the Northeastern Dune Islands used to be flooded and defined the shoreline at the northern limit of the lake. However as a result of reduced flooding events, between 1972 and 1973, (17.3 km^3 as against 40km^3 [Carmouze and Lemoalle, 1983]), the shoreline became displaced towards the centre of the lake basin. Consequently, the Northeastern Dune Islands became dessicated and devoid of vegetation.

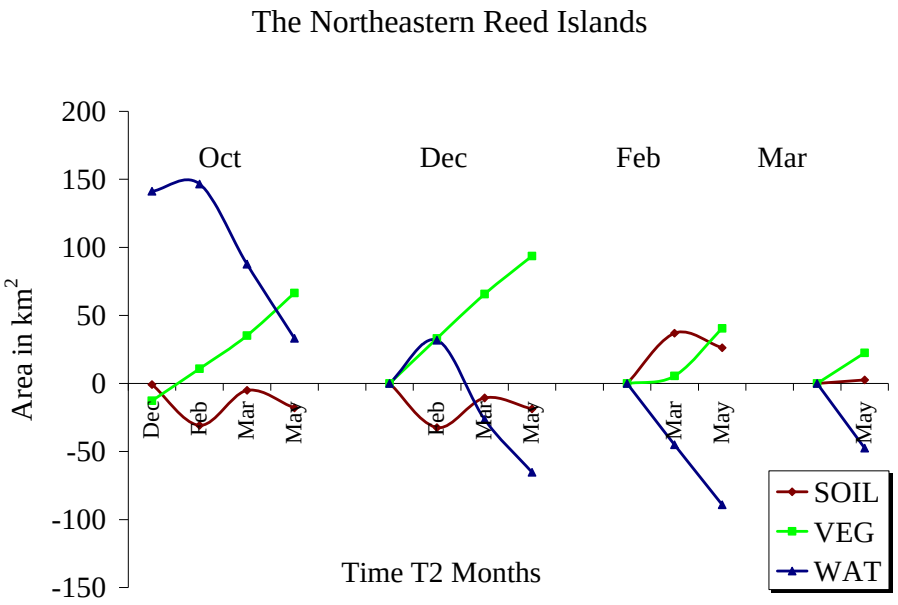

Fig. 4.21: Soil, vegetation and water change patterns in the Northeastern Reed Islands between Times T1 and T2 months.

iv) The Northern Open Swamps (Region 4).

The northern limit of the Northern Open Swamps is contiguous with the lower limit of inundation in the Northern Reed Islands (figure 4.22). The most notable changes in the Northern Open Swamps are the complete inundation which occurs between October and December (figures 4.22b and 4.23b) and the rapid transformation from water to vegetation between December and February, (figures 4.22c and 4.23c) due to evaporation and infiltration which has been estimated at 9.96 billion cubic metres per annum (Isiorho et. al, 1996). The vegetation density and extent reach a maximum in March (table 4.6 and figure 4.24).

As water in the northern lake basin is very saline it cannot support crop vegetation. Thus dunes in this area are not likely to be inhabited for farming. On the other hand, they are inhabited for fishing activities. Smoke plumes detected on images are evidence of habitation by fishermen, as the smoke plumes result from fish smoking and drying activities. This phenomenon was seen during field trips between December 2003 and May 2004.

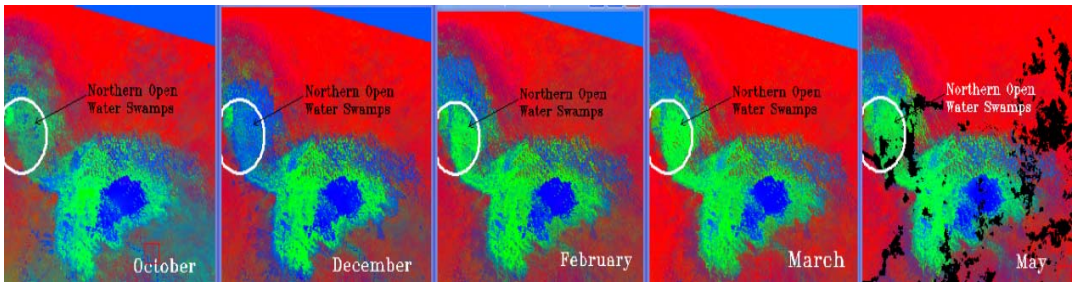

Fig. 4.22: The Northern Open Swamps between October and May.

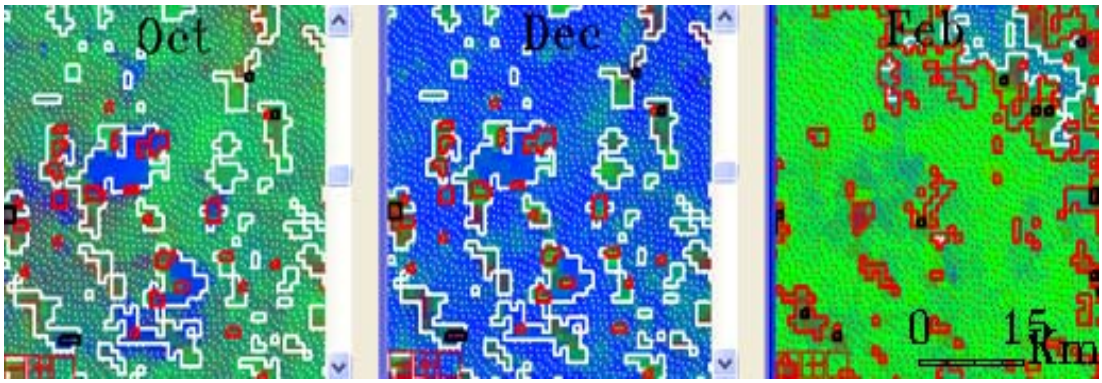

Fig. 4.23: Land cover changes between October and February in the Northern Open Swamps.

Table 4.6 Increase, decrease and net change in the area of soil, vegetation and water in the Northern Open Swamps between times T1 and T2.

Northern Open Swamps									
Increase in area of endmember fractions between times T1 and T2 (Km^2)				Decrease in area of endmember fractions between times T1 and T2 (Km^2)			Net change in area of endmember fractions between times T1 and T2 (Km^2)		
Oct	**Soil**	**Veg**	**Wat**	**Soil**	**Veg**	**Wat**	**Soil**	**Veg**	**Wat**
Dec	5.7	13. 7	615.7	-27.0	-62.5	-7.4	-21.2	-48.9	608.4
Feb	4.7	386.5	143.0	-33.5	-4.3	-89.0	-28.8	382.2	54.0
Mar	30.2	539.8	76.5	-30.8	-2.9	-207.2	-0.5	536.9	-130.7
May	11.5	299.7	43.5	0.32	-1.3	-143.5	11.8	298.4	-100.0
Dec	**Soil**	**Veg**	**Wat**	**Soil**	**Veg**	**Wat**	**Soil**	**Veg**	**Wat**
Feb	17.3	499.1	19.3	-10.1	-3.7	-619.7	7.11	495.4	-600.4
Mar	47.44	673.99	9.94	-4.51	-3.66	-832	42.9	670.3	-821.7
May	26.19	432.20	11.08	-8.43	-4.01	-641.8	17.76	428.2	-630.8
Feb	**Soil**	**Veg**	**Wat**	**Soil**	**Veg**	**Wat**	**Soil**	**Veg**	**Wat**
Mar	31.8	60.1	8.1	-3.8	-7.3	-109.9	28.0	52.9	-101.8
May	14.5	64.4	11.3	-3.4	-22.9	-133.8	11.1	41.5	-122.4
MAR	**SOIL**	**VEG**	**WAT**	**SOIL**	**VEG**	**WAT**	**SOIL**	**VEG**	**WAT**
May	6.4	13.7	13.7	-8.84	-49.0	-37.1	-2.43	-35.4	-23.4

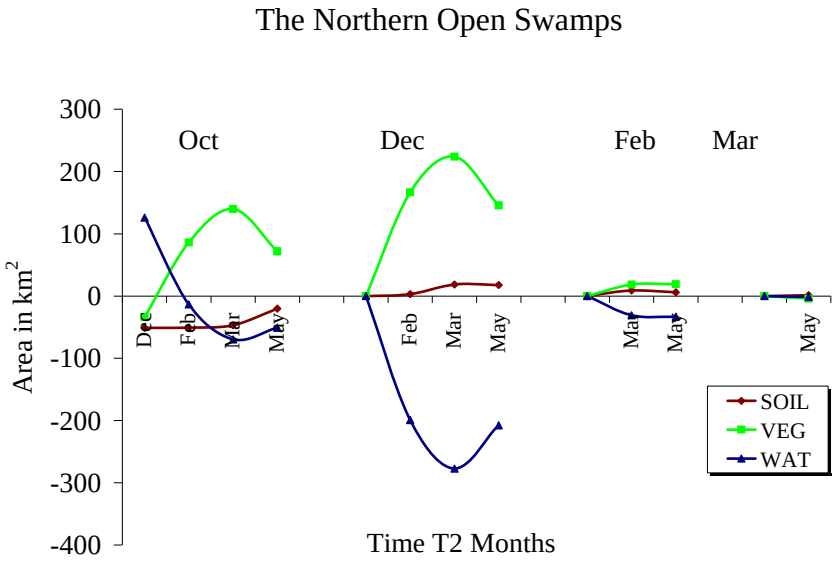

Fig 4.24: Soil, vegetation and water change patterns in the Northern Open Swamps between Times T1 and T2 months.

v) <u>The Southeastern Dune Islands (Region 6).</u>

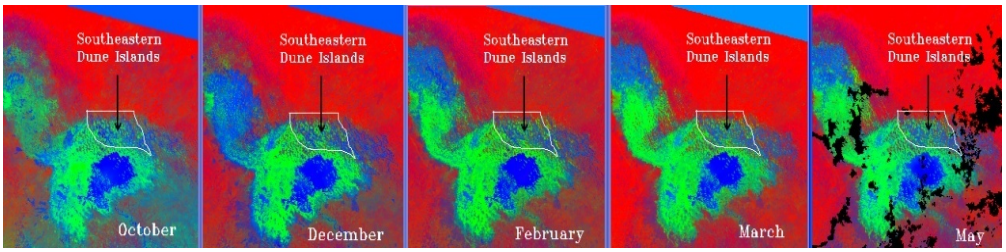

Fig. 4.25: The Southeastern Dune Islands between October 2003 and May 2004

The Southeastern Dune Islands lie adjacent to the Eastern Dune Islands on the southeastern coastal areas of the southern lake basin (figure 4.25). The islands occupy an area of 3200 km^2. The most important thing about this region is that the polder farmlands are found here. Change from one land cover to another was more fluid in the Southeastern Dune Islands due to the fact that the landform is a mosaic of dune islands and vegetated or inundated dune depressions. Therefore within the same vicinity, water replaced vegetation and vegetation replaced water and soil. The change from either water or vegetation to soil occurred over smaller areas and strips of land at the edges of the dunes and land water interfaces (magenta ellipses, figure 4.27). On the other hand changes from pixels with a high proportion of vegetation fraction to pixels with a high proportion of water fractions and vice versa, sometimes occurred

over large interdunal surfaces (yellow and blue ellipse, figures 4.26 and 4.27). This type of change directly from high water endmember fraction abundance to high vegetation fraction abundance is only peculiar to swamp vegetation, (which is sometimes represented by floating vegetation) and does not occur with cultivated crop vegetation. This is because cultivated areas must be drained of the water first before the crops are planted. The exception to this is if rice is being cultivated. However, the major crops grown on the polders are wheat and corn. Therefore this is an indication of the difference between cultivated and swamp vegetation. The increase in area of swamp vegetation mainly occurred in December in this region. Some dune islands which were either partially or completely flooded or had high vegetation abundance in October became dry and bare of vegetation in February (magenta ellipses figures 4.27 and figure 4.28).

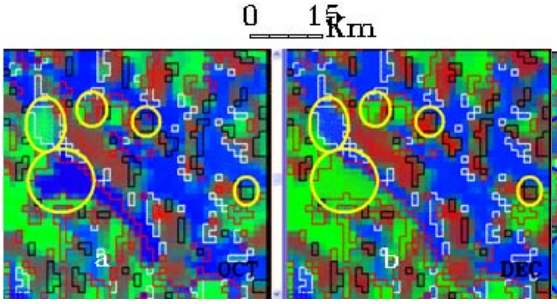

Fig 4.26: Changes from vegetation fractions to water fractions and vice versa between October and December in the Southeastern Dune Islands.

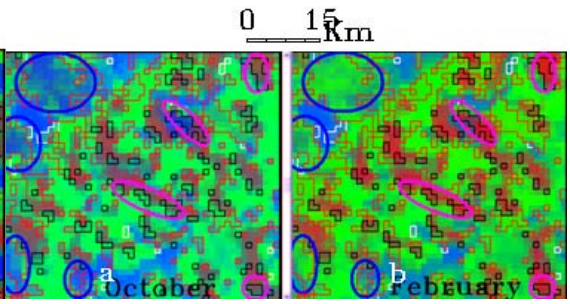

Fig. 4.27: Changes from vegetation fractions to water fractions and vice versa between October and February.

This is another difference between crop vegetation and swamp vegetation. Given that in February, most farmland crops are maturing and therefore crop vegetation fraction abundance is at a maximum in February, a change from vegetation to bare soil between October and February can only mean that the vegetation is not a crop. Soil fractions increased in March (figure 4.30 and table 4.7). There was also evidence of water advancing back over the dunes after its retreat in March indicating a rise in water level in the dune depressions.

This occurrence was observed in March and May (figure 4.29). The area of vegetation between October, December and February was fairly constant, but declined slightly between February and May. The consistency in the area of vegetation over time suggests the constant presence of swamp vegetation.

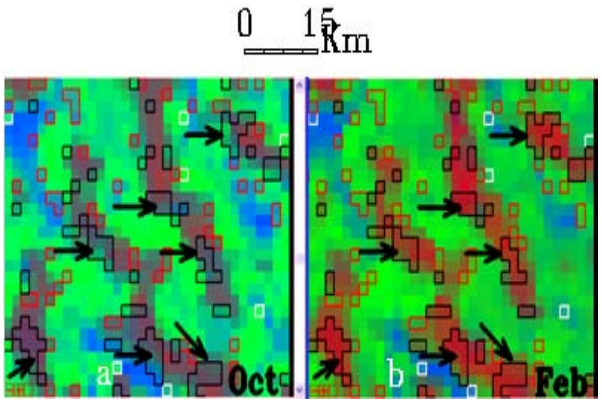

Fig. 4.28: Overland flooding in October on dune islands and evaporation of water from the dune islands in February.

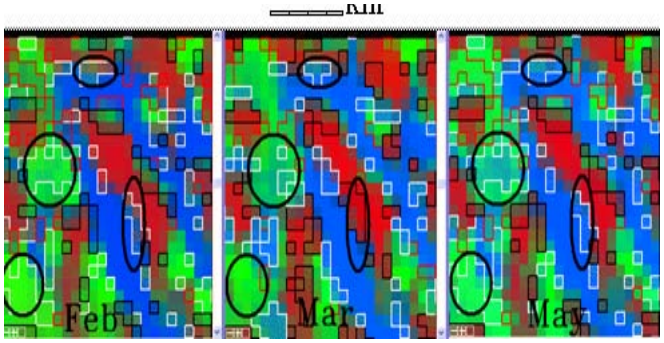

Fig. 4.29: Water advancing back into interdunes in May.

Table 4.7: Increase, decrease and net change in the area of soil, vegetation and water in the Southeastern Dunes Islands between Times T1 and T2.

South Eastern Dune Islands									
Increase in area of endmember fractions between times T1 and T2 (Km^2)				Decrease in area of endmember fractions between times T1 and T2 (Km^2)			Net change in area of endmember fractions between times T1 and T2 (Km^2)		
Oct	**Soil**	**Veg**	**Wat**	**Soil**	**Veg**	**Wat**	**Soil**	**Veg**	**Wat**
Dec	55.7	59.1	45.6	-19.6	-16.6	-82.8	36.1	42.4	-37.2
Feb	45.1	51.7	32. 6	-18.5	-12.6	-91.6	26.6	39.1	-59.1
Mar	128.6	46.1	26.0	-8.2	-12.0	-101.7	120.4	34.1	-75.7
May	102.1	46.5	39.8	-16.2	-21.4	-74.3	85.9	25.1	-34.5
Dec	**Soil**	**Veg**	**Wat**	**Soil**	**Veg**	**Wat**	**Soil**	**Veg**	**Wat**
Feb	67.1	51.2	60. 7	-45.0	-45.8	-83.9	22.0	5. 4	-23.3
Mar	106.8	39.3	52.6	-25.3	-45.8	-85.5	81.5	-6.5	-32.9
May	93.1	46.9	79.1	-33.2	-59.1	-75.9	59.9	-12.2	3.2
Feb	**Soil**	**Veg**	**Wat**	**Soil**	**Veg**	**Wat**	**Soil**	**Veg**	**Wat**
Mar	97.8	22.6	42.7	-16.7	-36.7	-47.2	81.1	-14.1	-4.5
May	75.9	32.0	69.1	-25.1	-49.7	-41.1	50.8	-17.7	27. 9
Mar	**Soil**	**Veg**	**Wat**	**Soil**	**Veg**	**Wat**	**Soil**	**Veg**	**Wat**
May	28.5	21.3	52.8	-33.0	-25.6	-26.0	-4.5	-4.2	26.8

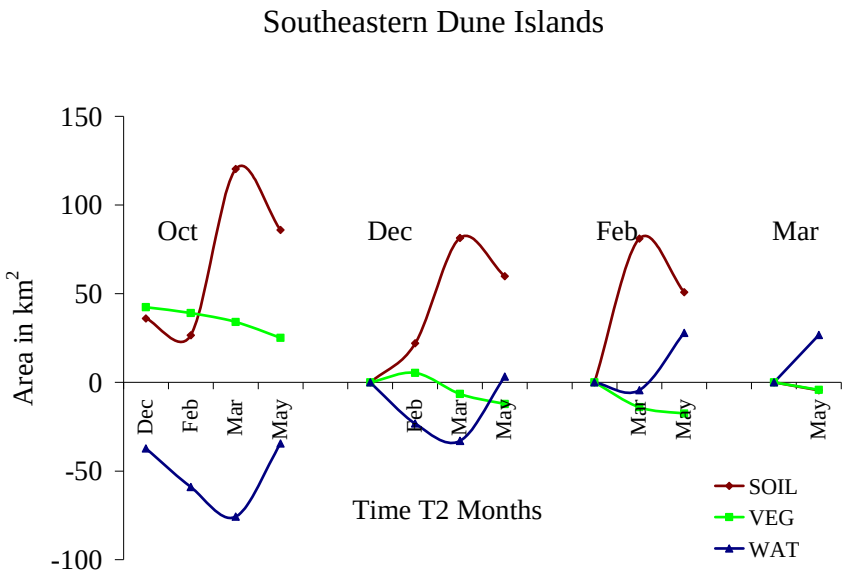

Fig. 4.30: Soil, vegetation and water change patterns in the Southeastern Dune Islands between times T1 and T2 months.

vi) The Southern Open Swamps and the Southern Reed Islands (Regions 9 and 10).

The Southern Reed Islands is a 5 km to 80 km wide stretch of reed clumps growing along the southwestern and southern coastline of the lake in shallow pools of water which increase in depth with distance from the shore.

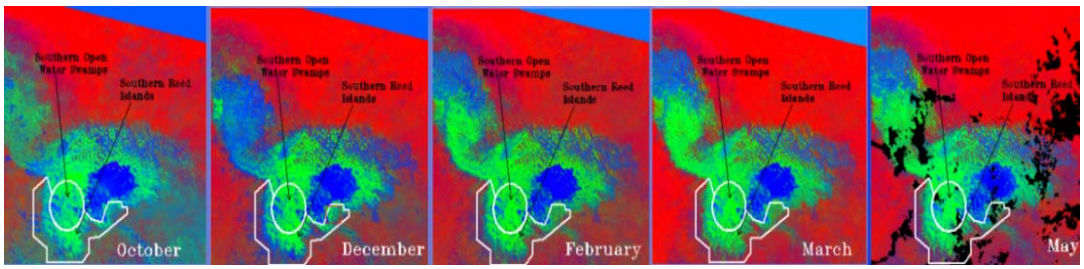

Fig. 4.31: The Southern Open Water Swamps and the Southern Reed Islands between October 2003 and May 2004.

The coastal region of the Southern Reed Islands is occupied by the Southwestern Lakeshore Farmlands, while the Southern Open Swamps lie immediately to the north of the Southern Reed Islands (figure 4.31). The Southern Open Swamps was previously open water when the water level was around 281.9 metres asl. Now only residual pools and dense vegetation are left and the swamp vegetation has become contiguous with the Southern Reed Islands.

The Southern Reed Islands were inundated between October and December due to a general rise in lake level in the Southern Open Swamps (white ellipses, figure 4.32). Increase in swamp vegetation in the Southern Open Water Swamps was noticed on the December MERIS LSU image as a result of the movement of water out of the Southern Open Swamps in a southwesterly direction towards the Southwestern Lakeshore Farms (figures 4.32 and 4.33). This caused a decrease in areal extent of water in the Southern Open Water Swamps and an increase in areal extent of water in the Southern Reed Islands in December. The decrease in areal extent of water on December MERIS LSU in the Southern Open Swamps implies that the rise in lake level in this region occurred in November and according to Carmouze and Lemoalle, (1983), the amount of water that enters the lake from October to November is 50% of the annual supply.

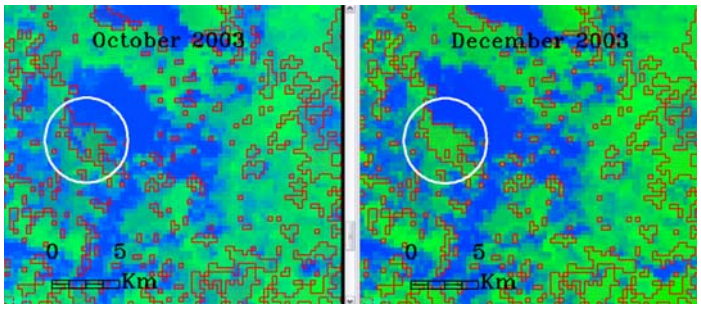

Fig 4.32: Inundation in October and emergence of vegetation in December in the Southern Open Swamps.

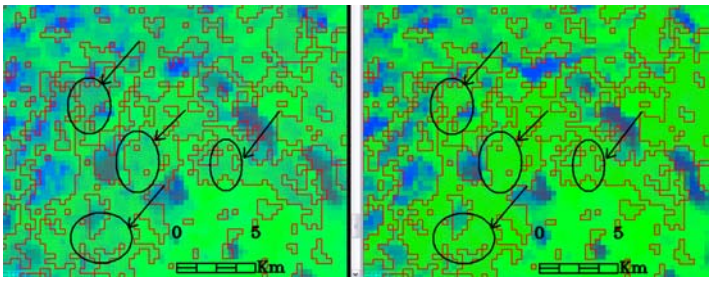

Fig 4.33: Passage of water between vegetation in October and vegetation increase in December in the Southern Open Swamps.

The area of swamp vegetation in the Southern Open Swamps remained constant between December and May (see graph, figure 4.36) while between December and May, the areal extent of vegetation in the Southern Reed Island fluctuated with a pronounced maximum areal extent in March because of the presence of crop vegetation growing on the Southwestern Lakeshore Farms which are located in this region. Thus the area of swamp vegetation was relatively constant between December, and May and

this stability in the area of swamp vegetation over time is an indication of the difference between swamp vegetation and cultivated vegetation because the area of cultivated vegetation does not remain constant between October and May in the two farmlands but tends to fluctuate.

It was noticed at the edges of small pools, in the Southern Open Swamps, that pixels with high water fractions in December, were converted to vegetation fractions on the eastern side of the pools in February (figure 4.34 white ellipses). Likewise pixels with vegetation fractions were converted to water fractions on the western side of the pools (figure 4.34 black ellipses). This showed the influence of the Harmattan winds which were blowing from a northeasterly direction at this time of the year (December and February) and pushing the water and vegetation in a southwesterly direction.

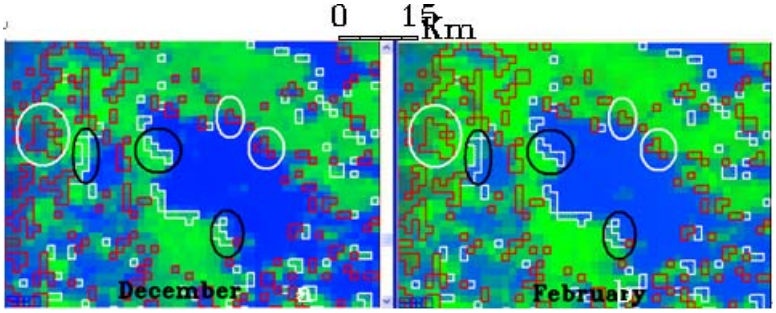

Fig 4.34: Vegetation replaces water and vice versa in the residual pools of the Southern Open Swamps between December and February.

Table 4.8: Increase, decrease and net change in the area of soil, vegetation and water in the Southern Reed Islands between Times T1 and T2.

Southern Reed Islands									
Increase in area of endmember fractions between times T1 and T2 (Km^2)				Decrease in area of endmember fractions between times T1 and T2 (Km^2)			Net change in area of endmember fractions between times T1 and T2 (Km^2)		
Oct	**Soil**	**Veg**	**Wat**	**Soil**	**Veg**	**Wat**	**Soil**	**Veg**	**Wat**
Dec	15.3	70.8	111.2	-3.2	-23.3	-66.6	12.1	47. 5	44.6
Feb	25.9	104.6	21.7	-2.3	-10.9	-149.1	23.7	93.8	-127.4
Mar	127.3	119.8	4.0	-0. 9	-10.2	-210.0	126.4	109.7	-206.1
May	84.3	75.6	10. 9	-1.1	-15.0	-108.0	83.2	60. 6	-97.1
Dec	**Soil**	**Veg**	**Wat**	**Soil**	**Veg**	**Wat**	**Soil**	**Veg**	**Wat**
Feb	14. 5	60.2	16.6	-1.4	-35.1	-126.9	13.0	25.1	-110.2
Mar	100.5	102.4	14.3	0.00	-36.5	-221.3	100.5	66.0	-207.1
May	73.7	85.1	33.5	0.00	-48.1	-155.8	73.7	37.0	-122.3
Feb	**Soil**	**Veg**	**Wat**	**Soil**	**Veg**	**Wat**	**Soil**	**Veg**	**Wat**
Mar	29.5	20.8	14.0	0.00	-8.1	-52.2	29.5	12. 7	-38.3
May	26.3	20.00	53.1	0.00	-25.8	-39.5	26.3	-5.8	13.7
Mar	**Soil**	**Veg**	**Wat**	**Soil**	**Veg**	**Wat**	**Soil**	**Veg**	**Wat**
May	5.9	5.9	42.8	-3.0	-19.0	-5.9	2.9	-13.1	37.0

Southern Reed Islands

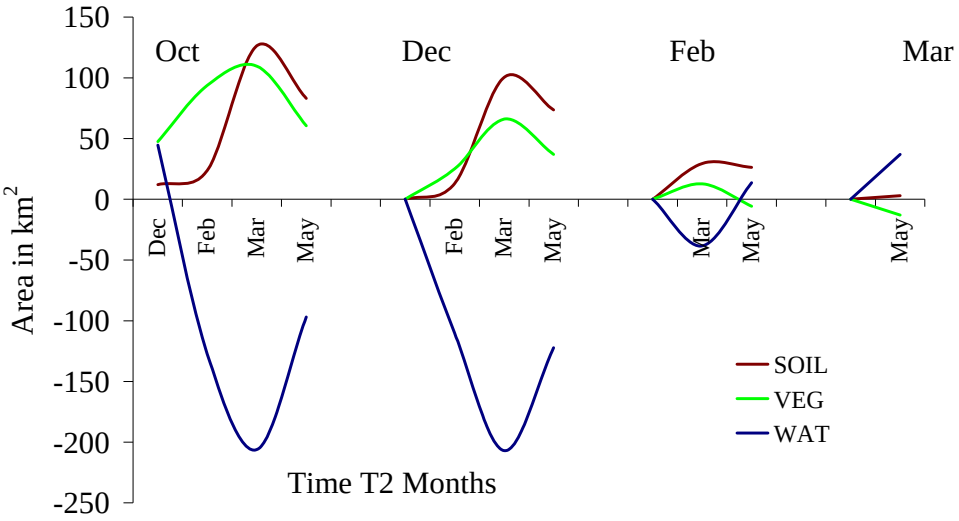

Fig.4.35: Soil vegetation and water change patterns in the Southern Reed Islands between times T1 and T2 months

Table 4.9: Increase, decrease and net change in the area of soil, vegetation and water in the Southern Open Swamps between times T1 and T2.

Southern Open Swamps									
Increase in area of endmember fractions between times T1 and T2 (Km^2)				Decrease in area of endmember fractions between times T1 and T2 (Km^2)			Net change in area of endmember fractions between times T1 and T2 (Km^2)		
Oct	**Soil**	**Veg**	**Wat**	**Soil**	**Veg**	**Wat**	**Soil**	**Veg**	**Wat**
Dec	0.02	85.0	17.3	0.00	-9.30	-97.7	0.02	75.7	-80.4
Feb	0.49	110.8	19.3	0.00	-11.8	-172.6	0.49	99.0	-153.3
Mar	2.30	140.6	16.0	0.00	-8.5	-168.2	2.30	132.1	-152.2
May	1.84	56.4	30.1	0.00	-13.1	-77.0	1.84	43.4	-46.9
Dec	**Soil**	**Veg**	**Wat**	**Soil**	**Veg**	**Wat**	**Soil**	**Veg**	**Wat**
Feb	0.94	27.5	29.7	0.00	-29.7	-54.0	0.94	-2.20	-24.32
Mar	3.03	41.4	29.5	0.00	-35.1	-52.5	3.03	6.3	-22.93
May	2.13	49.1	78.9	0.00	-45.6	-38.5	2.13	3.5	40.49
Feb	**Soil**	**Veg**	**Wat**	**Soil**	**Veg**	**Wat**	**Soil**	**Veg**	**Wat**
Mar	0.35	17.0	30.1	0.00	-11.4	-25.2	0.4	5.6	4.9
May	1.10	25.4	96.0	0.00	-23.5	-18.8	1.1	1.9	77.2
Mar	**Soil**	**Veg**	**Wat**	**Soil**	**Veg**	**Wat**	**Soil**	**Veg**	**Wat**
May	0.94	5.82	51.0	0.00	-13.9	-10.4	0.94	-0.87	40.6

Southern Open Swamps

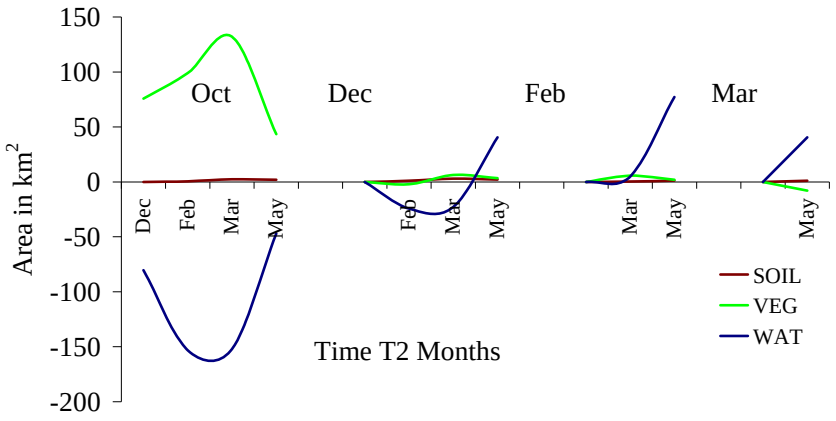

Fig.4.36: Soil vegetation and water change patterns in the Open Swamps between times T1 and T2 months

vii) The Southeastern Reed Islands (Region 11).

The Southeastern Reed Islands are situated immediately to the east of the Southeastern Open Water region (i.e the area of permanently open water where the Chari River enters the lake) and to the south of the Southeastern Dune Islands (figure 4.37). The Southeastern Reed Islands became permanently vegetated from1974 onwards during the 1970s drought years.

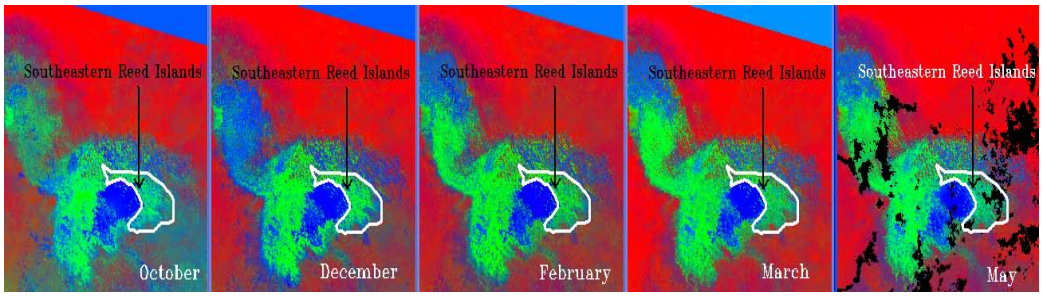

Fig. 4.37: The Southeastern Reed Islands between October 2003 and May 2004

Between October and February, vegetation fraction increased in pixels of partially inundated vegetation with a corresponding decrease in the water fractions. The area of vegetation was highest in December (see graph, figure 4.42). Between December and March, vegetation fractions changed to soil fractions on the eastern side of dune edges (white ellipses figure 4.38) and likewise soil fractions changed to vegetation fractions on the western side of dune edges (black ellipses figure 4.38). This indicated that the vegetation was moving in a westerly direction and as with the Southern Reed Islands,

this is also a function of the Harmattan wind which blows from a northeasterly direction between December and March.

Small water movements can be traced from December through to May. The black arrows in figure 4.39 show the movement of water from the pool which inundated vegetation at the edge of the pool in December. Therefore movement of water through the lake was not confined to the months of flood inundation (figures 4.40 and 4.41) and pixels in the May MERIS LSU recorded an increase in water fraction abundance thus making vegetation partially inundated.

Some of the dunes in this region are inhabited. This was seen from the smoke detected on an ASTER image. It is not likely that the reed covered dunes of the Southeastern Reed Islands are inhabited primarily for agricultural purposes although it is possible that some cultivation at the edges of the dunes occurs because cultivation on dune shorelines was noticed on all the dune islands visited during field observations. Additionally, the salinity of the lake water in the Southern basin is low enough to support cultivation. However, due to its proximity to the region of permanently open water, the swamp vegetation in the Southern Reed Islands is almost perennial and some of the reed vegetation is difficult to remove even in the dried areas of the lake (personal communication with LCBC staff).

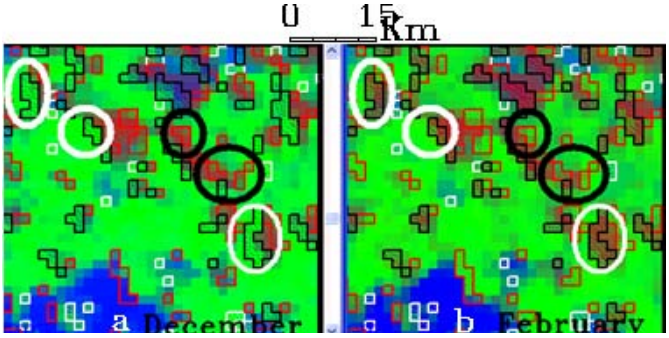

Fig. 4.38: Change from vegetation to soil in the Southern Reed Islands between December and February.

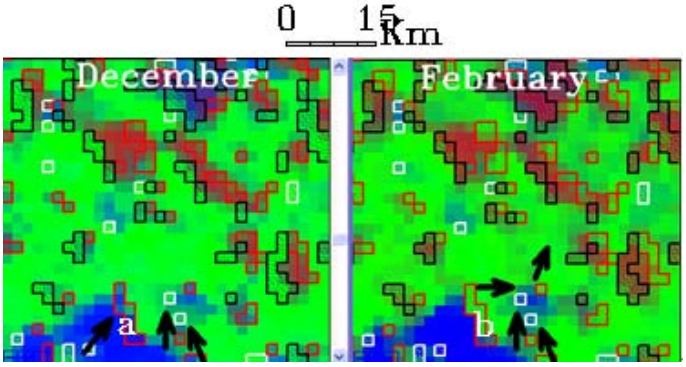

Fig.4.39: Movement of water through the Southeastern Reed Islands between December and February.

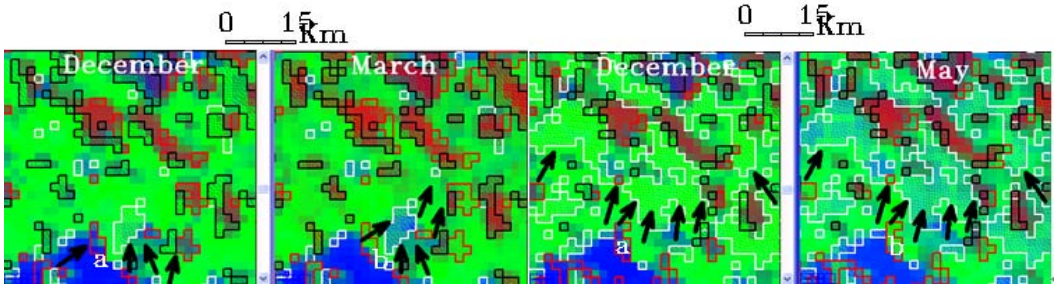

Fig.4.40: Movement of water through the Southeastern Reed Islands between December and March.

Fig 4.41: Movement of water through the Southeastern Reed Islands between December and May.

Also as mentioned earlier, because farmers follow the recession of water, most of the farmed lands lie nearer the lakeshore rather than within the hinterland of the lake. Therefore any habitation in the interior of the lake can be attributed to fishing villages. Table 4.10 and figure 4.42 summarize the pattern of change in the Southeastern Reed Islands between the T1 months and T2 months.

Table 4.10: Increase, decrease and net change in the area of soil, vegetation and water in the Southeastern Reed Islands between times T1 and T2.

Southeastern Reed Islands									
Increase in area of endmember fractions between times T1 and T2 (Km^2)				Decrease in area of endmember fractions between times T1 and T2 (Km^2)			Net change in area of endmember fractions between times T1 and T2 (Km^2)		
Oct	**Soil**	**Veg**	**Wat**	**Soil**	**Veg**	**Wat**	**Soil**	**Veg**	**Wat**
Dec	22. 9	134.9	49.2	-4.20	-7.58	-125.5	18.7	127.4	-76.3
Feb	38.7	63.7	21.7	-3.6	-5.4	-163.9	35.1	58.2	-142.2
Mar	93.1	60.1	16.3	-1.02	-5.72	-172.7	92.1	54.4	-156.3
May	68.3	27.6	20.3	-1.6	-14.4	-64.3	66.7	13.2	-43.9
Dec	**Soil**	**Veg**	**Wat**	**Soil**	**Veg**	**Wat**	**Soil**	**Veg**	**Wat**
Feb	39. 0	28.2	28.9	-15.4	-60.9	-75.2	23. 6	-32.7	-46.3
Mar	77.3	27.3	31.9	-7.2	-66.1	-99.8	70.1	-38.9	-67.9
May	55.7	17.9	85.6	-7.7	-89.5	-11.5	48.1	-71.6	74.1
Feb	**Soil**	**Veg**	**Wat**	**Soil**	**Veg**	**Wat**	**Soil**	**Veg**	**Wat**
Mar	37.5	14.1	23.9	-6.7	-19.4	-26.1	30.7	-5.3	-2.2
May	32.4	13.7	88.8	-7.2	-38.6	-21.3	25.2	-24.9	67.5
Mar	**Soil**	**Veg**	**Wat**	**Soil**	**Veg**	**Wat**	**Soil**	**Veg**	**Wat**
May	12. 3	7. 6	63.4	-13.8	-24.5	-8.5	-1.5	-16.9	55. 0

Southeastern Reed Islands

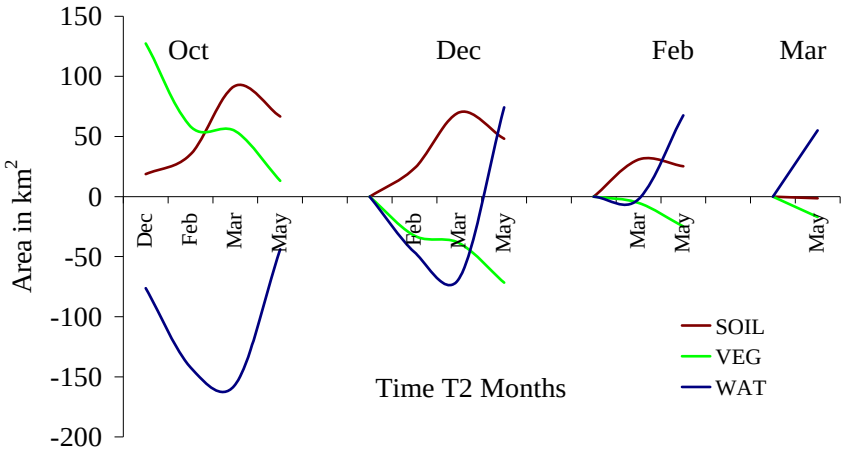

Figure 4.42: Soil, vegetation and water change patterns in the Southeastern Reed Islands between times T1 and T2 months.

4.2.3 A comparison between an identified farmland in the Northeastern Reed Islands and Southwestern Lakeshore Farms

The objective of this section is to examine patterns of change between endmember fractions in regions of the lake basin to see whether the changes could indicate other areas of farmlands apart from the Polder Farmlands and Southwestern Lakeshore Farmlands. Part of the shoreline of the Northeastern Reed Islands was found to have similar temporal change patterns with the farmlands of the Southwestern Lakeshore Farmlands therefore it is possible that recessional agriculture is practiced along the Northeastern Reed Islands shoreline. A time series mean fraction abundance value spectra of soil vegetation and water endmembers showing the temporal patterns of change for this area of the Northeastern Reed Islands were compared with those on the Southwestern lakeshore farms (figures 4.43 to 4.46. The mean fraction values in the two areas were found to be similar (table 4.11). The temporal pattern of change noticed in the Southwestern Lakeshore Farmlands (green curve, figure 4.43a) and the Northeastern Reed Islands (red curve, figure 4.43a) was not similar in October because soil fraction was very high in the Northeastern Reed Islands as a result of the presence of dessicated dunes and interdune depressions in the region. The presence of these dunes is because the Northeastern Reed Islands are contiguous with the region of Northeastern Dune Islands.

Table 4.11: Comparison of the mean monthly soil, vegetation and water fractions between the Southwestern lakeshore Farmlands and Northeastern Reed Islands.

	Southwestern lakeshore farms			Northeastern Reed Islands		
	SOIL	VEG	WATER	SOIL	VEG	WATER
OCTOBER	0.200	0.390	0.413	0.523	0.220	0.257
DECEMBER	0.113	0.270	0.651	0.450	0.171	0.393
FEBRUARY	0.150	0.408	0.449	0.163	0.422	0.440
MARCH	0.249	0.514	0.239	0.287	0.498	0.221
MAY	0.232	0.473	0.294	0.147	0.203	0.074

On the other hand, the Southwestern Lakeshore Farms are located in clay dominated soils which are waterlogged in some places.

It was found that in December, both areas show a rise in water and drop in vegetation fraction abundance (figures 4.43b and 4.44). In February, the two areas showed very identical mean fractions with increases in vegetation and a sharp decrease in soil fractions and slight decrease in water fractions, which suggest an inward contraction of the water (figures 4.43c and 4.45). In March, there was maximum increase in vegetation fractions in both the areas, with sharp declines in both water and soil fractions (figures 4.43d and 4.46). In May vegetation fraction abundance in both regions was higher than either soil or water fractions. However vegetation fraction abundance in the Southwestern Lakeshore Farmlands was much higher than the fraction abundance in the suggested farms of the Northeastern Reed Island. The reason for the apparent difference in vegetation fraction between the in May could be because of cloud contamination on some areas of the Northeastern Reed Island farmlands on the May LSU image which caused some pixels to be masked out and therefore lowered the mean fraction abundance value.

A visual examination of the northeastern shoreline of the Northeastern Reed Islands using high resolution ASTER VNIR 15m resolution image confirmed that some of the area was indeed farmlands, due to signs of mixed vegetation and disturbed soils and the appearance of rectangular partitions indicating farmlands on the ASTER image. There was also some fallow land, where the interdune vegetation appeared be smooth in texture and spatially continuous, an indication of grass vegetation (figures 4.47 and 4.48). Therefore this suggests that this area of the Northeastern Reed Islands is indeed cultivated and the similarities between the Southwestern Lakeshore Farmlands also suggest that recession agriculture is practiced on the shoreline of the Northeastern Reed Islands.

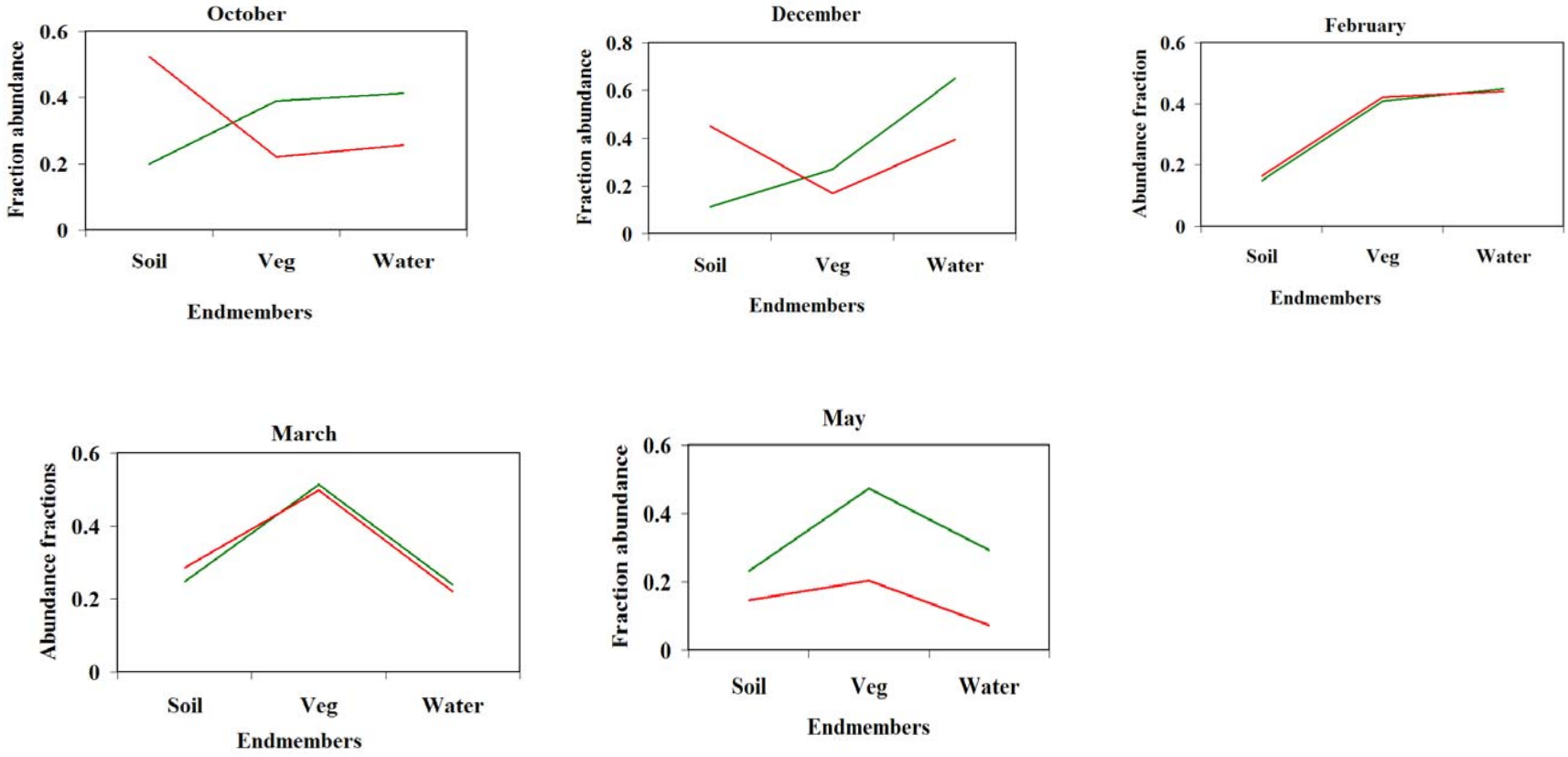

Fig. 4.43 a – e: A comparison of fraction abundance spectra in the Southwestern Lakeshore Farmlands and suggested farmlands in the Northeastern Reed Islands between October 2003 and May 2004 (green = Southwestern Lakeshore Farmlands; red = Northeastern Reed Islands Farmlands).

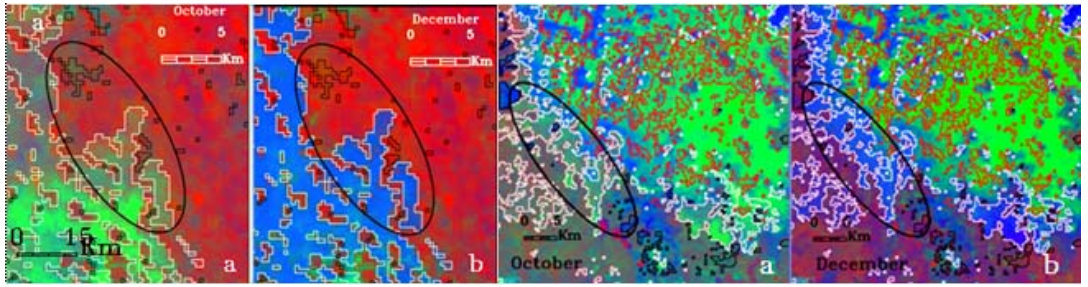

Fig 4.44: The suggested Northeastern Reed Islands Farmlands and the Southwestern Lakeshore Farmlands between October and December.

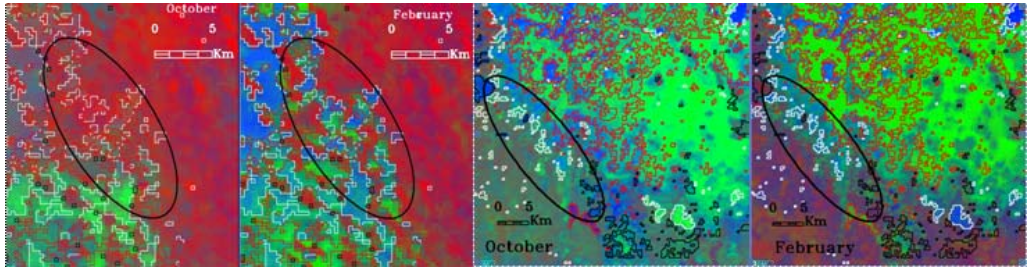

Fig 4.45: The suggested Northeastern Reed Islands Farmlands and the Southwestern Lakeshore Farmlands between October and February.

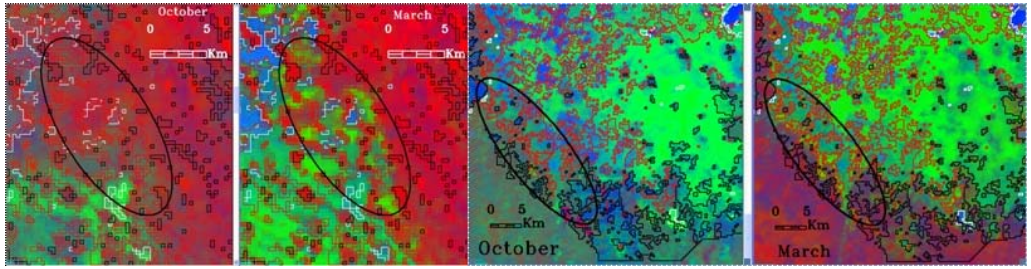

Fig 4.46: The suggested Northeastern Reed Islands Farmlands and the Southwestern Lakeshore Farmlands between October and March**.**

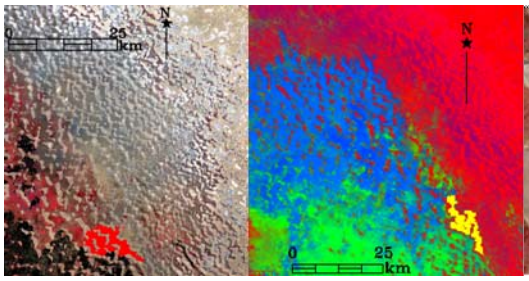

Fig. 4.47: Location of the suggested farms in the Northeastern Reed Islands on ASTER VNIR image and on MERIS LSU image.

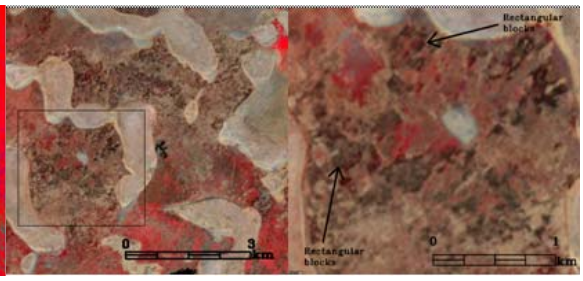

Fig. 4.48: A section of the farmlands in the Northeastern Reed Islands on ASTER VNIR (and magnified in next image of ASTER VNIR).

4.3 GENERAL DISCUSSIONS

4.3.1 Comparison between the Southwestern Lake Shore Farmlands and the Polder Farmlands of the Southeastern and Eastern Dune Islands.

Both the Polder Farmlands and the Southwestern Lakeshore farmlands are located along the shorelines of Lake Chad. The polder farmlands are located in dune depressions of the southeastern part of the lake and the Southwestern Lakeshore Farms are located on flat land in the southwestern part of the lake. Due to limited spatial resolution, the farmlands were initially identified on the MERIS images with the aid of information from fieldwork and reference to higher resolution optical images in which cultural features associated with cultivation e.g. dams, were seen.

The Southwestern Lakeshore Farmlands experienced pronounced seasonal inundation in December which was not apparent in the Polder Farmlands (except on traditional polder farmlands) because barriers keep out the lake water. Some of the polder farms may have become partially inundated in May due to ground water seepage to the surface and re flooding of these polder farms, given the earlier explanations of the re-advancement of the water in May.

On the MERIS LSU the highest vegetation fraction abundance in the Southwestern Farmlands was seen on the March and May images while on the Polder Farmlands, the highest vegetation fraction abundance was observed in February. This implied that crops matured between March and May on the Southwestern Lakeshore Farms, and in February on the Polder Farmlands. In the Southwestern Lakeshore Farms a decrease in vegetation was seen on the farmlands in May, in part due to the insect infestation observed during field work in May. It is possible that without the infestation, the mean vegetation fraction values in May might be higher.

On some areas of the modern polder farms that were intensively cultivated a high proportion of soil fraction was observed in February thus implying that not all the areas of Polder Farms had been cultivated. This was attributed to soil salinity which builds up as a result of seepage of water to the surface. This therefore is a limiting factor to cultivation on the polder farmlands. Vegetation turned to bare soil between February and May on some of the traditional polder farms due to one cropping cycle per year. On the government assisted polder farms however, three cropping cycles are possible and therefore the farms did not turn to soil in May. These differences mean that identification of farmlands using multi temporal MERIS should use different criteria for the two regions, i.e. the Polder Farmlands and the Southwestern Lakeshore Farmlands and possibly other regions as well.

4.3.2 Differences between swamp vegetation and farmland vegetation in the lake basin

The major difference between swamp vegetation and cultivated vegetation is that in general the areal extent of swamp vegetation was relatively constant between October and May, although it could fluctuate slightly between any two months. Therefore swamp vegetation could be considered as permanently present between October and May. Cultivated vegetation on the other hand was seasonal (except on the government assisted polder farms where three crops are harvested) and the areal extent of crop vegetation was more variable. Thus where interdune depressions become bare of vegetation, it is probable that this is farmland. Figures 4.49 and 4.50 show the mean fraction abundance for areas of swamp vegetation and areas of farmland vegetation.

It could be seen that the fluctuations in the area of swamp vegetation between time T1 and T2 in the interdune depressions was not large where as in comparison, there was a steady increase in vegetation from December to February on the Polder Farmlands and a steady increase in vegetation from December to March on the Southwestern Lakeshore Farmlands. In general, the area of swamp vegetation in the northern and southern lake basins was at a maximum in March and December respectively. The area of crop vegetation was at a maximum in February on the Polder Farmlands, and at a maximum March and May in the Southwestern Lakeshore Farmlands.

Some change patterns noticed in pixels which served to highlight the difference between the cultivated crops and swamp vegetation were:

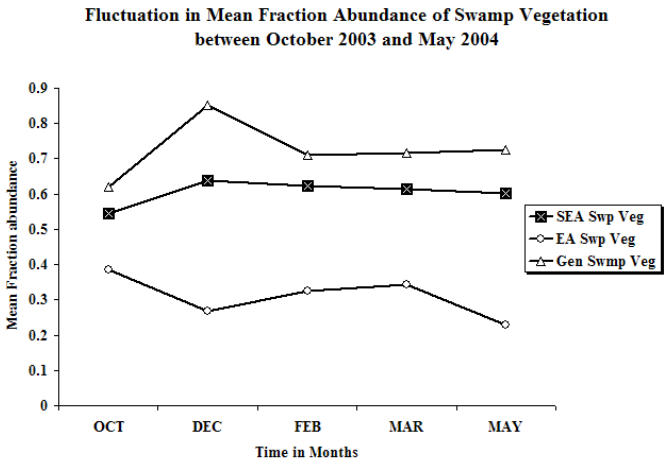

Figure 4.49 Mean swamp vegetation fraction abundance in some regions of Lake Chad. (SEA =Southeastern Dune Island; EA = Eastern Dune Islands; Gen Swmp = General Swamp Vegetation over whole Lake

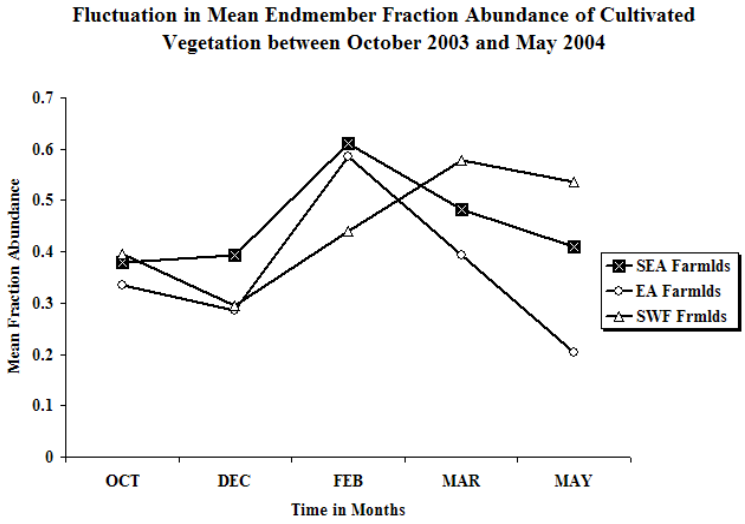

Figure 4.50 Mean cultivated vegetation fraction abundance in some regions of Lake Chad (SEA and EA Farmlands = Polder Farmlands in the Southeastern and Eastern Dune Islands; SWF = Southwestern Lakeshore Farmlands).

1) Swamp vegetation becomes inundated by water fractions at any time or month while crop vegetation is rarely inundated. However bare farmlands can become inundated. This was observed on the traditional polder farms of the Polder Farmlands in the Southeastern Dune Islands. Likewise during seasonal flooding between November and February, the Southwestern Lakeshore Farmlands are inundated.

2) Direct change from pixels with high proportion of water fractions to pixels with high proportion of swamp vegetation fractions occurs between times T1 and T2 (see figure 4.27). The change can be caused by floating vegetation islands which appear in the image at time T2. Therefore this also differentiates swamp or non crop vegetation from cultivated vegetation. With crop vegetation, a transitional period must occur where pixels with a mixed proportion water and soil fractions change to crop vegetation between times T1 and T2. This occurred with pixels on the Southwestern Lakeshore Farmlands which had a high proportion of water fractions in December and consequently became a mixture of water and soil fractions in February.

3) The change from swamp vegetation to soil is often localized and occurs mainly at edges of the dune where swamp vegetation makes an interface with dune islands. The areas of change are usually not large. On the other hand, when vegetation in cultivated farmlands changed to soil, the change occurred over a large area of land and it also occurred at specific periods of time for example after harvesting.

4.3.3 Overall change across the lake basin:

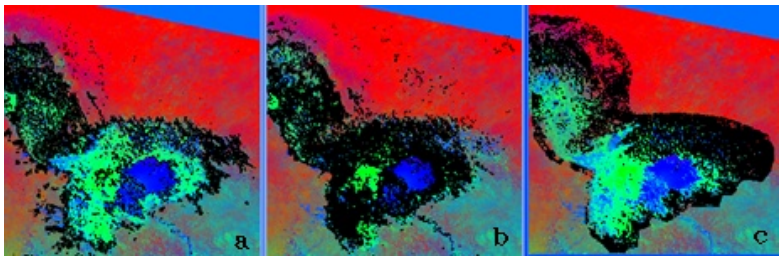

Fig 4.51: Spatial location of (a), water (b) vegetation and (c) soil change pixels

In general, the temporal changes across the lake revealed that in each month, a different type of change occurred. Between October and December, the significant changes observed were the flood inundation over the northern lake basin and the coastal area of the Southern Reed Islands. In February, the most significant change was the increase in crop vegetation abundance to a maximum in the polder farms and vegetation replaced water inundation in the northern basin. In March, the most significant changes were the general increases in soil and swamp vegetation fraction abundances to a maximum over the whole lake and the increase in crop vegetation to a

maximum in the Southwestern Lakeshore Farms. In May, the most significant change was the ubiquitous increase in water fractions observed over most of the lake regions.

i) Change in water endmember fractions:

Changes involving water fractions occurred in the following areas of the lake: the Northern and Northeastern Reed Islands, the Southeastern and Eastern Dune Islands, the Southern Reed Islands and Southwestern Lakeshore Farmlands, the Northern and Southern Open Swamps and the Grand Barrier Ridges (figure 4.51a). Between October and May, over the whole lake, water increased predominantly in the southwestern lake shoreline and in the Southeastern and Eastern dune islands and the extreme northern part of the lake basin. Water generally settled in these areas from December to May except in the southwestern shore of the lake where water retreated and was replaced by recession cultivation. The movement of water in the southern lake basin is not confined to the months with the peak flood levels but seemed to be occurring in all the months. This is due to the constant discharge of the Chari water into the lake which results in the northward and lateral movement of the water observed in section 4.2.2 (vi) in the Southeastern Reed Islands.

Water found in the northern basin from February suggested the northward movement of the water and a rise in lake level in the northern basin. The area of water remained relatively constant between February and May implying that from February, the volume of discharge entering the lake had decreased. It also implied that the limit of the movement of water had been reached in the northern basin.

The movement of water into the northern open water swamps can be traced from the spatial distribution of the change pixels representing decrease in water fractions from October and March (figure 4.52). The red, yellow, green cyan and blue pixels in the southern lake and northern lake basins indicated the location and spatial distribution of water endmember fractions that were replaced by vegetation from October through to February. It can be seen that the color of the pixels appeared to be arranged serially in relation to the order in which the months followed one another. This implied that the position of the pixels show how the water moved through the lake and where it was located in each month. This ability to trace the transitional movement of the water over the whole lake is one of the advantages of the MERIS wide swath width. This transitional movement of water is shown schematically in figure 4.53.

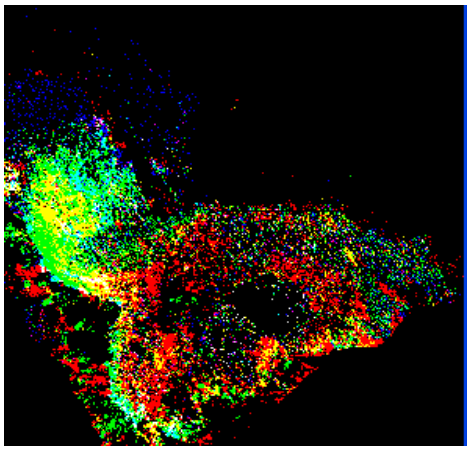

Fig 4.52: Spatial distribution of change pixels mapping out the movement of water fractions over the lake basin from October 2003 to March 2004.

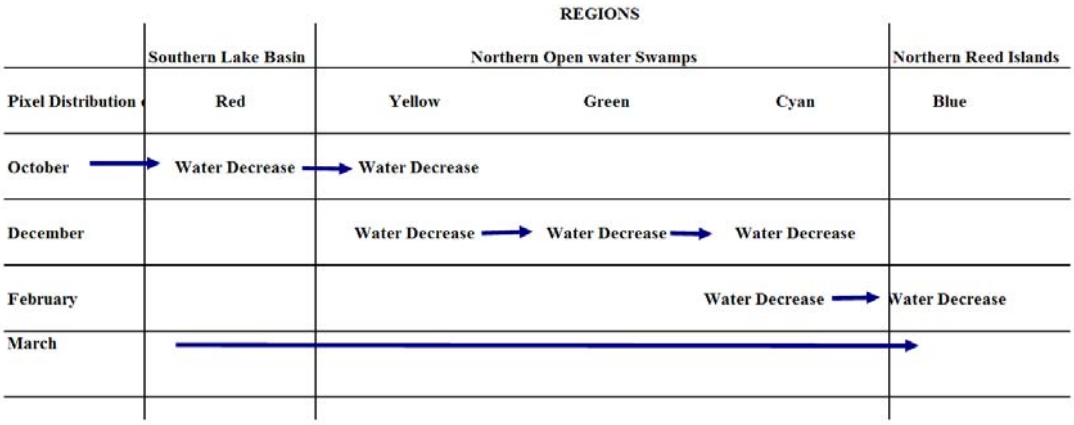

Fig. 4.53: Decrease in water fractions between October 2003 and March 2004 reflecting water movement across the lake

ii) Change in vegetation endmember fractions

Changes in vegetation fractions mostly occurred in the following areas of the lake: the Northern Open Swamps, the Southern Open Swamps, the Northeastern Reed Islands, the Grand Barrier, the Southern Reed Islands, the Southeastern Reed Islands and the Southeastern Dune Islands (figure 4.51b).

It was generally noticed that the fluctuations in the area of swamp vegetation in the northern and southern lake basins were at a maximum in March and December respectively (table 4.12). It was concluded that this had to do with the time of the departure of the flood waters from the northern and southern lake basins. A comparison of areal extent of vegetation and water from October to May for the northern and southern basin showed that the mean vegetation fraction value was highest in

December in the southern basin when flood water has moved away from the southern basin and highest in March in the northern basin when flood water has moved away from the Northern Open Water Swamps and reached its limit of inundation in the Northern Reed Islands.

Table 4.12: A comparison of mean endmember fractions and areal extent of vegetation and water from October to May, 2004

	Southern Lake Basin				Northern Lake Basin			
	Mean Vegn EMF	Areal extent of Vegn	Mean Water EMF	Areal extent of water	Mean Vegn EMF	Areal extent of Vegn	Mean Water EMF	Areal extent of water
Oct	0.490	3288.2	0.542	3637.5	0.410	1799.7	0.389	1704.9
Dec	0.587	3940.0	0.444	2975.3	0.381	1671.6	0.602	2643.0
Feb	0.564	3787.6	0.415	2779.8	0.583	2559.1	0.379	1659.1
Mar	0.568	3808.3	0.424	2841.5	0.638	2801.7	0.285	1246.5
May	0.513	3442.2	0.452	3033.3	0.485	2130.6	0.237	1039.5

This phenomenon of optimal vegetation growth being dependent on time of flood arrival and retreat was not observed for crops. With crops, there is a delay period between the flood retreat and optimal crop growth in which time the soil becomes well drained to support cultivation. The polder farms are independent of flood arrival and retreat, due to the movement of the water into the polders being controlled by farmers.
The highly saline nature of the northern basin prevents the dune areas of the northern basin from being cultivated when water retreats from their edges. Likewise, the dune elevations which are lower in the northern basin than in the southern basin preclude their utilization as farmlands because they could be constantly under inundation. However, settlements are found on the northern basin dunes where the main activity is fishing.

iii) Change in soil endmember fractions

Change in soil fractions occurred in the following areas of the lake: the Northern, and Northeastern Reed Islands the dried out Northeastern Dune Islands, the Grand Barrier dune ridges, the Southeastern Dune Islands Southeastern Reed Islands and the Eastern Dune Islands (figure 4.51c).
Change from pixels with high water or vegetation fraction abundance to pixels with high soil fraction abundance occurred between February March and May in the Southeastern where some Polder Farmlands went from being densely vegetated in

February to 100% bare soil in May. Change from pixels with high water fractions to pixels with high soil fractions also reflected the rapid retreat and drying out of the water in some parts of the lake that have been hitherto inaccessible except by canoe. This phenomenon was experienced during field trip. For example, in December and January, the island of Nbulwa, which could not be reached except by canoe became accessible in a four wheel drive by July (Plate 3).

Plate 3: Waterway at Nbulwa village in January 2004 and May 2004.

Other changes are those at the boundary between soil, vegetation and water fractions at the edges of dune islands. These include the proportion of water to vegetation in a pixel, and the proportion of soil to vegetation in a pixel (the higher the proportion of water, the more likely it is to be swamp vegetation, and the higher the proportion of soil the more likely it is to be crop vegetation).

Many dune islands in the hinterland of the lake are inhabited for fishing activities. The edges of the dune islands or land surrounding the dune islands are cultivated (observations from fieldwork). The settlements include those types which constitute risk zones i.e. areas of cultivable or potentially cultivable land that is prone to inundation and the possible loss of crops. On the MERIS LSU, it was not easy to determine whether the vegetation at the edges of the dune was crop vegetation or not, because these pixels were spatially fragmented despite having similar change patterns and usually pixels with the same change patterns representing farmlands are adjacent to each other in arrangement and spatially contiguous enough to be identified as farmlands. Additionally, the average size of farmland plots on the dune islands estimated from IKONOS was about 0.64 ha. This is approximately 7% of the ground area seen on a MERIS pixel and therefore it was not possible to separate the farmland vegetation from non farmland vegetation on these pixels.

4.3.4 Change patterns which indicate farmlands in other regions of the lake

Similar temporal patterns of change were found between the Southwestern Lakeshore Farmlands and some areas of the Northeastern Reed Islands. The time series of mean endmember fraction spectra for the two regions were also very similar. The similarity in the patterns of change in the two regions was based on location, arrangement of features in space and seasonality. Seasonality is the timing of events like harvesting and flooding which is repeated at the same time of the year and for which the same change patterns are produced by their representative pixels every time the events occur. This similarity suggested the existence of farmlands in the coastal areas of the Northeastern Reed Islands. Therefore for the MERIS data, the spatial location and arrangement of features in space and seasonality was important in helping to identify similar features through change detection. A visual analysis of ASTER VNIR high resolution images confirmed the presence of some farmlands in the Northeastern Reed Islands. Thus auxilliary information is also required to match the observations on the MERIS LSU images with activities that occur at the time of year or month under consideration.

4.4 CONCLUSION

The objectives of this chapter were to investigate the patterns of change which could indicate the presence of croplands in the known areas of farmlands and to identify any such pattern which could indicate croplands over the whole lake basin. Swamp vegetation change patterns included conversion from vegetation fractions to water fractions which occur at any time of the year while crop vegetation fractions only change to water at specific times of the year. Change from vegetation to soil fractions is small and localized for swamp vegetation whereas farmland is represented by large areal conversions of vegetation fractions to soil fractions at specific times of the year. A direct change from water fractions, to vegetation fractions and vice versa, (i.e. no soil phase in between), is also indication of swamp vegetation. On the other hand, a transitional period occurs when water fractions change to crop vegetation. Swamp vegetation is permanently present in the interdune depressions throughout between times T1 and Tn, whereas cultivated vegetation is only periodically present in the interdunes. The areal extent of swamp vegetation is at a maximum immediately after

the passage of flood water. Bare soil in interdune depression is a sign of an area under cultivation because under normal circumstances, interdune depressions are always swampy. Therefore interdune depressions without vegetation are indicative of farmlands especially in the months known to be harvest months, like March on the Polder Farmlands.

Differences in cultivation practices observed in the Polder Farms and on the Southwestern Lakeshore Farms mean that different criteria are to be used for the identification of farmlands using multi temporal MERIS in the two regions, and possibly other regions as well. Similarities in spatial location and the temporal pattern of change between a known area and an unknown area suggest that the known and unknown areas have the same land cover features. Therefore spatial location and arrangement of features in physical space and seasonality, (i.e. the recurrence of one or a set of temporal change patterns produced as a result of the time of the year) are important in helping to identify similar features through change detection.

Temporal changes across the lake revealed that the area of water was maximum in December and minimum in March. Water re-advanced back into the lake in May. The areal extent of swamp vegetation was at a maximum in December and March in the southern and northern basins respectively and at a minimum in October and December in the southern and northern basins respectively. The areal extent of soil was maximum in March and minimum in October.

4.5 RECOMMENDATIONS

Cultivation using residual moisture is practiced in the southwestern and southeastern parts of the lake. However, the major crops grown in the two regions and the cropping cycles are not the same, thus their patterns of change were not similar. So in order to identify cropland in parts of the lake using MERIS, prior information on the areas being investigated is required so that the temporal change patterns can be established and used to compare with similar temporal change patterns found in other regions of the lake.

Since the spatial resolution of MERIS is relatively coarse, it is important to obtain in situ data through fieldwork, in order to establish whether changes between soil vegetation and water fractions which occur at on dune islands can be attributed to the presence of farmlands or natural vegetation.

It is important to acquire a calendar year of MERIS data in order to monitor temporal changes in the farmland areas on a monthly basis. Fine temporal resolution images allowing 2 to 3 day revisit time, are essential for analyzing flooding periods as well as harvest periods. In this way, the passage of flood and its effects on the surrounding land can be monitored in greater temporal detail and during the harvesting period, differences between crop and non crop vegetation will become more apparent.

CHAPTER FIVE

RELATING TOPEX/POSEIDON ALTIMETER MEASUREMENTS TO RIVER VOLUME DISCHARGE AND HYDROM GENERATED LAKE HEIGHT VALUES

5.1 INTRODUCTION

The overall objective of section one is to discover whether the areal extent of water and vegetation detected on MERIS LSU can be related to altimeter values. In order to estimate missing altimeter lake level values in the year 2004 corresponding to the image dates, a relationship between time series river discharge data and time series lake level altimeter data is established. Another relationship is established between time series lake level measurements obtained in situ with the HYDROM software and time series lake level altimeter data. Finally the estimated radar altimetry data for the year 2004 is related to the horizontal areal extent of water as well as to vegetation growth in some of the regions of the lake derived from the MERIS LSU classification.

5.2 PROCEDURES

5.2.1 Datasets

Datasets used were

- Chari river discharge data (1998 to 2002) measured at the Ndjamena station;
- Water level measurements (1999 to 2004) at the settlement of Bol where the principal lake level measurements for Lake Chad are obtained. The water level measurements were generated from the HYDROM software.
- Archived geo-physically corrected radar altimeter measurements (1999 to 2002) derived from the TOPEX/Poseidon satellite. (See appendix B for all data).

The Chari River discharge data were used because manual gauge data were unavailable. Also the Chari river discharge system has a predominant influence on the seasonal and annual fluctuation of the water balance of the lake to the extent that predictions of future lake levels are possible (Coe and Birkett, 2004). Additionally, the radar altimeter readings were acquired in the region of permanently open water where the Chari river enters the lake Chad. The lake water level data at Bol generated from the HYDROM software were used because they provided data for the years 2003 and 2004 which were missing from the river discharge data

and also they acted as validation for the regression analysis between the river discharge data and the available TP altimeter measurements. The HYDROM generated data are currently used by the Lake Chad Basin Commission since the manual gauges for recording the water level are dysfunctional (Bila Mohammed, LCBC staff, Personal communication).

Bol is a dune settlement on the Lake Chad located in the Southeastern Dune Island. This particular part of Lake Chad was chosen to investigate the relationship between the altimeter data and the areal extent of the lake because

- The HYDROM lake level measurements were obtained from the inundated dune depressions surrounding the Bol dune settlement.
- Bol is relatively close to the satellite ground track over the open water (pass 248) where the accepted TOPEX POSEIDON measurements were obtained.
- That part of the lake is an important source of water for irrigation for farmers.
- All the major Polder Farms are located in the area.

Both river discharge measurements and the radar altimeter measurements are time series data. The river volume discharge data are daily measurements of the Chari River measured at the hydrological station at Ndjamena, approximately 108 km from the entrance of the lake and approximately 131 km from the point where the altimeter satellite values were acquired (figure 5.1). The data span the years from 1998 to 2003.

5.2.2 TOPEX/POSEIDON Satellite Tracks

The TOPEX/POSEIDON satellite has two ground tracks that cross over the lake basin. These are ascending pass 109 and descending pass 248. The descending pass 248 crosses over the region of permanently open water. Ascending pass 109 enters the lake at between latitude 12° and 13° N and longitudes 13º and 14º E from the southwestern end of the lake and exits the lake at between latitudes 13° and 14° N and longitudes 14° and 15° E in the northern part of the lake. Descending pass 248 enters the lake from the northeastern side at between latitude 14º and 15 º N and longitudes 13º and 14 º E and descends across the dune islands. It passes over the open water region and exits the lake between latitudes 12° and 13° N and longitudes 14° and 15° E. The latitude and longitude range at which the lake level values measured from the descending pass 248 were recorded by the radar altimeter started at 13.07°N and 14.37° E and ended at 12.87°N and 14.44°E (figure 5.1).

5.2.3 Data Limitations

Each reading of the altimeter data is the mean of 10 days' relative height variation values (Birkett, 2000). Therefore there are only three data values per month. The reference datum for the values of the lake height variations is the TOPEX/POSEDON 10 year mean level, measured in metres. The estimated error of the values of the lake height variations ranges from 0.045m to 0.166m (CNES/NASA, 2006). This seems reasonable because Birkett (2000) was able to detect seasonal water level variations with an accuracy of greater than 10cm RMSE (i.e. 0.1m).

The altimeter and river volume discharge data are not continuous from beginning of data measurements to the end of data measurements and do not always correspond temporally. There are river discharge data from October 1992 to April 1998 and from 1st November 2003 to 23 March 2006. The altimeter data time span was from October 1992 to October 2002. The time period between the data sets corresponded was from 7th May 1998 to 11th October 2002.

Some of the altimeter readings are noisy due to seasonal variability, i.e. low water levels were not recorded accurately by the altimeter. Therefore it was more difficult to interpret the radar backscatter signals in the months when water level was low. The presence of growing vegetation also attenuated some signals. (Birkett, 2000).

5.2.4 Relating River Volume Discharge to T/P Data

In order to calculate missing data values and also establish whether the seasonal pattern of fluctuations of Chari river volume discharge and altimeter data were similar, the river volume discharge and altimeter lake level data were plotted on the same graph with time in days as the x axis and river discharge and lake level as y axis (figure 5.2).

Because each single altimeter reading is a mean value of 10 days' readings, the river volume discharge data were also averaged to 10 day values to correspond with the altimeter values. A cross correlation analysis was performed in order to establish the phase lag between the time the Chari River water leaves N'Djamena and reaches the point where the altimeter measurements were obtained (figure 5.3). The following formula was used to find the phase lag (Bourke, 1996):

$$r = \frac{\sum_i [(x(i)-mx)(y(i-d)-my)]}{\sqrt{\sum_i (x(i)-mx)^2}\sqrt{\sum_i (y(i-d)-my)^2}} \quad (1)$$

Where x is river volume discharge; y is altimeter values; mx is mean of river volume discharge; my is mean of altimeter values; d is delay phase.

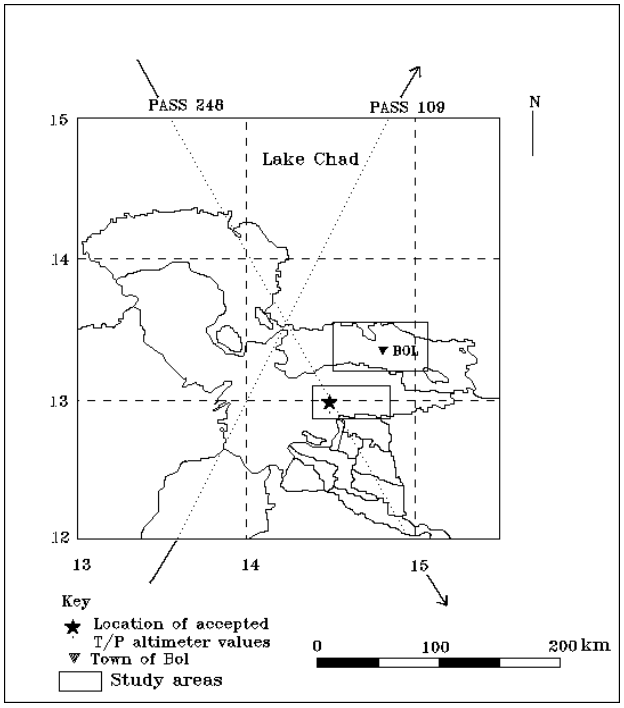

Fig. 5.1 TOPEX/POSEIDON satellite tracks over Lake Chad.

A 30 day phase lag was determined from the cross correlation analysis. This meant that there was a displacement of 30 days between every altimeter value and its corresponding river volume discharge value. Using the phase lag, the altimeter values were regressed against the river discharge values (figure 5.4). A coefficient of correlation (r^2) of 0.8545 was obtained with a logarithmic regression, while a linear correlation coefficient gave an r^2 value of 0.7261. The logarithmic regression was accepted because the trend line took into account all negative values which were representative of the periods of low water levels. The logarithmic regression was also indicative of the possible morphology of the lake where small river

discharges at low water level resulted in an initial steep rise of the curve where the lake bottom was narrow, and then a leveling off of the curve as the lake became wider.

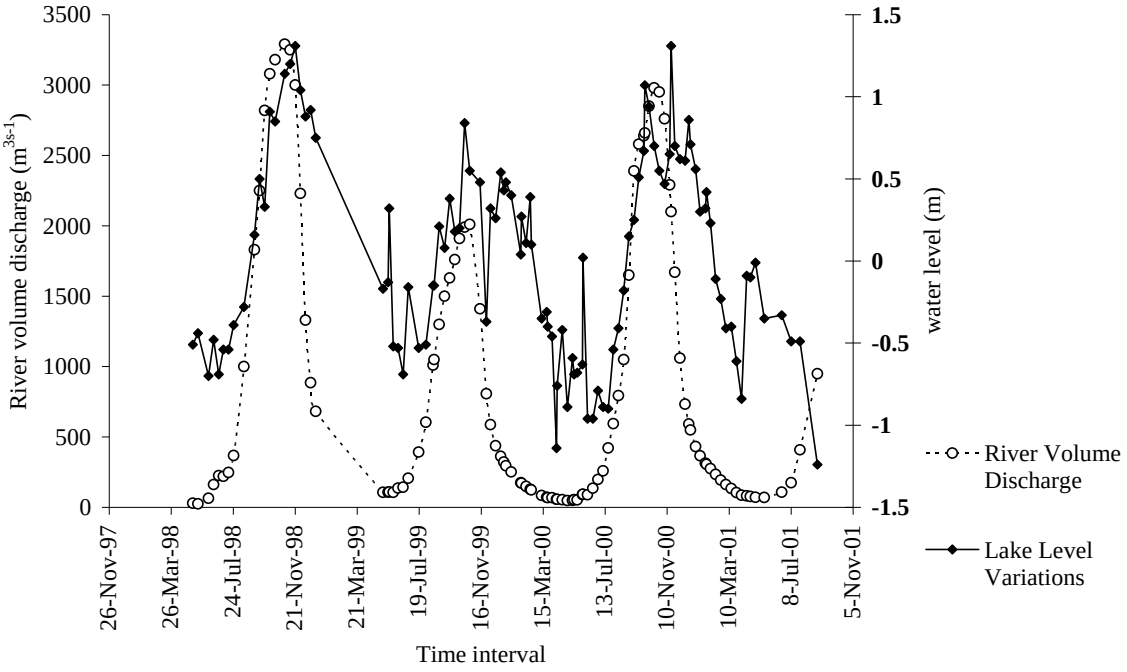

Fig 5.2: Relationship between river volume discharge and lake level measured from TP altimeter

Because there were neither river volume discharge data nor altimeter data for the precise dates of MERIS images, the Chari river discharge data for the MERIS image of October 8th 2003, December 17th 2003 and February 25th 2004 were derived from river volume discharge graphs of the Chari river found in AGRHYMET[1] monthly bulletins of February 2004, and August 2004.

[1] The AGRHYMET bulletin is a monthly magazine produced in collaboration with FEWS NET detailing some agricultural, hydrological and meteorological events pertaining to the francophone region of West Africa only. There is no regional cooperation between them and the lake Chad Basin Commission. The reason for using the AGRHYMET bulletins was because there was no reply to numerous enquiries made to the centre in Niamey, Niger, for a complete set of the river volume discharge data published in their monthly bulletins.

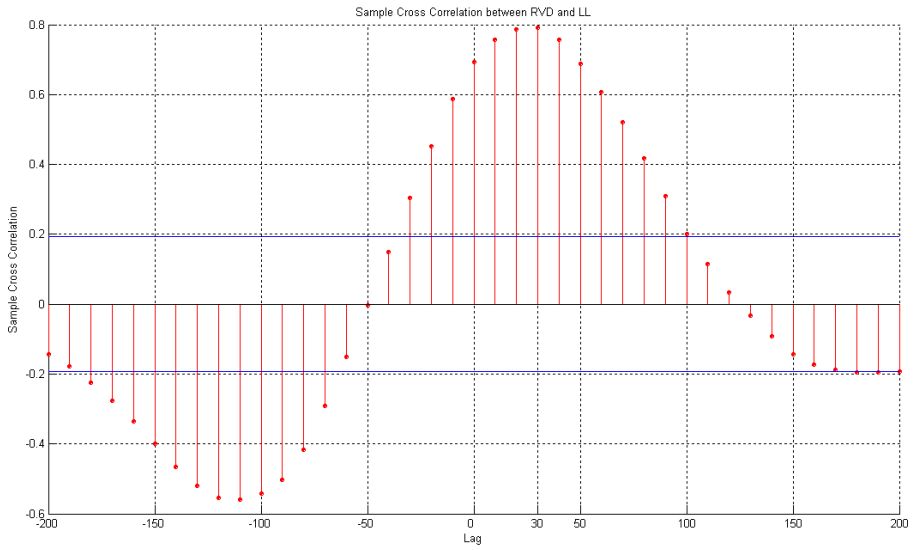

Fig. 5.3: Cross Correlation between river volume discharge and lake level

The river discharge data for Dec 17th 2003, January 21st 2004 were calculated from interpolation, because the AGRHYMET graphs are limited to river discharge values between January and November. Additionally, the river volume discharge data derived from the AGRHYMET graphs took account of the 30 day phase lag and therefore the recorded river discharge values were 30 days in advance of the dates of the images.

The river volume discharges that were interpolated were the dates of December and January and both represented river volumes near maximum. Therefore the high values obtained from the interpolation seem reasonable. The formula used for the interpolation was:

$$L_m = L_l + \left[\left(\frac{L_h - L_l}{D_h - D_l}\right) x\, D_m - D_l\right] \qquad (2)$$

Where L_m is the missing lake level between 2 values; L_l is the lower lake level value; L_h is the higher lake level value; D_h is the date of the higher lake level value and D_l is the date of the lower lake level value and D_m is the date of the missing lake level value. The river discharge values obtained from the AGRHYMET bulletins were used to calculate the altimeter height levels of the lake using the logarithmic regression equation:

$$y = 0.4136Ln(x) - 2.4047 \quad (3)$$

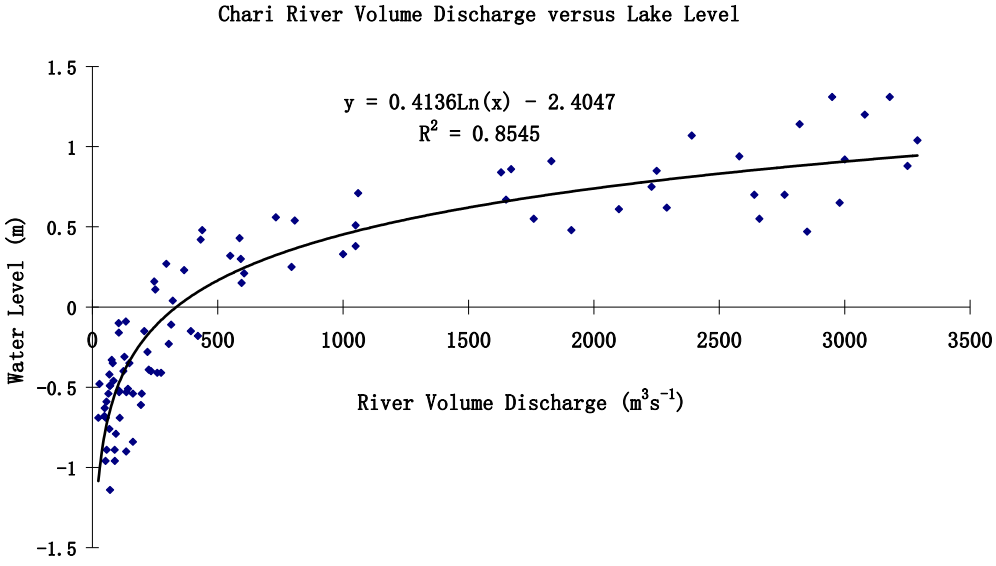

Fig. 5.4: Relationship between river volume discharge and lake level

Table 5.1 presents the values of the derived river volume discharges and estimated altimeter height levels for MERIS data and the seasonal trends in water level shown in figure 5.5 indicate a good agreement between river discharge volume and estimated altimeter height levels.

Table 5.1: Dates of MERIS images river volume discharge and lake levels estimated for the T/P altimeter.

Actual Dates of MERIS Images	River Volume Discharge Derived from AGRHYMET (m^3s^{-1})	Calculated Altimeter height levels (m)
Oct 8th 2003	1872.78	0.712
Nov 12th 2003	2890.39	0.891
Dec 17th 2003	2054.72	0.750
Jan 21 2004	1457.81	0.608
Feb 25th 2004	383.38	0.056
Mar 31st 2004	115	-0.442
May 5th 2004	50	-0.787

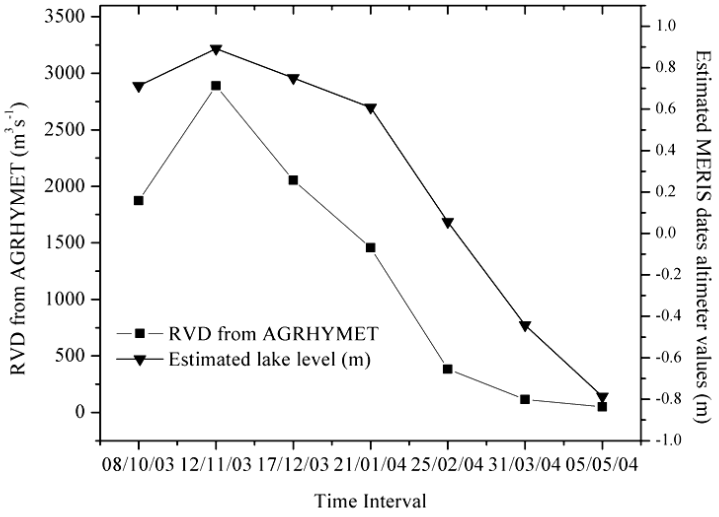

Fig. 5.5 Comparison of river volume discharge against estimated altimeter value dates of MERIS images

5.2.5 Relating T/P Data to HYDROM generated Lake Level Data

The second set of data was the lake height level data from Bol (See table C2 appendix C). The lake height level data was generated using a software called HYDROM[2] at *Institut de Recherche pour le Developpement* (IRD formally ORSTOM) in France and then disseminated to staff at LCBC (Mohammed Bila, staff LCBC, Pers. Comm).

A Coefficient of Determination (R^2)was established between the HYDROM generated lake level data and the radar altimeter lake level data through regression analysis. The R^2 of 0.693 was obtained, which showed that there was a good agreement between the generated lake level values and the radar altimeter lake level values (figure 5.6).

A time series graph of the generated lake levels and the radar altimeter lake height levels was plotted and a good agreement between the two data regarding the seasonal fluctuation of the lake was seen (figure 5.7). The time span for the generated lake level data was from 1999 to 2004 while that of the altimeter data was 1998 to 2002. Therefore the graph was divided into two parts. The blue colored part of the graph represents periods where there was both generated lake level data (blue line) and altimeter data (black triangles), while the green

[2] The HYDROM is a software for managing and processing hydrometrical data. It was developed under MS/DOS in the 80s by Gerard Cochonneau and widely used for hydrological data processing in South American and African countries (HYDRACCESS help manual).

colored part of the graph represents the generated lake level data. Using the dates of the generated lake level data, the altimeter lake level values for the MERIS images were calculated using the regression equation derived from the graph of figure 5.6:

$$y = 0.008x - 1.4874 \quad (4)$$

The estimated altimeter values for the dates of MERIS images were plotted on the graph (red squares, figure 5.7). The estimated values for the dates of MERIS images also showed a good fit with the generated lake level data. Table 5.2 presents the lake height level values calculated from the regression equations (4) and HYDROM generated lake level data. Figure 5.8 also indicates a good agreement between the HYDROM generated lake height values and the estimated altimeter height levels. Table 5.3 gives a comparison of estimated altimeter values derived from equations 2 and 4 respectively.

From table 5.3, it can be seen that the two sets of estimated altimeter values (i.e. from (a) equation derived from the regression between river volume discharge and the available TP altimeter data and (b) equation derived from the regression between using HYDROM generated lake level values and the available TP altimeter data are not the same. This is because the region of the lake for which the HYDROM generated lake height data was obtained was not the same region as that of open water where the satellite altimeter lake level values were acquired.

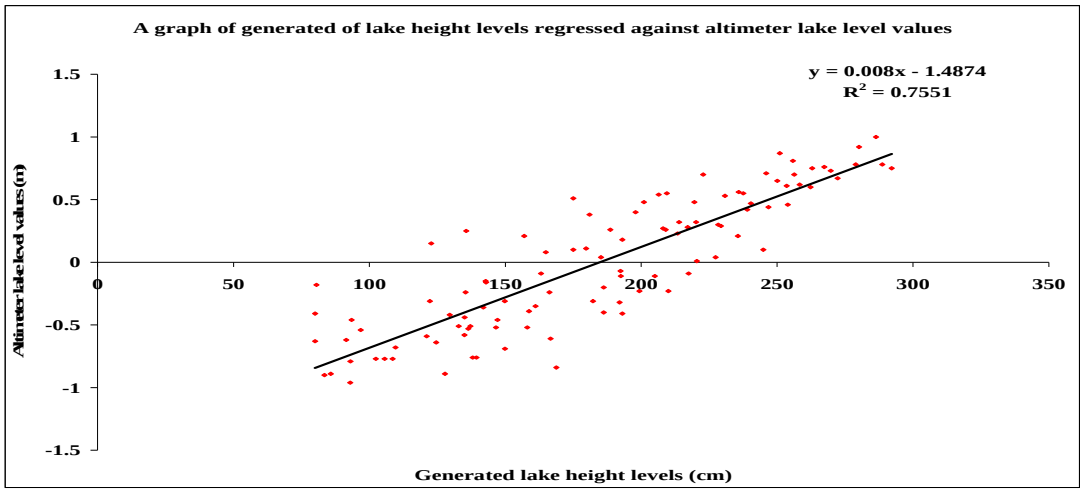

Fig 5.6: Graph of HYDROM generated lake height levels regressed against radar altimeter lake level values.

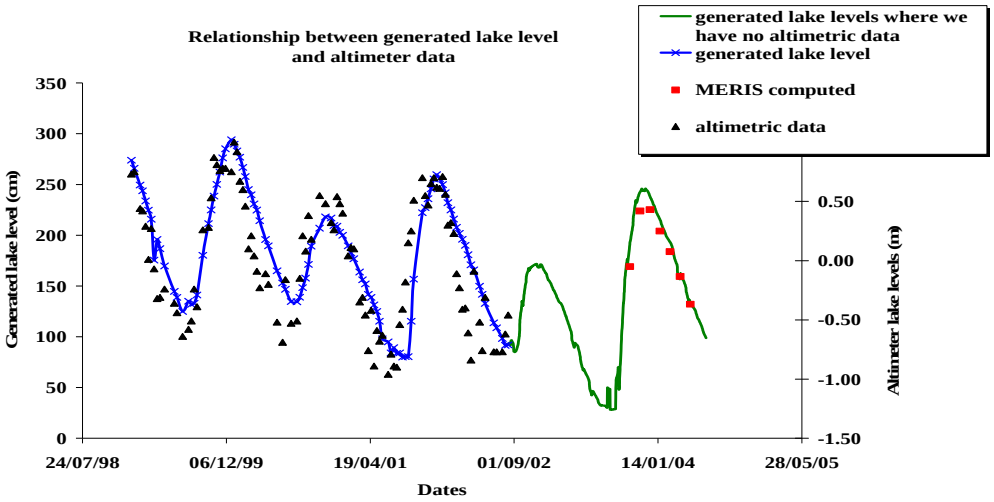

Figure 5.7: The relationship between the generated lake level values and T/P altimeter data.

Table 5.2: HYDROM generated lake height levels and estimated altimeter values for MERIS images

MERIS Dates	Altimeter values derived from equation 4 (m)	HYDROM generated lake levels (cm)
Oct 8th 2003	-0.05	178.4
Nov12th 2003	0.42	240.2
Dec 17th 2003	0.43	241.7
Jan 21 2004	0.25	218
Feb 25th 2004	0.08	195
Mar 31st 2004	-0.13	167.6
May 5th 2004	-0.37	136.7

However, the graphical representation of the values (figures 5.5 and 5.8) shows the same seasonal trend of a rise in water level between October and February, and a fall between March and May. The coefficients of determination between estimated altimeter values of MERIS image dates were 0.8575. Therefore the derived altimeter lake height values were deemed acceptable for use in relating the areal extent of surface inundation derived from MERIS with lake height levels from altimetry.

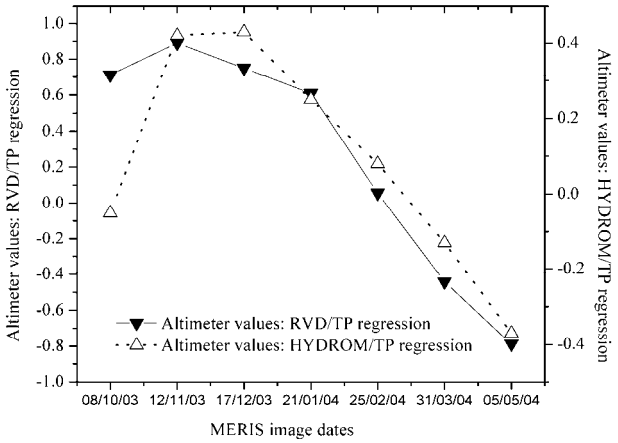

Fig. 5.8: Comparison between the HYDROM generated lake height levels and estimated altimeter values for MERIS dates.

Table 5.3: A comparison of the estimated altimeter values for the MERIS images dates

MERIS Dates	Estimated Altimeter data from RVD and TP regression (MERIS)	Estimated Altimeter data from HYDROM and TP regression (MERIS)
Oct 8th 2003	0.712	-0.05
Nov12th 2003	0.891	0.42
Dec 17th 2003	0.750	0.43
Jan 21 2004	0.608	0.25
Feb25th 2004	0.056	0.08
Mar31st 2004	-0.442	-0.13
May 5th 2004	-0.787	-0.37

The altimeter data derived from regressing the Chari river volume discharge data against TP altimeter data, were compared with the areal extent of water seen on MERIS images in the open water area, and in the Southeastern Reed Islands. The altimeter data derived from the HYDROM software were compared with the areal extent of water with lake height levels in the Southeastern and the Eastern Dune islands where the polder farms and the town of Bol are located.

5.2.6 Relating the Lake Level to the Areal Extent of Water and Vegetation

One of the objectives of the thesis is to relate radar altimetry data of water levels in Lake Chad to fluctuations in extent of water from MERIS images. In this section, the relationship

between altimetry data and areal extent of water was investigated using MERIS data. The monthly fluctuations in surface areal extent of water were related to the estimated altimeter lake levels (see section 1). Only the regions of the southern part of the lake basin were analyzed. This is because the southern lake basin experiences annual flooding from the Chari river discharge whereas water only crosses over to the northern lake basin when the Chari flood discharges exceeds 15 km^3. When the Chari river discharge exceeds 18km^3 flood reaches up to the latitude of the town of Bosso in Niger Republic (figure figure 1.3 section 1 chapter 1). This appears to be a common occurrence. The whole lake basin is flooded when river discharges exceed 28km^3. This occurred in the 2003/2004 flood season, when a total of water volume of 28.1 km3 was discharged between 1st May 2003 and 29th February2004 (AGRHYMET BULLETIN 2004). No radar altimeter data are available for the northern lake basin.

5.2.7 Binary Masking

On the five MERIS LSU images of October and December 2003, and February, March and May 2004, the water and vegetation bands were isolated. On the water and vegetation band of each month, subsets of the following sub regions of the southern lake basin were made: the Southeastern Dune Islands (region 6); the Open Water Region (region 7); the Southern Reed Islands (region 10) and the Southeastern Reed Islands (region 11). On the water band of each region, inundated interdune depressions were isolated by masking out all other features. Likewise on the vegetation band of each region, swamp vegetation was isolated by masking out all other features.

As Polder Farmlands were located in the Southeastern Dune Islands, the farms were isolated by masking out all other areas on the water and vegetation bands of the Southeastern Dune Islands. Likewise, the Lakeshore Farmlands were isolated by masking out all other areas on the water and vegetation bands of the Southern Reed Islands where they are located.

5.2.8 Estimating Area of Water and Vegetation from MERIS LSU Binary Files

The total areal extents of water and vegetation shown on the time series MERIS LSU water and vegetation fraction bands were calculated, for the sub regions of the southern lake basin. The areal extents of the water and the areal extent of the vegetation respectively, in the Southeastern Reed Islands, the Southern Reed Islands, the area of open water and the

Southwestern Lakeshore Farms were compared with the altimeter lake level reading estimated for the date of each image from the regression between river volume discharge data and radar altimeter lake level readings. Likewise the areal extent of the water and the areal extent of the vegetation respectively in the Southeastern Dune Islands and the Polder farmlands were compared with the altimeter lake level reading estimated for the date of each image from regression between HYDROM lake level data and the radar altimeter lake level data. Time series graphs of areal extent of water against estimated altimeter lake level and areal extent of vegetation against estimated altimeter lake level were produced. The relationships between areal extent of water or vegetation and the estimated lake level in each region of the southern lake basin were determined from the coefficient of determination (R^2).

5.3 RESULTS

Tables 5.4 to 5.5 show the estimated lake levels for the dates of MERIS LSU compared with the surface areal extent of water and vegetation respectively, extracted from MERIS LSU. The graphs of the relationship between surface areal extent and lake height level plotted over time (figures 5.9a to d to 5.14a to d) are given for each of the regions mentioned. The coefficients of determination (R^2) are given in table 5.6

Table 5.4: MERIS Surface area of lake at different regions of the lake and estimated T/P altimeter lake height level values (regression using river volume discharge)

Estimated Level for		South-eastern Reed Islands		Southern Reed Islands		South-western Lake shore farms		Open Water Region
MERIS	m	Areal extent of water/vegetation (in km^2)						
		water	veg	water	veg	water	veg	water
Oct	0.71	194.86	697.65	345.08	880.46	42.36	59.64	767.09
Dec	0.75	241.59	752.68	446.57	772.77	67.73	80.81	754.29
Feb	0.06	152.07	776.64	148.89	928.96	45.28	72.53	745.16
Mar	-0.44	132.88	770.34	91.23	904.63	24.30	83.30	741.03
May	-0.79	155.67	714.00	107.37	824.69	30.47	88.12	741.16

Table 5.5: MERIS surface area of lake at different regions of the lake and estimated T/P altimeter lake height level values (HYDROM regression)

MERIS		Southeastern Dune Islands		Polder farmlands	
Estimated Lake Level		Areal extent (km^2) of		Areal extent (km^2) of	
Dates	(m)	water	vegetation	water	vegetation
Oct	-0.05	235.98	323.99	37.91	38.81
Dec	0.43	216.32	384.78	34.14	35.36
Feb	0.08	184.41	413.00	20.90	52.73
Mar	-0.13	186.74	408.04	17.58	43.38
May	-0.37	202.79	380.82	23.44	35.14

Table 5.6: The Coefficient of determination R^2 showing the relationship between lake level and areal extents of water and vegetation.

Region	Coefficient of determination (r^2) for relationship between lake level and	
	Areal extent of water	Areal extent of vegetation
Southeastern Dune Islands	0.0983	-0.0027
Region of Open Water	0.7405	Not determined.
Southern Reed Islands	0.8397	-0.0524
Southeastern Reed Islands	0.6638	-0.0163
Polder Farmlands	0.3015	0.0009
Southwestern Lakeshore Farmlands	0.6409	0.7288

5.3.1 Southeastern Dune Islands

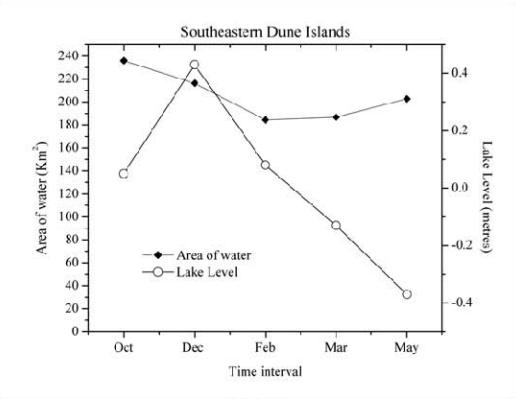

Fig. 5.9a

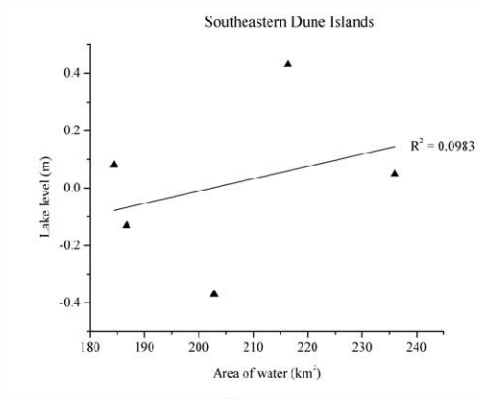

Fig. 5.9b

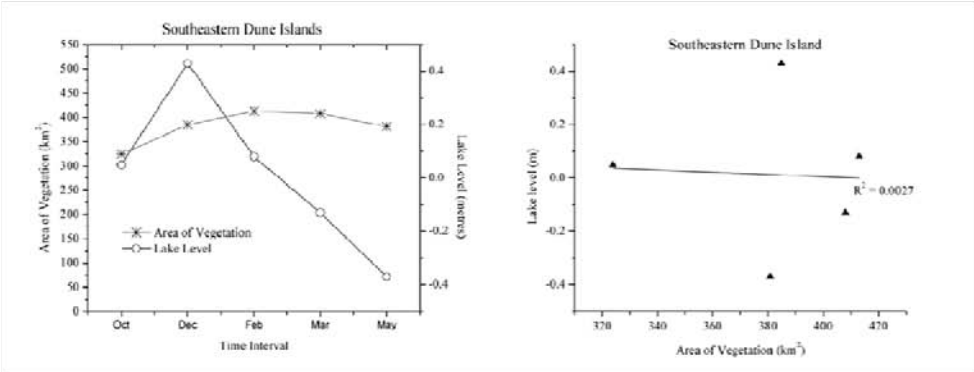

Fig. 5.9c Fig. 5.9d

Fig. 5.9a – d: Relationships between estimated lake level and surface area of water and vegetation respectively in the Southeastern Dune Islands

5.3.2 Open Water Region

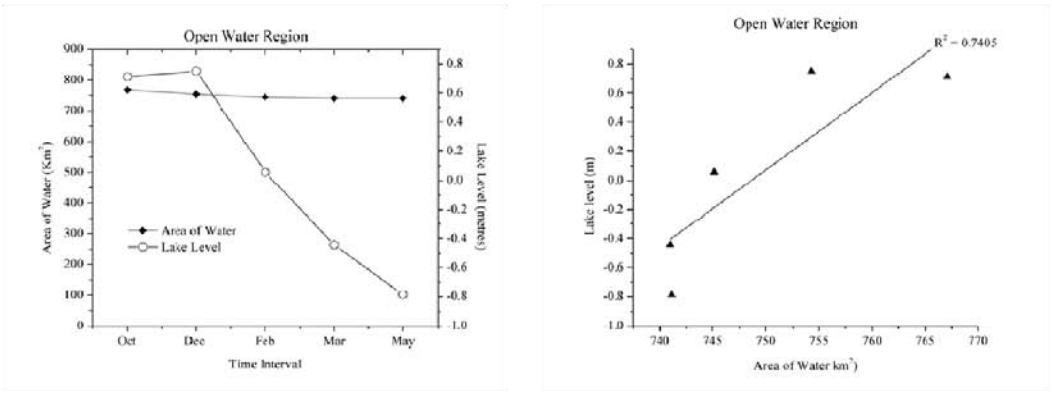

Fig. 5.10a Fig. .5.10b

Fig. 5.10a – b: Relationships between estimated lake level and surface area of water in the Open Water Region

5.3.3 Southern Reed Islands

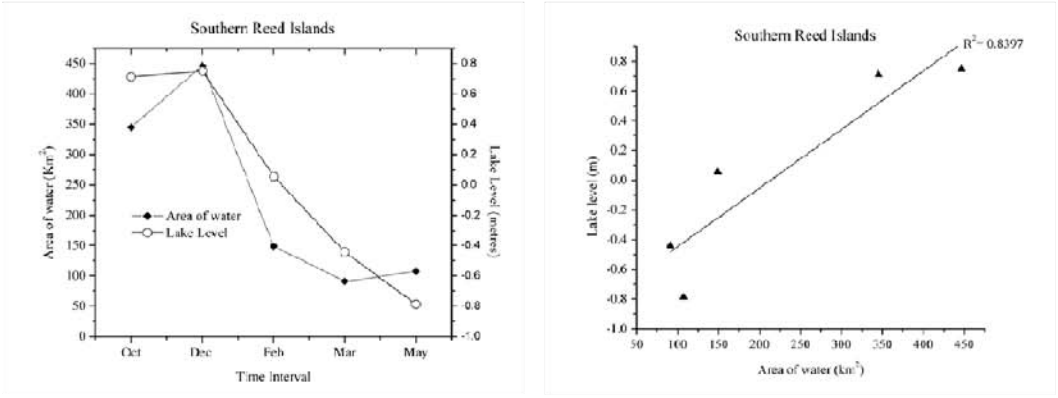

Fig.5.11a Fig.5.11b

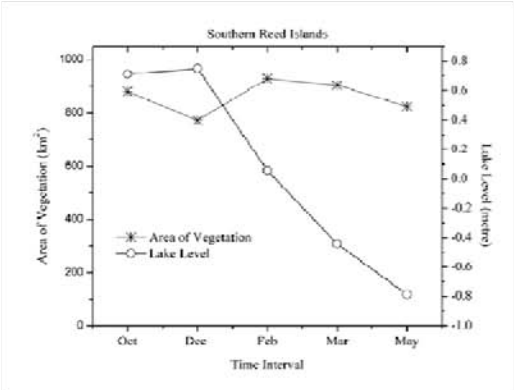

Fig. 5.11c

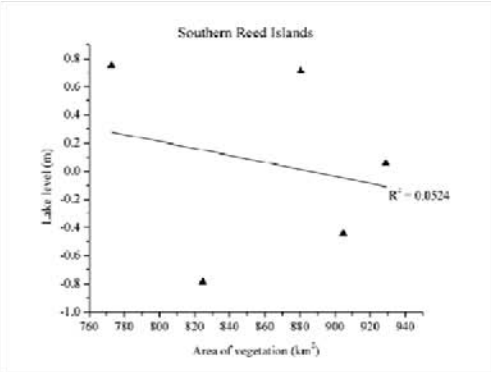

Fig. 5.11d

Fig. 5.11a – d: Relationships between estimated lake level and surface area of water and vegetation respectively in the Southern Reed Islands

5.3.4 Southeastern Reed Islands

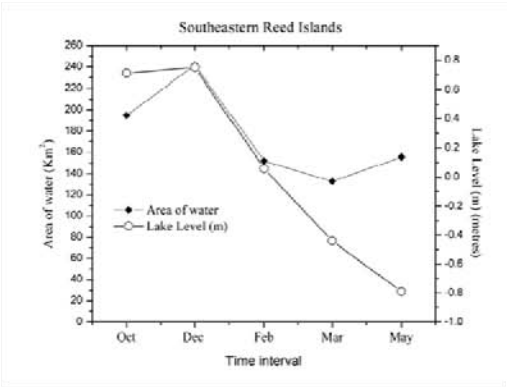

Fig.5.12a

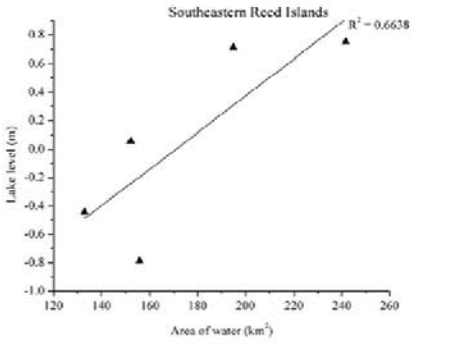

Fig. 5.12b

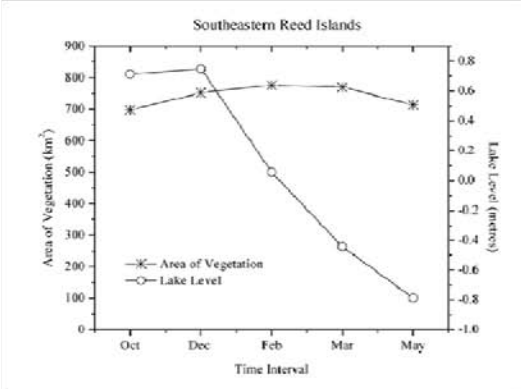

Fig.5.12c

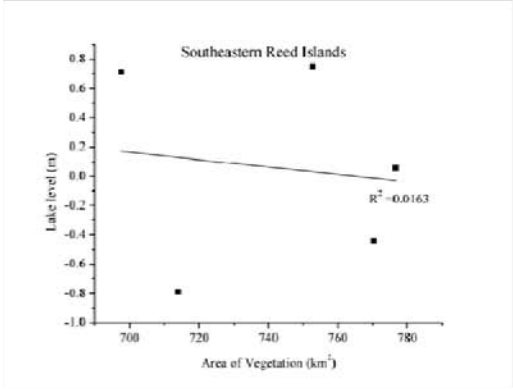

Fig. 5.12d

Fig. 5.12a – d: Relationships between estimated lake level and surface area of water and vegetation respectively in the Southeastern Reed Islands

5.3.5 Polder Farmlands

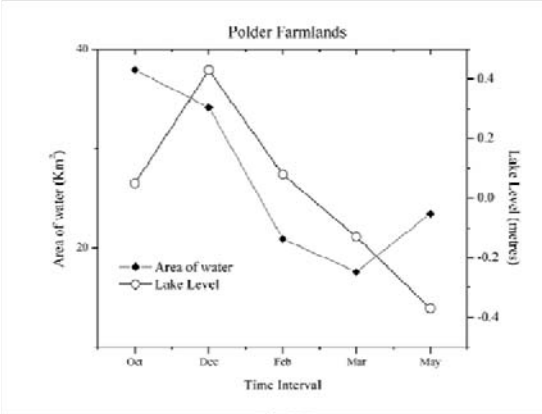

Fig. 5.13a

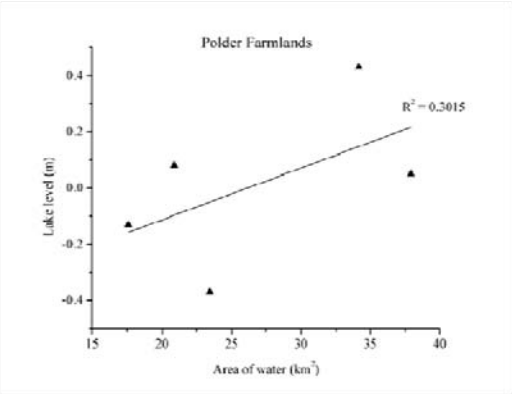

Fig. 5.13b

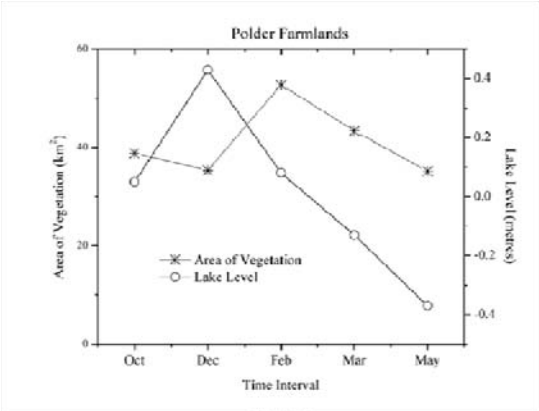

Fig.5.13c

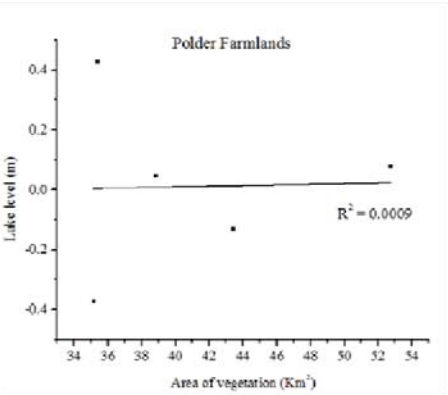

Fig. 5.13d

Fig. 5.13a – d: Relationships between estimated lake level and surface area of water and vegetation respectively on the Polder Farmlands

5.3.6 Southwestern Lake Shore Farms

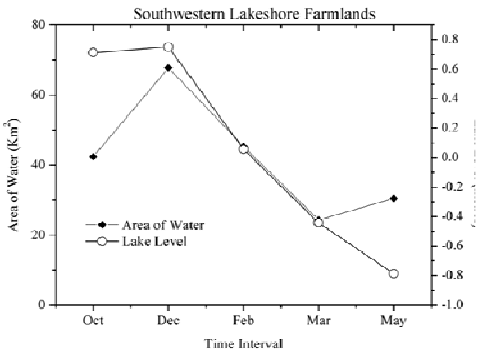

Fig.5.14a

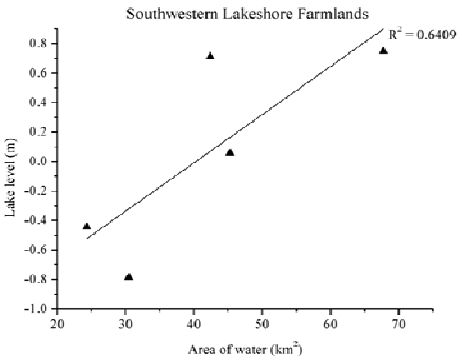

Fig.5.14b

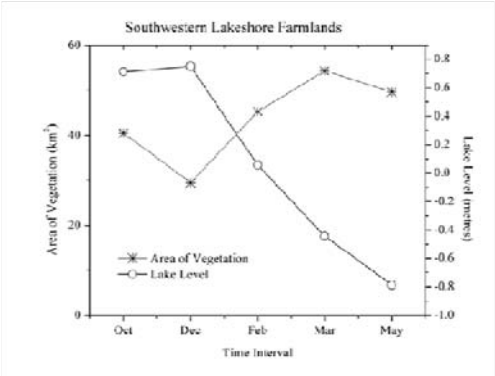

Fig. 5.14c

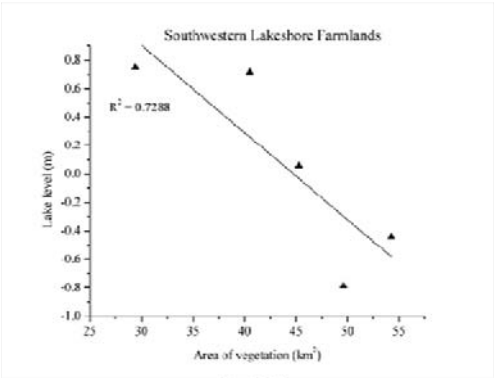

Fig. 5.14d

Fig. 5.14a – d: Relationships between estimated lake level and surface area of water and vegetation respectively on the Southwestern Lakeshore Farmlands.

5.4 DISCUSSIONS

5.4.1 Comparison between Areal Extent of Water and Altimeter Lake Level Data.

The relationship between variation in the level of the lake and variation in the surface area of water between October 2003 and May 2004 on MERIS images shows a moderately strong and positive correlation in the permanently Open Water Region (5.10a and b), the Southern Reed Islands (figures 5.211a and b), the Southeastern Reed Islands (figures 5.12a and b), and the Southwestern Lakeshore Farmlands (figures 5.14a and b). The coefficients of determination (R^2) for the permanently Open Water Region, the Southern Reed Islands, the Southeastern Reed Islands and the Southwestern Lakeshore farm were 0.7405, 0.8397**,** 0.6638 and 0.6409 respectively (table 5.6).

For the MERIS image dates, the altimeter levels showed a steady decrease between October 2003 and May 2004. For the area of water, a maximum extent occurred between October and December, in the Southeastern Reed Islands, the Southern Reed Islands and the Southwestern Lakeshore Farmlands. This was followed by a decrease between December and March and thereafter an increase between March and May. The decrease from December to March corresponded with the altimeter decline in lake level from December to March only.

The reason for the maximum areal extent of water between October and December in the Southeastern Reed Islands, the Southern Reed Islands and the Southwestern Lakeshore Farms was that the Southeastern Reed Islands and the Southern Reed Islands lie adjacent to

topographically very flat land (of which the Southwestern Lake shores form a part), and there are no dune elevations to cause obstruction to water flow. The hydraulic gradient of flow of underground water also favors the southwestern part of the lake (Isiohor et.al, 1990) because it is at a lower elevation than the Southeastern part of the lake. Thus, a variation of about 3 metres in the level of the lake can cause flood water to extend laterally from the shoreline by as much as 20 km (Isiorho et. al, 1993).

On the other hand, in the area of permanently open water (the Open Water Region), the fluctuations in the surface extent of water from one month to the next were negligible. The graph curve of areal extent of water versus lake level in the permanently open water region was approximately a straight line (figure 5.10a), showing that the areal extent of the open water did not fluctuate significantly from one month to the next. This is due to the sheltered condition of the permanently open water which is hedged in by reed and papyrus islands. Birkett, (2000) attributed the open water area's relatively large backscatter coefficient of 28 dB to its sheltered (by reeds and papyrus) state.

In the Southeastern Dune Islands (figures 5.9a and b), there was no definable relationship (r^2 = 0.0983) between the lake level and the area of water between October 2003 and May 2004. The areal extent of water between October and March in the interdune depressions of the Southeastern Dune Islands was also more or less constant (figure 5.9a).

On Polder Farmlands (figures 5.13a and b), the relationship between variation in lake level and area of water on the farms was very weak (r^2 = 0.3015) due to the fact that the interdunes on the Polder Farms are deliberately drained and farmed, therefore at some time the area of water will be replaced by crops. The fluctuation in areal extent of water was also more pronounced on interdune depressions of Polder Farms than in the interdune depressions of the Southeastern Dune Islands.

One common trend running through all the graphs was the increase in the area of water between March and May 2004. This is in contrast to the lake level which continued to decline between March and May. The reasons for the increase in area of water between March and May were explained earlier in chapter 4 as being due to a shallow water table caused by the large flood event which occurred in the 2003/2004 Lake Chad flooding season and a reduced evapotranspiration in March due to aquatic plant senescence. This plant senescence causes less water to be taken up by plants for evapotranspiration and therefore this keeps the water table from decreasing rapidly and increased rates of seepage to the surface results. Thus the

areal extent of the water maybe more influenced in some areas by the local ground water regime and the seasonal climatic conditions than the overall regional water levels.

In regions of the lake lying adjacent to, or close to the area of permanently open water where the areal extent of the water and lake level are positively correlated, the amount of water discharged in to the lake and the topography of the regions appear to influence the relationship between lake level and areal extent of water; the more flat the topography of the regions, the greater the spread of water by inundation when the lake level rises and flows overland. That is why there was a maximum areal spread of water in the Southern Reed Islands and the Southwestern Lakeshore Farmlands.

In the Southeastern Dune Islands and on Polder Farmlands where, the relationship between the areal extent of the water and lake level was not obvious the confining effects of the dunes on the water and the effects of cultural activities like farming influence the relationship. When draining the interdune depressions, the water in the polders is allowed to evaporate rather than be drained back into the lake. Seepage to the surface occurs which eventually contributes to the lowering of the lake level.

In general, the relationship between the areal extent of the water and lake level is controlled by factors such as the amount of precipitation, evapotranspiration, rate of seepage and the depth of the local water table. Dieleman and Ridder, (1963) showed that groundwater flowed from the lake through the dunes to polder areas. The ground water eventually seeped to the surface as seepage flow. However, the seepage flow varies from place to place because it is dependent on subsurface geological conditions, namely the thickness of a subsurface silt loam stratum which acts as a barrier to the flow of the water to the surface. Thus the potential of a polder for utilizing residual moisture for agricultural purposes depends on the rate of seepage to the surface. The faster the rate of seepage to the polder surface, the better the potential of the polder for cultivation. It also means that interdune depressions which have been drained through evaporation, for agricultural purposes and in which the rate of seepage to the surface is slow will likely remain dry due to high evaporation rates and slow seepage and therefore there will be no relationship between the level of lake and the areal extent of water in the polders since there will be no water to speak of. However if the polders are traditional polders i.e. having temporary earth (rather than concrete dams which are used to stop the lake water from entering the polder), then during the rainy or the flooding season, the temporary earth dam could be overwhelmed by rising water from the lake as it is not a

permanent structure and the polder concerned could become inundated. Therefore some sort of correlation between variation in lake level and areal extent could occur. On the other hand if it is a polder which has a concrete, then there will not be any correlation because the dams will effectively keep the rising lake water from entering the cultivated polder. However, if the subsurface strata of the polder with the concrete dam do not create resistance to seepage, then water will seep to the surface and depending on the level of the water table and time of year, there will be some correlation between the areal extent of the water and the lake level variations. Thus the relationship between the areal extent of water and the lake level variation is not so apparent when surface distributions alone are examined, as with the use of visible remote sensing images such as MERIS.

5.4.2 Comparison between Areal Extent of Vegetation and Altimeter Lake Level Data.

There was no definable relationship between the estimated lake level and areas of vegetation on MERIS images of the Southeastern Dune Islands (figures 5.9c and d) the Southern Reed Islands (figures 5.11c and d) and the Southeastern Reed Islands (figures 5.12c and d). The coefficients of correlation were -0.0027 and -0.052 and -0.0163 for the Southeastern Dune Islands, the Southern Reed Islands and the Southeastern Reed Islands respectively (table 5.6). The areas of vegetation in the three regions did not fluctuate as significantly as the drop in lake level and this shows that the area of vegetation in the three regions was more or less constant and supports the finding in section 5 that the area of swamp vegetation was found to be relatively constant over time.

There was no definable relation between estimated lake level and area of vegetation on the Polder Farmlands (figures 5.13c and d). The Coefficient of correlation (r^2) was 0.0009. This is because the timing of the cropping cycle at the polder farms is not dependent on the rise and fall of the level of the lake, in fact cultivation occurs in spite of the variations in the level of the lake because the polder farms are either irrigated or make use of residual moisture for plant growth and irrigated cultivation takes place seven months of the year from November to May and rainfed cultivation takes over afterwards. Therefore periods of crop maturation could coincide with periods of a fall or a rise in lake levels and the availability of irrigation water or residual moisture does not in part depend on lake level because where there is no sufficient water, wells are either dug and the water either pumped to the farms (seen during

field work), or the shadoof system of irrigation is employed method (Dieleman and Ridder, 1963).

On the other hand, there was a strong negative correlation between estimated lake level and areal extent of vegetation on the Southwestern Lakeshore Farmlands (r^2 = -0.7288, figures 5.14c and d). This was the result of a decrease in vegetation with increase in lake level between October and December (due to flooding of the cultivated areas) and an increase in areal extent of vegetation from December to March with a corresponding drop in lake level values between January and May due to planting as the flood recedes. As mentioned earlier, the topography of the Southwestern Lakeshore farms is flat and featureless, with the elevation ranging between 281m to 285m asl, and the hydraulic gradient of the lake (and therefore the groundwater flow) is inclined towards the southwestern lakeshore and the water table is shallower in this region. Thus lateral flooding occurs which coincides with the rise in lake level. When the flood recedes, this area is farmed and crop vegetation replaces the area of water. The crop vegetation matures in March and May when the lake level is at its lowest. Thus the timing of the cropping cycle at the Southwestern Lakeshore Farmlands is influenced by the rise and fall of the level of the lake hence a high correlation level. However the recessional farming itself, affects the type of relationship between estimated lake level and area of vegetation in the Southwestern Lakeshore Farms because if recessional farming were not practiced, the water would be replaced by swamp vegetation. Since there is no definable relationship between estimated lake level and area of swamp vegetation then no observable relationship will exist between lake level and areal extent of vegetation in the Southwestern Lakeshore Farmlands.

5.4.3 Using altimetry as early warning system for risk zones

Sarch and Birkett (2000) proposed the idea of using altimetry as an early warning system for areas of the lake which are subjected to inundation with the possible crop losses to the farmers. These areas were termed as risk zones. From the analysis of the relationship between lake levels measured from altimetry and areal extent of water and vegetation, it has been found that modern or government assisted polder farms in the Polder Farmland regions cannot be considered as risk zones because inundation is controlled by using dykes to control the flow of water into the interdune depressions. Likewise polder farms depend on residual moisture or irrigation for water needed by plants. Thus subsurface geology which controls

the rate of seepage to the surface and irrigation practices have a greater influence on crop growth and survival. On the other hand, traditional polder farms with temporary earth dams for controlling the flow of water are more prone to water spilling over the earth dams and inundating the farms. Therefore such farms can be considered as risk zone areas. An element of risk for all the polder farms is the potential build up of saline soil due to seepage and evaporation on the polder farms. Dieleman and Ridder (1963) however noted that this is not significant because the less saline water migrates to the surface as seepage.

The Southwestern Lakeshore Farmlands where seasonal inundation of cultivated land occurs are more likely to constitute risk zones. However, not all the inundated farmlands are risk zones. The farmlands which are furthest away from the lake experience flood retreat earlier than farmlands closer to the lake and are cultivated immediately the soil becomes well drained for cultivation. Therefore the risks associated with these farms are minimized since the crop maturation periods do not coincide with the period of flood inundation and land preparation and planting starts as soon as flood retreats and the soil becomes well drained (fieldwork observations). On the other hand, for the farmlands which are further into the lake shores initial planting starts as late as April when the first crops from some farm lands further away from the lake shore are becoming ready for harvesting. Therefore farmers who have a late start in cultivating their farms but have more than one cropping cycle per annum are more likely to experience crop loss either at the start of the rainy or flooding season. Therefore these farmlands constitute risk zones.

Temporary settlements which follow flood retreat such as those documented in Sarch and Birkett (2000) are also at risk of losing crops to flooding. Many of the temporary settlements are located on dune islands inside the lake. The response to fluctuations in the lake level since the 1970s, has been for fishermen to follow the lake (during low water level periods), establish temporary settlements on dune islands and switch to farming the exposed lake beds in the dry season period. Due to the uncertainties in the volume of water discharged into the lake by the Chari every year, some villages experience severe inundation (for example the 1981 to 1983 flooding seasons; the 1985/86, 1988/89 seasons and more recently 1997 to 1999 and 2003/04 flood seasons) while some years there are hardly any flooding over the whole lake basin for example in 1984/85 season. Thus villages are caught unawares and those dry season crops whose growing season is extended into and beyond the rainy season (as a result of the taking advantage of the rainy season) become liable to flooding before

harvesting, (Sarch and Birkett, 2000). Permanent settlements are also found on dune islands and they constitute risk zones for the same reasons as the temporary settlements. Some of these settlements are among those in which the average size of farmland plots were too small to be resolved by MERIS and therefore it was not possible to identify them based on separating farmland vegetation from non farmland vegetation (see chapter 4, section 4.4.3c). It can be concluded that factors such as location, type of settlement (permanent temporary, or dune island settlements) subsurface geology and farming practices are important in determining which areas are risk zones and a generalized relationship between lake level and area of water or vegetation cannot be made over the lake basin because these factors have to be taken into consideration when proposing the use of altimetry as an early warning system.

5.5 CONCLUSIONS

In regions of the southern lake basin where the topography is relatively flat and undulating and no dunes are present, an overall positive relationship was observed between the level of the lake and areal extent of water. These regions include the Southeastern Reed Islands, the Southern Reed Islands, and the Southwestern Lakeshore farms and the permanently open area of water. There was no definable relationship in the Southeastern Dune Islands and the Polder Farmlands because the confining effects of the dunes on the water and the effects of cultural activities like farming influence the relationship. Overall, the relationship between the areal extent of the water and lake level is controlled by factors such as the amount of precipitation, evapotranspiration, rate of seepage and the depth of the water table.

The relationship between lake level and areal extent of swamp vegetation in the areas of the southern lake basin was not definable because the area of swamp vegetation on the whole was found to be relatively constant over time. On the Polder Farms, the relationship was also not definable because the timing of the cropping cycle in the more intensively cultivated Polder Farms is not dependent on the rise and fall of the level of the lake. On the other hand the strongly negative relationship in the Southwestern Lakeshore farms showed that the timing of the cropping cycle is dependent on the rise and fall in level of the lake and this explains the practice of recessional farming in the area.

Factors such as location, type of settlement, subsurface geology and farming practices also have to be taken into account when considering the use of altimetry as an early warning

system in areas designated as risk zones, because these factors determine whether an area can be called a risk zone or not, and therefore this also indicates that a general relationship between altimetry and areal extent cannot be applied over the whole lake basin.

CHAPTER SIX

GENERAL CONCLUSIONS

6.1 VALIDATION OF MERIS USING ASTER

The Lake Chad Basin, as defined in Chapter 1, is a vast area of 25,000 km², although the current area of permanently open water is 1642 km². Due to cyclical as well as seasonal variations, the areal extent of surface water is in a state of constant change, as are the relationships between water, soil and vegetated land cover and the human activities which accompany these changes. This makes the Lake Chad Basin a region of high risk in terms of the economic activities carried out there, and authorities managing the region's resources require tools for monitoring and inventorying this large and remote region in order to respond to the changes. The types of resources which are of greatest interest include those involving cultivated and cultivable land.

The aim of this research was to use a multi sensor multi temporal approach to evaluate the potential of ENVISAT MERIS optical data as:

- A means of establishing a data base for Lake Chad farmland resources;
- A means of investigating the relationship between the variation in surface water level and lake areal extent using TOPEX/POSEIDON altimeter data.

The study has examined two methodologies, Spectral Mixture Analysis and Threshold Change Detection which use remote sensing for change monitoring and resource inventory over the Lake Chad Basin, and which take into account the region's overall size in relation to the relatively small size of land cover units. The advanced mapping technique of LSU was found to be more suitable than a traditional per pixel classifier and permits the use of the wide swath but low resolution sensor for monitoring the whole basin.

The suitability of ASTER as reference data for validating MERIS depended on several assumptions which were demonstrated for other sensors having higher spatial resolution than MERIS. These are firstly that fieldwork as well as land cover observations on IKONOS multi spectral images can be considered representative of the true ground situation. Secondly, that the validation of land cover mapping on ASTER using these 'ground truth' sources is good enough to permit ASTER to act as a substitute 'ground truth' for validating MERIS. In fact the overall accuracy achieved for validating ASTER with IKONOS data was 96% with a Kappa of 0.9505 so the assumption is upheld.

In validating MERIS with ASTER, a good agreement was obtained from the point pixel sampling between ASTER and MERIS (86.7% accuracy and Kappa coefficient of 0.806) due to the high degree of homogeneity of the land. Linear Spectral Unmixing was applied to land cover classification of MERIS data and validated by comparing the total area of MERIS LSU soil, vegetation and water fractions respectively with ASTER ML class areas of soil vegetation, and water. A good agreement between corresponding classes, with a correlation coefficient of 0.96 was obtained. The high accuracy level was very likely due to the simpler and more spectrally distinctive land cover types in the study area comprising the basic classes of vegetation, soil and water. Additionally, the spatial distribution of the three dominant land cover types, soil, vegetation and water over an annual cycle was the most obvious and readily identifiable indicator of resource availability. Thus the three endmembers used for the study, provided the basis for a viable methodology for resource inventory over the whole lake basin using MERIS. Overall, the results mean that using SMA with a combination of MERIS and ASTER data for monitoring and inventorying Lake Chad resources, is a simple and cost effective way in terms of money and time for adapting a technology in regions of the world where it has not gained a firm foothold.

6.2 LAND COVER MONITORING FROM MERIS

Using MERIS, patterns of change which indicated differences between croplands and natural vegetation were identified. For example, the study showed that over time, fluctuation in the area of swamp vegetation was small when compared to crop vegetation, which exhibited significant seasonal fluctuations. It also showed that the maximum area of swamp vegetation occurred immediately after flood retreat. This was not observed for crops because a delay period occurs between the flood retreat and optimal crop growth in which time the soil becomes well drained to support cultivation.

Differences were also found in cultivation practices in the Polder Farmlands and the Southwestern Lakeshore Farmlands and this leads to the conclusion that identification of farmlands using multi temporal MERIS should use different identification criteria in different parts of the lake basin. Furthermore, when identifying croplands over the whole lake basin, it was concluded that spatial location, the arrangement of features in physical

space and seasonality were important for understanding and interpreting the change detection patterns derived from the MERIS images.

6.3 WATER LEVEL RELATIONSHIPS FROM ALTIMETRY.

One of the major objectives of this study was to investigate if there was a predictable relationship between altimetric heights of the water surface and the areal extent of water bodies in the lake basin identified by MERIS. Such a theory seems reasonable given that the study is an extremely shallow lake basin so that small changes in water depth would be expected to produce large changes in the extent of surface water. However it was found that the overall relationship between the respective areal extents of water and vegetation and lake level are not so apparent when surface distributions alone are examined because the relationship is controlled by factors invisible on satellite images, such as topography, landforms, precipitation, evapotranspiration, rate of seepage, depth to water table and the cultural farming practices. Different regions of the lake basin exhibited different relationships based on the prevalence of one or more of the above factors. The regions of the lake, which have a flat topography showed a positive relationship between lake level and areal extent of water. There was no definable relationship between swamp vegetation and lake level because the area of swamp vegetation remained relatively constant over time. With cultivated vegetation however, the relationship in the Southwestern Lakeshore Farmlands suggested that the timing of farming activities were dependent on the rise and fall in lake level.

The dune islands of the southeastern part of the lake basin and the Polder Farmlands associated with the interdune depressions also showed no definable relationship between lake level and areal extent of water. For the dunes islands this was partly because of relief and the steep slopes restrict the horizontal spread of water. For the Polder Farmlands, it was due to the local ground water regime and the seasonal climatic conditions than the regional water levels. Farming practices on the Polder Farmlands were independent of the rise and fall in lake level and therefore only a weak relationship was exhibited between lake level and vegetation extent.

Increase in the areal extent of water, over the lake basin in May was observed to occur and this was not reflected by the altimeter lake level values which show a constant decline in the dry season months. This increase in water is probably due to the presence of a

shallow water table as a result of the unusually heavy flooding season of 2003/2004, but it is also probably not a temporary phenomenon since it has been commented upon by Dieleman and Ridder (1963).

6.4 ALTIMETRY OVER LAKE CHAD BASIN

As Lake Chad is a shallow lake with mean depths of about 4m (Carmouze and Lemoalle, 1983), a rise in the lake level translates to floods and areal expansion of water which can be quantified from satellite imagery. The water level relationships from altimetry discussed previously have shown that a predictable relationship between lake level and area of water or vegetation on the lake basin can be shown for certain areas of the lake (e.g. the Southwestern Lakeshore Farmlands) and not for others (e.g. the Southeastern Dune Islands). Thus due to factors related to the basin's complexities, an overall relationship between the lake level and area of water (or vegetation) over the whole lake is only a generalization and cannot be applied over the whole lake basin as was done by Birkett (2000). Therefore only discrete regions in the basin show a useful and predictable relationship between altimeter data and the areal extents of water or vegetation. These relationships are not predictable for the whole basin.

The long term drying out of Lake Chad makes altimetry a less viable option as a tool for an early warning system because at present only the area of permanently open water is available for the altimeter to acquire an instant "lock" on the surface and therefore record data with a high degree of precision. If this area of permanently open water does not contract, then it will be possible to continue monitoring the lake using this small area of water but even then, this data will only be relevant in the southern lake basin. However if it dries out then getting good data in other parts of the lake, will not be possible due to the complexity of the terrain and because the presence of (swamp) vegetation attenuates backscatter signals.

The amount of water entering the lake every season is dependent on how much water is discharged by the Chari and this determines the magnitude and extent of flooding. As mentioned in chapter 2, Africa and Lemoalle (1996) showed that the flow of water towards the northern lake basin was a function of the annual river discharge of the Chari. They established that inflow from the Chari of less than 15km^3/yr meant that no flow of water reached the northern basin. An inflow of about 18 km^3/yr meant that flooding was

possible up to the town of Bosso in the Northern Reed Islands (figure 1.3 section 1 chapter 1) while an inflow of 28km^3/yr meant that the whole lake was flooded. Therefore in order for altimetry to be effective as an early warning system, these critical lake levels must first be ascertained from a correlation between an altimeter reference frame and a river stage reference frame that are indicative of flood severity.

6.5 RISK ZONES

The concept of the risk zone used in this study refers to the area of cultivable land which is subjected to inundation with a high risk of crop loss to the farmers, thus leading to farming in uncertain conditions. Modern or government assisted polder farms in the Polder Farmland regions are not risk zones under this concept because the use of dykes prevents seasonal inundation of the interdune depressions and thus the movement of water is effectively controlled. Polder farming also depends on residual moisture and seepage flow to the surface. Furthermore, the subsurface geology controls the rate of seepage to the surface and therefore has a greater influence on crop growth and survival. Water seepage in traditional polder farms also comes under the influence of subsurface geology. However the temporary earth dams used for controlling the flow of water are not as effective as the concrete earth dams used on modern polder farms. Thus they are more prone to seasonal flooding since water can overwhelm the earth dams and inundate the farms. As such, these farms can be considered as risk zone areas.

In the Southwestern Lakeshore Farms where seasonal inundation of cultivated land occurs, not all the inundated farmlands constitute a risk zone. The permanently settled farming communities of the Southwestern Lakeshore Farmlands, which live with the annual flood inundation minimize the risk of crop loss by planting so that the crop maturation periods of March to May do not coincide with the period of flood inundation from November to January and land preparation and planting starts as soon as flood retreats and the soil becomes well drained (fieldwork observations).

On the other hand, temporary settlements which follow flood retreat such as those documented in Sarch and Birkett (2000) are those that are at risk of losing crops to flooding. Some of these settlements are among those in which the average size of farmland plots were too small to be resolved by MERIS and therefore it was not possible to identify them based on separating farmland vegetation from non farmland vegetation.

Nevertheless it can be concluded that location and type of settlement are important in determining which areas are risk zones. Farmlands which are prone to inundation but are located near the present shoreline in permanently settled areas are not likely to be risk zones because farmers will minimize the risk of crop losses by choosing the times of harvesting that will not coincide with flood inundation. However, farmlands which are on dune islands where many of the temporary settlements are located are liable to crop loss due to uncertainties in the volume of discharge from the Chari that will determine the severity of flooding for the year.

Thus factors such as location, type of settlement, subsurface geology and farming practices have to be taken into account when considering the use of altimetry as an early warning system in areas designated as risk zones, because these factors determine whether an area can be called a risk zone or not, and therefore this also indicates that a general relationship between altimetry and areal extent cannot be applied over the whole lake basin.

6.6 POTENTIAL OF MERIS FOR ESTABLISHING A LAKE CHAD FARMLAND RESOURCES DATABASE

The ENVISAT/MERIS multispectral sensor was shown to be suitable for its wide swath width (which makes it cost effective). The high radiometric qualities i.e. 12 bit quantization and a radiometric error of less than 2% of detected signal (Curran and Steele, 2005) allow the sensor to give acceptable results when the spectrally demanding technique of LSU is applied. The study shows that MERIS is able to establish seasonal patterns of land cover changes which occur over the whole lake basin, and which are associated with specific human activities, in known areas of farmlands. This information is now available from this study and was not available previously, as most descriptive literature on the Lake Chad was written before water levels fell to their current low extent and heights and recent literature covers only specific regions of the lake, namely those which are more accessible and densely settled.

In addressing land cover change over the whole lake using remote sensing, the study has demonstrated a methodology for identifying areas which are cultivated, based on spectral unmixing of MERIS images. Such areas involve changes from water to increasing proportions of bare soil, often with increasing low vegetation fractions representing some

grass cover (as opposed to the more dense vegetation of cropland) marking a transition from inundated land to cultivated land as was observed in the Southwestern Lakeshore farmlands (figure 6.1 Southwestern Lakeshore Farmlands black ellipses encircle farmlands and magnified farmlands) . Furthermore in the study, a change map composite was generated from MERIS LSU (refer to figure 4.48 section 4.4 chapter 4) showing the movement of water across the lake between October 2003 and March 2004. The usefulness of such maps is that with MERIS images at the higher temporal resolutions of 2-3 days the rate of flow of water can be estimated.

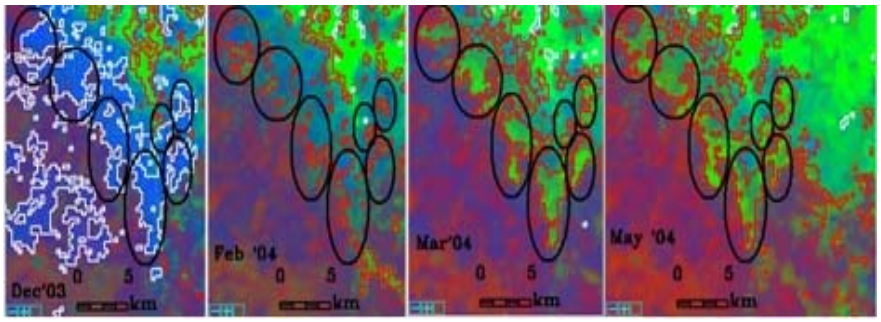

Fig. 6.1: Transitional change from inundation to vegetation between December 2003 and May 2004 on the Southwestern Lakeshore Farmlands

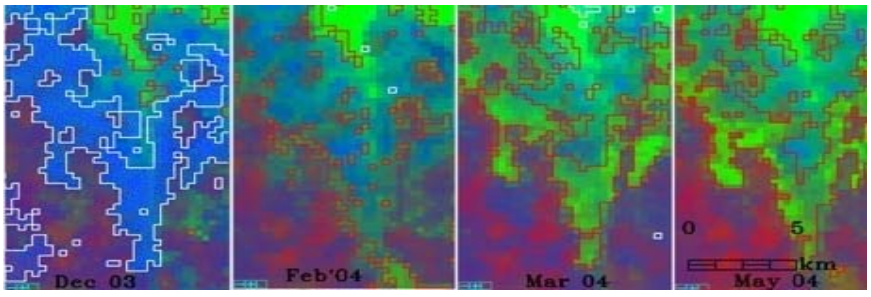

Fig. 6.2: Magnified images of transitional change from inundation to vegetation between December 2003 and May 2004 on the Southwestern Lakeshore Farmlands

The rate of water movement has already been estimated at 1.8 km/day using METEOSAT data (Africa and Lemoalle, 1996). But the 2.5 km spatial resolution of METEOSAT in the VIR channel makes the estimate a very general one and MERIS data offers more advantages with better spatial, spectral and radiometric resolutions. Even so, the relative coarseness of MERIS spatial resolution makes it necessary to obtain in situ data through fieldwork and/or, higher resolution imagery in order to identify and establish changes which occur in areas that are difficult to interprete at the edges of the dune islands.

6.7 RECOMMENDATIONS.

The wide swath width and 3 day revisit period of MERIS makes it a cost effective tool in monitoring and inventorying data for establishing a resource data base especially for remote and inaccessible regions like the Lake Chad. High temporal resolution images are needed during the flooding and harvest periods in order to get detailed information on the flood and also to differentiate areas of crop from non crop vegetation. The coarse spatial resolution of MERIS means that auxiliary data and apriori information for the regions to be investigated will always be required.

The amount of water entering the lake every season is dependent on how much water is discharged by the Chari and this decides the magnitude and extent of flooding. Therefore in order for altimetry to be effective as an early warning system, it is important to generate flood forecasts early in the season which can be generalized over the whole lake. This can be done by determining threshold lake levels from a correlation between an altimeter reference frame and a Chari River stage reference frame located upstream of the lake. This can then indicate different categories of flood severity depending on the volume of water discharged by the Chari River It is also important to recognize a phase lag between the time water passes over the stage reference and the time it enters the lake so that flood forecasts are issued in time for stakeholders to take mitigating measures.

On the whole, the study has shown that using SMA and change detection on MERIS data can provide a cost effective way for monitoring large regions such as the Lake Chad basin as well as a methodology which is simple and easy to adopt in areas where acquiring state of the art technology can be prohibitively expensive.

APPENDIX A

A1 FIELD OBSERVATIONS IN NIGERIA

Field observations were conducted between Dec 2003 and July 2004 Field work consisted of land use /land cover observations. The areas visited included the clay plain, the sand ridges and the swamps inside Lake Chad. GPS points and land use / land cover characteristics were recorded. A canoe trip was taken inside the lake and at various places GPS points were taken in order to fix the positions of the edge of the lake in March. The field observations were repeated in May and July.

The whole of the study area is characterized by lacustrine sediments. However from figure A1.1, it can be seen that the area can be subdivided into three land forms.

- Dark lagoonal clay plains called Firki. These are approximately 12 km wide at the narrowest extent
- A sand ridge about 30 km long
- Lake Chad covered by permanent swamp vegetation.

The general arrangement of landuse land cover along the transect routes encountered were settlements found on the sandy soils which are at a slightly higher altitude than the surrounding clay soil areas. On ASTER images a combination of shade trees and the bare soil characterized settlements which appeared as pink patches on the back ground of sandy or sandy loam soils. The soil changes from very sandy in the villages to bare grey black sandy clay loam away from the villages. The landscape is made up of scattered shrubs with predominantly scattered *Calotropis procera* in some places and in others dense concentrations of the plant. Thorn bushes were found sporadically. These plants are mainly responsible for the pinkish appearance of some sandy areas on ASTER images. In some places by the roadside, the vegetation had been burnt. Sometimes, dried *Ipomea* bushes were encountered. Areas where the *Ipomea* were found, were evidence of the presence of flooding at sometime in the past.

The village nearest the lake which is also located on sandy ground was as about two kilometers distance from the lake. During the flood, the village is cut off from the surrounding hinterland region by water. Near the lake, the land cover is farmlands and water logged grassland. All farmlands are located outside the settlement areas and usually on the exposed clay sediments. The soils nearer the intake canal retain more moisture all year and support more annuals therefore cultivation occurs on these soils, while further away inland, perennial vegetation dominates, therefore only rainfed cultivation occurs on the upland sandy loam soils.

A1.1 **Land use Land cover.**

A land use land cover map of the area was drawn from the ASTER RGB image of April 2004 (figure A1.2). The following is an explanation of the various landscapes encountered.

A1.1.1 **A: Region of open water with swamp vegetation**

This is the area of permanent swamp vegetation fringing the lake shore and extending out into regions of open brackish water (plate A1.1). The vegetation consists of floating grass vegetation like *Echinocloa*, *Ipomoea aquatica* and water lily *Nymphaea*. Swamp vegetation include Hippo grass, *(Voscia cuspidate)*, papyrus *Cyperus papyrus.* The Hippo grass and papyrus line the banks of the water intake

canal and where the canal extends into the lake, the hippo grass has completely blocked water flow in the canal and caused overflowing onto surrounding farmlands. This was also observed in Nbulwa in July 2004. *Ipomoea* can grow into a full shrub and can survive on residual moisture. In many relatively dry land areas, its presence is an indicator that the land is liable to inundation. Dune islands were encountered some of which are settled by farmers and fishermen.

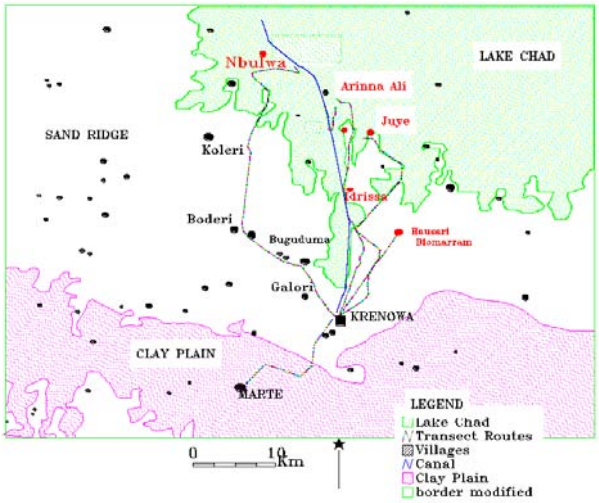

Figure A1.1: Three dominant land cover types (swamp vegetatation, sand ridge and clay plain) in the Lake Chad Basin

A1.1.2 **B: Exposed clay sediments.**

The landscape (plate A1.2) is made up of exposed clay sediments (Thiemeyer, 2000) in a predominantly sandy region. The land is very flat with a gradient of (0.000125) (Isiorho, et.al, 1996). Annual flooding of the area contributes to sustaining agricultural activities in the vicinity of the canal and the appearance of a perennially moist clayey region on the satellite image. Towards the extreme southwestern end of the lake is a river flood plain and the clays become an extension of the dark Firki clay plains.

Plate A1.1: Vegetation types found in the Lake Chad swamps

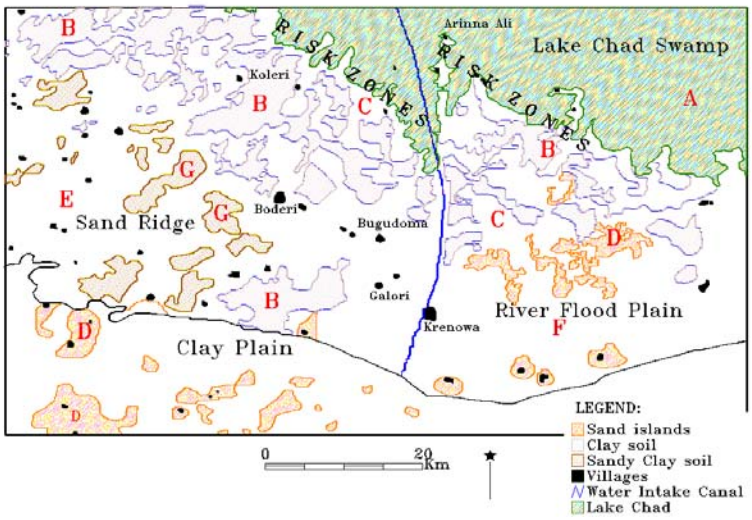

Figure A1.2: Land Use Land Cover Map (Source: drawn from April 2004 ASTER RGB**)**

Plate A1.2 Clay soil on farmlands

A1.1.3 **C: Dry sandy loam soils.**

This is a region of drier sand clay soils. Most settlements and motorable tracks are found on this type of land (plate A1.3). The dominant vegetation is the shrub *Calotropis procera*, although there are thorn trees like *A. raddiana, Z. mauritania* as well and other types of shrubs. *C. procera* is ubiquitous and its presence is a sign of a disturbed environment such as the outskirts of villages. Around the settlements shade trees like *A. indica* were observed.

Plate A1.3: Dry Sandy Clay Loam soils

A1.1.4 **D: Sandy alluvial soil on clay plain and river flood plain.**

In the areas around the river flood plain in the extreme southwestern part of the lake and also on the black clay plains to the south of the lake, there are protrusions of sandy alluvial soil islands on the clay

plains. On the satellite image, these areas appear bright against the background of the dark clay soils. These sandy soils are exposed tops of buried dune fields (Thiemeyer 2000).

A1.1.5 **E: Beach sand ridge.**

This is an area of predominantly sedimentary sandy soil that is part of the sand ridge, a relic of the former shoreline of Lake Chad (Thiemeyer 2000). It is sandwiched between the dark clay plains and the swamp filled lake. Sahelian woodland vegetation is found in this region. However, the vegetation is visible only as tiny red dots that gives the sand ridge a very faint pink tinge. Many settlements are located on the sand ridge.

A1.1.6 **F: Flood Plain**

This is the flood plain of river Yedseram which is a former tributary of the Lake.

A1.1.7 **G: Redistributed Aeolian sediments**

The landscape is made up of aeolian redistributed sediments which have given rise to barchan dunes. It is also transitional because sections of the dark lagoonal clays protude into the sand ridge from the south.

A1.1.8 **Black Clay Plain**

The Firki plains (plate A1.4) are characterized by soils of very high clay mineral content. This area is not flooded at all and any water reaching the soil is seasonal rainfall. The area is also characterized by a series of irrigation channels that have become obsolete due to the shrinking of lake Chad. The land is also featureless in terms of relief. The average gradient is 1:5000 (Wickens, 1974).

A1.1.9 **Water Intake Canal**

The Krenowa canal (plate A1.5) was constructed in order to channel water from the lake for irrigation purposes. It is about 32 km long from Krenowa to where it ends in an open water area of the lake. Its banks are choked with hippo grass and papyrus reeds. On both sides of the canal there are farmlands and settlements. The farmlands constitute part of the risk zone.

Plate A1.4: The dark clay plain landscape and associated soil

Plate A1.5: The water intake canal and the farmlands on both sides of the canal

A1.2 **Risk Zone Village**

Nbulwa is a sand dune island (plate A1.6) about 0.71 km^2 in size with an elevation of about 287 m asl. The surrounding area is at a lower elevation (about 284 m asl) which gets immersed in water during the flooding season between December and March. When the water evaporates and recedes, the surrounding area is farmed. The total area of farmlands surrounding the island was approximately 31. 65 km^2.

In January, the land water interface of the island is planted with beans. In July when the water had evaporated, the surrounding farmlands were found to be intensively cultivated with maize. Farmlands near the water intake canal were also flooded because the canal was choked with papyrus and bulrushes which caused overland flooding.

The soil of the island is sandy clay loam, however at the edge of the dune island, the soil had a higher clay content.

Plate A1.6: Dune island settlement seen from high resolution 5th May 2000, IKONOS RGB and the actual settlement

A1.3 **The Cropping Calendar**

The major crops cultivated are beans and maize. There are three periods in which land is cultivated every year. These are in December April and June. The first series of plantings start in December. Both maize and cowpeas are planted and it takes about four months to harvest a bean crop depending on the variety. Maize takes three months to mature therefore harvesting takes place in April and simultaneously, the second phase of the planting gets underway in which cowpeas and maize are planted again. Harvesting occurs in June and the third phase of planting commences with maize being the main crop of the third cycle.

These are general guidelines for the cropping calendar because there are no hard and fast rules. Not every farmer plants at the same time of month. Farmers migrate towards the lake as the water retreats. Thus the start of any preparation and cultivation depends on the time that the soil is drained enough to support crops. Therefore some farmers plant at an earlier time than others. Farmers who start later are liable to suffer crop losses in the event of flooding because their crops stay longer in the field. As maize is planted all year round, it is always subject to loss before harvesting.

A2.0 ASSESSING THE SUITABILITY OF ASTER AS REFERENCE DATA FOR VALIDATING MERIS

An IKONOS image (figure A2.1) was acquired on 12th May 2000, at 9:25 AM, GMT. It covers an area of 11 km by 11 km and has a centre latitude of 12.6°N and 13.96°E. The scene covered was of the southwestern lake shore located in Nigeria, West Africa. It consists of the farmlands located along an

water intake canal. The difference in time between IKONOS and ASTER was four years. However, the land use land cover changes in the Lake Chad have remained relatively stable in the past 20 years, due to the overall low population of around 38 persons/km^2 (National Population Commission, 1991) of the region i.e. Marte Local Government, where the field work was under taken. The population density which would have resulted in changes in the land use and land cover has not increased significantly, as the projected economic benefits to the region have not materialized due to the failure of the large scale irrigation projects such as the South Chad Irrigation Project (Odada et.al, 2003) that were implemented in the 70s. Therefore the landuse, land cover features found in ASTER and IKONOS images were the same (figures A2.2a and b). Thus IKONOS was used as additional supplement to field observations.

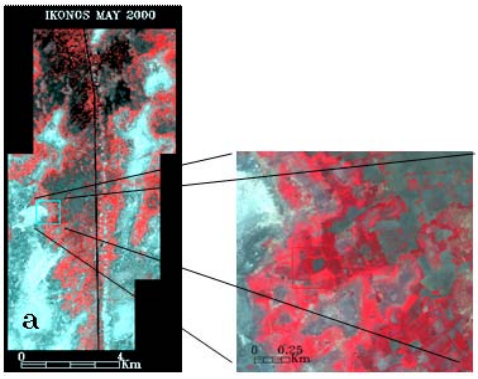

Fig. A2.1: IKONOS RGB and closeup of sites visited during field observations.

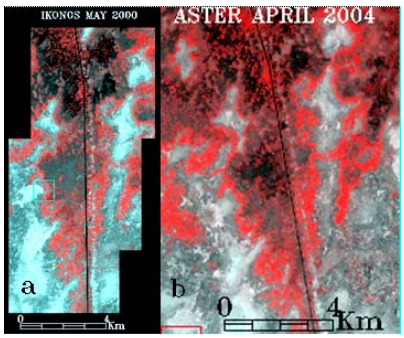

Figure A2.2: a) May 2000 IKONOS RGB; b) April 2004 ASTER RGB of the same scene; ASTER RGB of the same scene, all showing farmlands.

A3.0 VALIDATION OF MERIS USING ASTER

A3.1 Supervised Classification of ASTER and MERIS Data

Training areas of seven classes for ASTER dataset 1 and seven classes for ASTER dataset 2 were digitized and used in the Maximum Likelihood Classification. Five classes were digitized for ASTER dataset 3. The seven classes were swamp vegetation, sandy soil, clay soil, sandy clay soil, water, crop vegetation and vegetated sandy soil. The five classes of Firki Plains were clay, sandy clay loam, water, crop vegetation and vegetated sandy soil. The number of training classes differed because the datasets 1 and 2 were scenes of areas inside the lake while dataset 3 was a scene of an area located in the clay plains, therefore class of swamp vegetation and sandy soils were not found on the dataset 3. Confusion matrix tables were generated using ROIs obtained from the images. The ROIs used for assessing the accuracy of the resulting classes in the supervised classifications, were generated from the ASTER images. They were derived on the basis of identified land use /land cover from the IKONOS image and field observations. Therefore using ROIs obtained from the images as input for generating confusion matrix tables was considered acceptable.

Scenes on MERIS data representing the same ground area as the scenes on the ASTER images, were extracted as MERIS subset data 1, 2 and 3. Training regions based on fieldwork were identified on

corresponding MERIS subset data. The same training regions were digitized on MERIS and used for the Maximum Likelihood Classification. Similar to ASTER, seven classes were identified on the MERIS subsets 1 and 2 and five classes were identified on MERIS subset (figures A3.1 and A3.2).

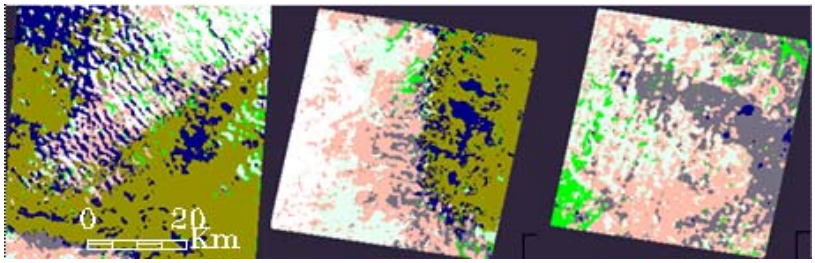

Fig A3.1: Maximum Likelihood Classified ASTER datasets 1 to 3

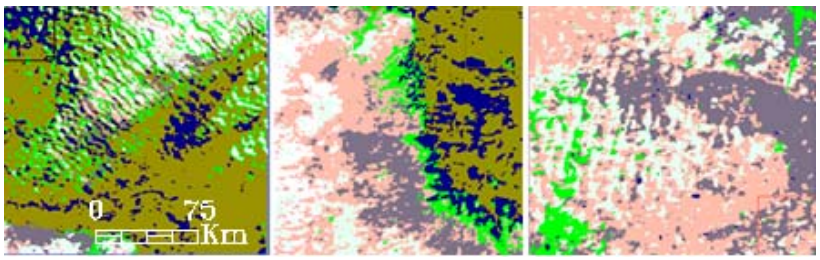

Fig: A3.2: Maximum Likelihood Classified MERIS subset data 1 to 3

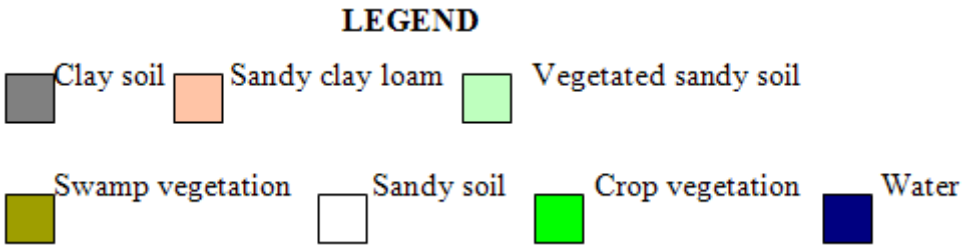

A3.2 **Confusion Matrix Tables for ASTER Maximum Likelihood Classification**

Table A3.1: Confusion Matrix tables for classified ASTER Dataset 1 : Grand Barrier Region

	Swamp	Sand	Clay	SCL	Water	Crop	VSS	Total
Swamp	747	0	0	0	14	41	0	802
Sand	0	944	0	29	0	0	0	973
Clay	0	0	444	0	7	0	0	451
SCL	0	0	46	156	0	0	3	205
Water	38	0	0	0	1373	0	0	1411
Crop	0	0	0	0	0	143	0	143
VSS	0	0	0	0	0	0	515	515
Total	785	944	490	185	1394	184	518	4500

ASTER Grand Barrier Overall Accuracy = 96.44%; Kappa Coefficient = 0.9505
(SCL = Sandy Clay Loam; VSS = Vegetated Sandy Soil)

Table A3.2: CONFUSION MATRIX Classified ASTER Dataset 2: Lake Swamp

	Swamp	Sand	clay	SCL	water	Crop	VSS	Total
Swamp	1489	0	1	0	83	10	0	1583
Sand	0	1304	8	45	0	10	24	1391
Clay	0	8	1201	25	0	13	11	1258
SCL	0	0	30	856	0	19	37	942
water	42	0	0	0	925	0	0	967
Crop	16	3	8	0	0	244	0	271
VSS	0	19	24	13	0	6	2844	2906
Total	1547	1334	1272	939	1008	302	2916	9318

ASTER Lake Swamp Overall Accuracy: (8863/9318) = 95.12%.; Kappa Coefficient = 0.939
(SCL = Sandy Clay Loam; VSS = Vegetated Sandy Soil

Table A3.3: CONFUSION MATRIX Classified ASTER Dataset 3: Clay Plain

	Clay	SCL	Water	Veg[1]	VSS	Total
Clay	1491	51	4	0	146	1692
SCL	23	879	0	0	26	928
Water	116	0	746	55	0	917
Veg[1]	1	19	9	2125	91	2245
VSS	0	49	0	0	4211	4260
Total	1631	998	759	2180	4474	10042

Aster Firki Clay Plain: Overall Accuracy = (9452/10042) 94.125% ; Kappa Coefficient = 0.9183
(SCL = Sandy Clay Loam; VSS = Vegetated Sandy Soil)

A3.3 **Validating MERIS with ASTER using Pixel Point Sampling**

In order to assess the agreement between information derived from ASTER and MERIS, pixel point sampling was performed on each of the MERIS subset data. Pixel point sampling is a technique whereby a correspondence is established between classification provided by the thematic map at a point and the reference classification associated with the same point location on the earth (Stehman and Czaplewski, 1998). Point sampling units are usually selected from an area frame and probability sampling concepts are applied to the point sampling such as random and stratified random and systematic sampling.

The three ASTER images were used as reference data. Initially, the **unclassified** subsets of MERIS were saved as separate files and for each file. To resample the MERIS pixel size from 300m to 15m, an image to image registration was performed using ASTER which corresponded to the MERIS subset as the base or master image, and the MERIS subset as the warp image. The images were resampled using nearest neighbor algorithm. Twenty four, twenty eight and thirty one ground control points were used for MERIS datasets 1, 2 and 3 respectively. The RMS errors associated with the coregistration of the MERIS dataset 1, 2, and 3, were 0.4026, 0.2538 and 0.3934 respectively i.e. half a pixel for all three datasets. Next, image to image coregistration was performed again, on the **classified** subsets of the MERIS data. This was done by simply applying the saved ground control points obtained from the first

[1] Vegetation in this classification means all vegetation occurring on land and not necessarily crops only.

co-registration between the unclassified MERIS data and the ASTER data, on the classified images and resampling them.

A3.3.1 **Sample Size**

A sample size *n* was determined at a 95% confidence level and an error tolerance within 1% of the total number of pixels in the sampling frame using the following formula (Biging et. al.,1999):

$$n = \frac{t^2 pq}{\delta^2}$$

where *n* is the sample size;

t^2 is the $1-\alpha/2$ quantile of the standard normal distribution at a certain confidence level.

p is the estimated proportion of correctly classified pixels

q is the estimated proportion of incorrectly classified pixels $(1-p)$

δ is the error tolerance.

α is equal to 0.05 at 95% confidence level

The total number of pixels in the whole classified MERIS dataset was taken as the population from which the sampling frame was drawn; the number of pixels in the classified subset MERIS dataset (MERIS datasets 1, 2 and 3) were taken as the sampling frames.

p was calculated as

$$\frac{number\ of\ \ pixels\ in\ classified\ \ subset\ MERIS\ dataset}{total\ number\ of\ \ pixels\ in\ classofoed\ whole\ scene\ of\ \ MERIS\ dataset.}$$

The sample size used for each dataset was 2000 pixels. This was done to account for any pixel that would have to be discarded due to being out of range.Two sets of 2000 random numbers were generated. One random number from one set was paired with another random number from the other set to obtain a paired set of 2000 random numbers. The random numbers were used as the x, and y, coordinates (cells and lines) to locate the position of a pixel on both the ASTER reference data sets and the corresponding subset MERIS data sets.

APPENDIX B

TABLE B1: MEAN 10 DAY TOPEX POSEIDON ALTIMETER DATA AND RIVER VOLUME DISCHARGE (m^3/s)

Dates	No of Days	Lake Level m	River discharge (m3/s)	Dates	No of Days	Lake Level m	River discharge (m3/s)	Dates	No of Days	Lake Level m	River discharge (m3/s)	Dates	No of Days	Lake Level m	River discharge (m3/s)
5/7/98	1	-0.51	28.9	8/15/99	466	-0.15	1010	5/1/00	726	-0.89	47.80	12/25/00	964	0.71	550
5/17/98	11	-0.44	24.3	8/17/99	468	-0.15	1050	5/11/00	736	-0.59	49	1/4/01	974	0.56	432
6/6/98	31	-0.7	63.8	8/27/99	478	0.21	1300	5/14/00	739	-0.69	54	1/13/01	983	0.3	366
6/16/98	41	-0.48	162	9/6/99	488	0.08	1500	5/20/00	745	-0.68	52	1/23/01	993	0.32	314
6/26/98	51	-0.69	225	9/16/99	498	0.38	1630	5/30/00	755	-0.63	89	1/25/01	995	0.42	305
7/5/98	60	-0.54	220	9/26/99	508	0.18	1760	5/31/00	756	0.02	93	2/2/01	1003	0.23	274
7/15/98	70	-0.54	247	10/5/99	517	0.2	1910	6/9/00	765	-0.96	89	2/12/01	1013	-0.11	234
7/25/98	80	-0.39	368	10/15/99	527	0.84	1990	6/19/00	775	-0.96	135	2/22/01	1023	-0.23	194
8/14/98	100	-0.28	1000	10/25/99	537	0.55	2010	6/29/00	785	-0.79	197	3/4/01	1033	-0.41	162.00
9/3/98	120	0.16	1830	11/14/99	557	0.48	1410	7/9/00	795	-0.89	259	3/14/01	1043	-0.4	134
9/13/98	130	0.5	2250	11/26/99	569	-0.37	807	7/19/00	805	-0.9	421	3/24/01	1053	-0.61	105
9/23/98	140	0.33	2820	12/4/99	577	0.32	587	7/29/00	815	-0.54	595	4/3/01	1063	-0.84	86.3
10/3/98	150	0.91	3080	12/14/99	587	0.26	438	8/8/00	825	-0.41	794	4/13/01	1073	-0.09	81.3
10/13/98	160	0.85	3180	12/24/99	597	0.54	362	8/18/00	835	-0.18	1050	4/20/01	1080	-0.1	77.5
11/1/98	179	1.14	3290	12/30/99	603	0.43	321	8/28/00	845	0.15	1650	4/30/01	1090	-0.01	71.1
11/11/98	189	1.2	3250	1/3/00	607	0.48	295	9/7/00	855	0.25	2390	5/17/01	1107	-0.35	69.8
11/21/98	199	1.31	3000	1/13/00	617	0.4	251	9/16/00	864	0.51	2580	6/20/01	1141	-0.33	107
12/1/98	209	1.04	2230	2/1/00	636	0.04	174	9/26/00	874	0.67	2640	7/8/01	1159	-0.49	174
12/11/98	219	0.88	1330	2/2/00	637	0.27	171	9/28/00	876	1.07	2660	7/25/01	1176	-0.49	408
12/21/98	229	0.92	885.00	2/11/00	646	0.11	148	10/6/00	884	0.94	2850	8/28/01	1210	-1.24	949
12/31/98	239	0.75	682.00	2/19/00	654	0.39	128	10/16/00	894	0.7	2980				
5/10/99	369	-0.17	106.00	2/21/00	656	0.1	124	10/26/00	904	0.55	2950				
5/20/99	379	-0.13	107.00	3/12/00	676	-0.35	84.5	11/5/00	914	0.47	2760				
5/22/99	381	0.32	109.00	3/22/00	686	-0.31	70.80	11/15/00	924	0.65	2290				
5/30/99	389	-0.52	106.00	3/24/00	688	-0.4	67.80	11/18/00	927	1.31	2100				
6/8/99	398	-0.53	136.00	4/1/00	696	-0.46	67.60	11/25/00	934	0.7	1670				
6/18/99	408	-0.69	142.00	4/10/00	705	-1.14	57.20	12/5/00	944	0.62	1060				
6/28/99	418	-0.16	207.00	4/11/00	706	-0.76	56.30	12/15/00	954	0.61	732				
8/1/99	452	-0.51	605.00	4/21/00	716	-0.42	53.40	12/22/00	961	0.86	592				

TABLE B2: MEAN 10 DAY TOPEX POSEIDON ALTIMETER DATA AND HYDROM LAKE HEIGHT LEVEL DATA

Date	10 Day Values	TP Data (m)	Lake Level	Date	10 Day Values	TP Data (m)	Lake Level cm	Date	10 Day Values	TP Data (m)	Lake Level cm	Date	10 Day Values	TP Data (m)	Lake Level cm
01/01/99	1			24/10/99	297	0.87	238.5	15/08/00	593	-0.15	138	12/05/01	863	-0.59	125
10/01/99	10	0.73	273.8	03/11/99	307	0.81	250.1	17/08/00	595	-0.15	139	21/05/01	872	-0.68	115.2
20/01/99	20	0.75	266	13/11/99	317	0.76	262.2	27/08/00	605	0.21	148.3	31/05/01	882	-0.63	98
09/02/99	40	0.44	249.47	23/11/99	327	0.78	276.1	06/09/00	615	0.08	157.8	10/06/01	892	-0.96	98
18/02/99	49	0.42	243.7	03/12/99	337	0.78	285.1	16/09/00	625	0.38	171.3	20/06/01	902	-0.96	95
28/02/99	59	0.29	233.8	23/12/99	357	0.75	294	26/09/00	635	0.18	189.3	30/06/01	912	-0.79	84
10/03/99	69	0.01	224.7	02/01/00	367	1	289.7	10/10/00	649	0.2	200.3	10/07/01	922	-0.89	89.3
20/03/99	79	0.27	215.8	12/01/00	377	0.92	283	15/10/00	654	0.84	204	20/07/01	932	-0.9	83.7
30/03/99	89	-0.07	175.5	22/01/00	387	0.67	276.8	25/10/00	664	0.55	207	30/07/01	942	-0.54	84
09/04/99	99	-0.32	195.8	01/02/00	397	0.6	266.8	14/11/00	684	0.48	218	09/08/01	952	-0.41	80
19/04/99	109	-0.31	186.8	10/02/00	406	0.46	257.8	04/12/00	704	0.32	217	19/08/01	962	-0.18	80.54
05/05/99	125	-0.24	169.8	21/02/00	417	0.1	244.9	14/12/00	714	0.26	209.5	29/08/01	972	0.15	80.4
19/05/99	139	-0.52	160.5	01/03/00	426	0.21	239.8	24/12/00	724	0.54	208.8	08/09/01	982	0.25	115.2
29/05/99	149	-0.94	149.5	11/03/00	436	0.04	230.8	03/01/01	734	0.48	202.8	17/09/01	991	0.51	156.8
08/06/99	159	-0.36	144.7	21/03/00	446	-0.09	224.8	13/01/01	744	0.4	200	27/09/01	1001	0.67	194.3
17/06/99	168	-0.44	138.8	31/03/00	456	-0.23	214.3	01/02/01	763	0.04	189.5	07/10/01	1011	0.94	215.2
07/07/99	188	-0.64	125	20/04/00	476	-0.11	195.8	11/02/01	773	0.11	182.7	17/10/01	1021	0.7	222.2
27/07/99	208	-0.58	134.95	30/04/00	486	-0.2	189.5	21/02/01	783	0.1	176.8	27/10/01	1031	0.55	227.2
06/08/99	218	-0.51	131.9	30/05/00	516	-0.52	165	13/03/01	803	-0.35	163.8	06/11/01	1041	0.47	236
16/08/99	228	-0.24	133	08/06/00	525	-0.53	157.8	23/03/01	813	-0.31	156.1	16/11/01	1051	0.65	245.7
26/08/99	238	-0.39	141.2	18/06/00	535	-0.69	153	02/04/01	823	-0.46	152	26/11/01	1061	0.7	255.4
15/09/99	258	0.26	180.2	28/06/00	545	-0.16	146.7	12/04/01	833	-0.76	141.8	06/12/01	1071	0.62	259.7
05/10/99	278	0.28	211.4	18/07/00	565	-0.53	134.8	22/04/01	843	-0.42	138.8	16/12/01	1081	0.61	255.7
14/10/99	287	0.53	225	07/08/00	585	-0.51	134.5	02/05/01	853	-0.89	131.3	26/12/01	1091	0.71	249.8
05/01/02	1101	0.56	241.8	23/02/02	1150	-0.23	201.8	14/04/02	1200	-0.09	166	12/06/02	1259	-1.05	125.5
14/01/02	1110	0.3	232	05/03/02	1160	-0.41	196	04/05/02	1220	-0.52	149.7	22/06/02	1269	-0.77	113.8
24/01/02	1120	0.32	225	15/03/02	1170	-0.4	190	13/05/02	1229	-0.76	141.8	02/07/02	1279	-0.77	108.8
03/02/02	1130	0.23	216	25/03/02	1180	-0.61	180.8	23/05/02	1239	-0.31	132.8	22/07/02	1299	-0.77	98.4
13/02/02	1140	-0.11	207.8	04/04/02	1190	-0.84	170.8	02/06/02	1249	-0.79	126.3	01/08/02	1309	-0.62	91.51

Appendix B3. Binary file images of the regions of the Southern basin analyzed for relationship between altimeter data and surface areal extent of water.

B3.1 **The Southeastern Dune Islands**

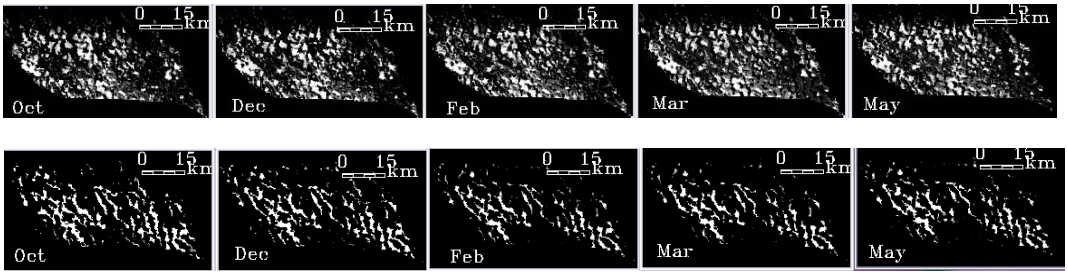

Fig B3.1: MERIS water and vegetation bands of the Southeastern Dune Islands between October 2003 to May 2004 (water bands top; vegetation bands bottom).

B3.2 **The Southern Reed Islands**

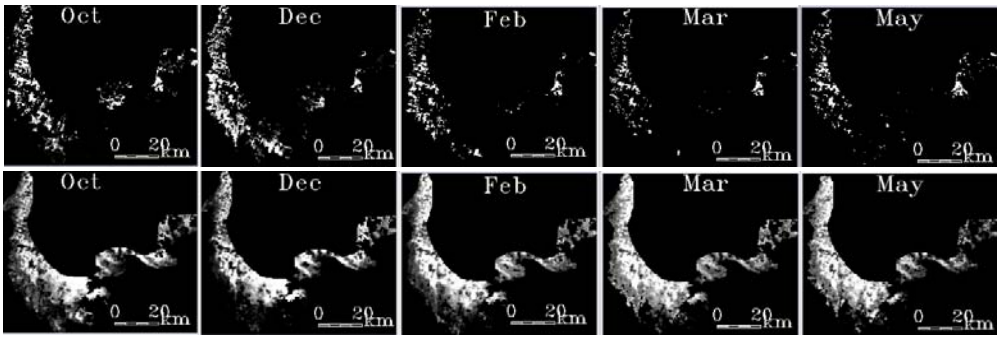

Fig B3.2: MERIS water and vegetation bands of the Southern Reed Islands between October 2003 and May 2004 (water band top; vegetation bands bottom).

B3.3 **The Southeastern Reed Islands**

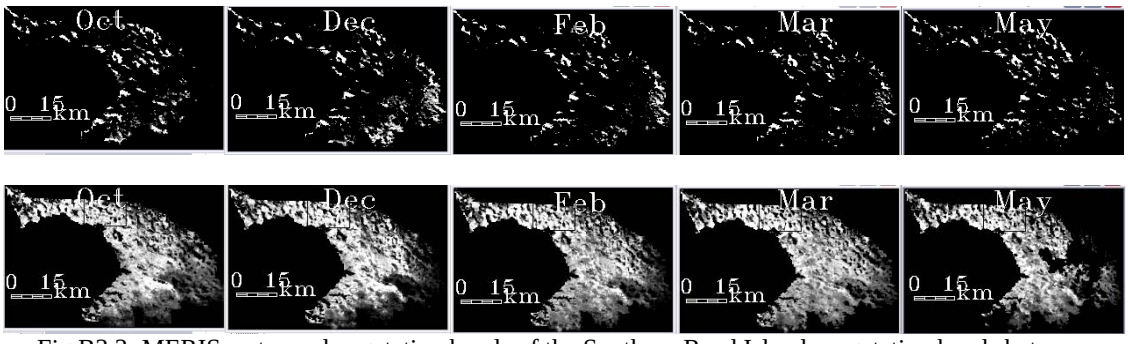

Fig.B3.3: MERIS water and vegetation bands of the Southern Reed Islands vegetation bands between October 2003 to May 2004 (water bands top; vegetation bands bottom).

B3.4 **The Polder Farmlands**

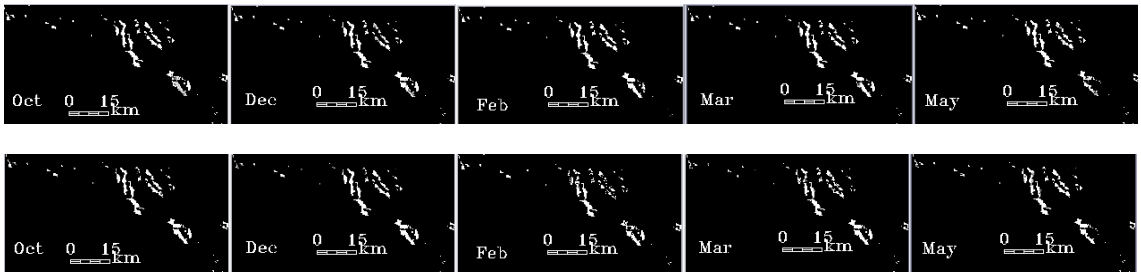

Fig. B3.4: MERIS water and vegetation bands of the Polder Farmlands between October 2003 and May 2004 (water bands top; vegetation bands bottom).

B3.5 **The Southwestern Lakeshore Farmlands**

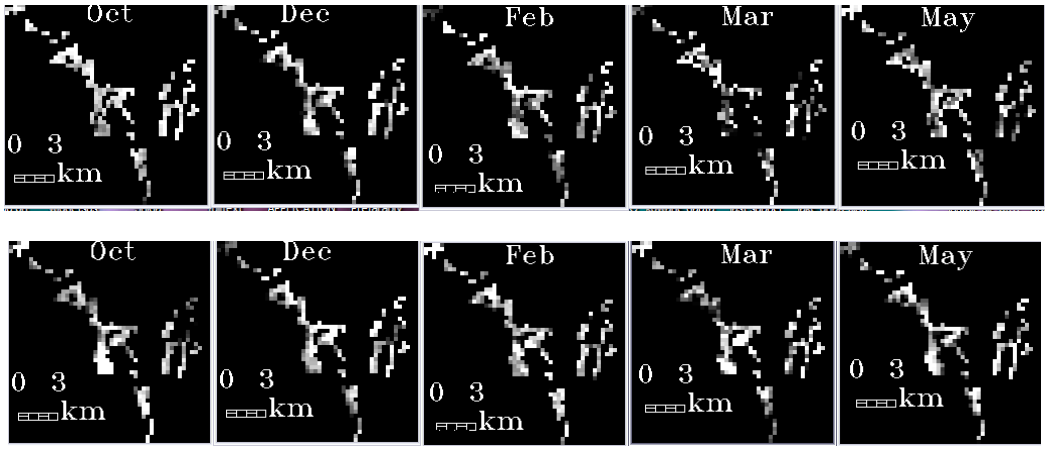

Fig. B3.5: MERIS water and vegetation bands of the water bands for Southwestern lakeshore farmlands between October 2003 to May 2004(water bands top; vegetation bands bottom).

B3.6 **The Open Water Region**

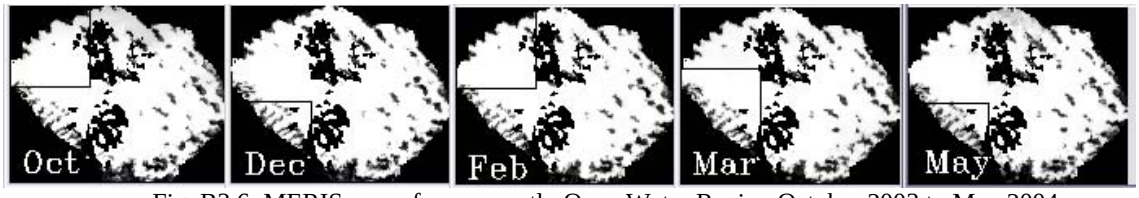

Fig. B3.6: MERIS area of permanently Open Water Region October 2003 to May 2004

BIBLIOGRAPHY

Adams, J. B., Sabol, D. E., Kapos, V., Filho, R.A., Roberts, D. A., Smith, M.O., and Gillespie, A. R (1995). 'Classification of multispectral images based on fraction of endmembers: application to landcover change in the Brazilian Amazon'. *Remote Sensing of Environment* **52** (1995) 137-154.

Adams, J. B., Smith, M. O. and Johnson, P.E., (1986). 'Spectral mixture modeling: a new analysis of rock and soil types at the Viking Lander 1 site' *J. Geophys. Res.* **91**: 8098-8122

Africa, O. E. and Lemoalle, J. (1996). 'Remote sensing of the water area of Lake Chad'. *Livestock Atlas for the Lake Chad Basin,* CIRAD/CTA.

AGRHYMET (2003a). 'Seasonal forecasts for 2003 - 2004 Cropping season'. *AGRHYMET Monthly Bulletin*. May 2003

AGRHYMET (2003b) 'Regional meteorological situation' *AGRHYMET Monthly Bulletin*. September 2003

AGRHYMET (2004) 'Regional meteorological situation' *AGRHYMET Monthly Bulletin.* February 2004

AGRHYMET (2005). 'Onset of rainy season underway in northern Sahelian areas.' *AGRHYMET Monthly Bulletin*. June 2005

AVISO, 2006 'How altimetry works.' http://www.aviso.oceanobs.com en/altimetry/principle/index.html

Ayana, E.K. (2007) 'Validation of radar altimetry lake level data and its application in water resource management.' Unpublished M.Sc. Thesis. International Institute for Geo information Sciences and Earth Observations, Enschede. The Netherlands

Badolo, M., N'Djafa Ouaga, H. Sidibe B., Sagnia, S.B. and Diallo, A.A. (2003). 'The project for strenthening the CILSS member states capacity to adapt to climate change.' *AGRHYMET INFO*. **5:** 9-10.

Bannari, A., Pacheco, A. Staenz, K., McNaim, H., and Omari, K. (2006). 'Estimating and mapping crop residues cover on agricultural lands using hyperspectral and IKONOS data." *Remote Sensing of Environment* **104**: 447-459.

Berberoglu, S., Evrendilek, S. F., Ozkan, C. and Donmez, C. (2007). 'Modelling forest productivity using ENVISAT MERIS data.' *Sensors* **7**: 2115-2127.

Boardman, J. W. (1994). 'Geometric mixture analysis of imaging spectrometry data.' *Proc. Int. Conf. Geoscience and Remote Sensing*.

Braswell, B. H., Hagen, S. C., Frolking, S.E., Salas, W.A. (2003). 'A multivariate approach for mapping subpixel land cover distributions using MISR and MODIS:

application in the Brazilian Amazon region.' *Remote Sensing of Environment* **87**(2003) 243-256.

Beauvilain, A. (1996). 'La pluviometrie dans bassin du lac Tchad.' *Livestock Atlas for the Lake Chad*, CIRAD/CTA.

Birkett, C. M. 1994 'Remote sensing of the water area of Lake Chad.' *EOS Transactions. American Geophysical Union,* Vol 75 No. 24, pp 273 – 275.

Birkett, C. M. (1995). 'The contribution of TOPEX/POSEIDON to the global monitoring of climatically sensitive lakes.' *Journal of Geophysical Research*. **Vol 100** (12): 179 – 204.

Birkett, C. M. (2000). 'Synergistic remote sensing of Lake Chad: variability of basin inundation.' *Remote Sensing of Environment* **72** (2000) 218 - 236.

Biging, G. S. and Congalton R. G. (1999). 'Sampling systems for change detection accuracy assessment.' *Remote Sensing Change Detection: Environmental Monitoring and Applications.* R. S. Lunetta and C. D. Elvidge. Taylor and Francis.

Brown, C.W., Connor, L.N., Lillibridge, J.L. Nalli, N.R., and Legeckis, R.V (2005) 'An introduction to satellite sensors, observations and techniques.' *Remote sensing of coastal aquatic environments.* Miller R.L et.al (eds) Springer Netherlands 2005.

Carlson, T. N. and Azofeifa, G. A. S. (1999). 'Satellite remote sensing of land use changes in and around San Jose, Costa Rica.' *Remote Sensing of Environment* **70** (1999) 247-256.

Carmouze, J. P. (1983). 'Hydrochemical regulation of the lake'. *Lake Chad:Ecology and Productivity of a Shallow Tropical System Monographiae Biologica* 53 Carmouze, J. P., J. R. Durand, and C. Leveque, (eds.). Dr. W. Junk Publishers.

Carmouze, J.P., and Lemoalle, J. (1983). 'The Lacustrine Environment.' *Lake Chad: Ecology and Productivity of a Shallow Tropical Ecosystem. Monographiae Biologica* 53 Carmouze, J. P., J. R. Durand, and C. Leveque, (eds.). Dr. W. Junk Publishers.

Chabrillat, S., Goetz, A. F. H., Krosley, L., and Olsen, H.W. (2002). 'Use of hyperspectral images in the identification and mapping of expansive clay soils and the role of spatial resolution.' *Remote Sensing of Environment* **82** (2002) 431-445.

Clevers, J. G. P. W., De Jong, S. M., Epema, G.F., Van Der Meer, F.D., Bakker, W.H., Skidmoter, A.K., and Scholte, K. H. (2002). 'Derivation of the red edge index using MERIS standard band setting.' *International Journal of Remote Sensing* **23**(16): 3169-3184.

Clevers, J. G. P. W., Schaepman, M. E., Mucher, C.A., De Wit, A.J.W., Zurita-Milla, R., and Batholoeus, H.M. (2007). 'Using MERIS on ENVISAT for land cover mapping in the Netherlands.' *International Journal of Remote Sensing* **3-4**: 637-652.

Coe, M. T. and Birkett C. M. (2004). 'Calculation of river discharge and prediction of lake height from satellite radar altimetry: example for the Lake Chad basin.' *Water Resour. Res.*, **40,** (10).

Coe, M. T. and Foley J. A. (2001). 'Human and natural impacts on water resources of the Lake Chad basin.' *Journal of GeoPhysical Research*, **106**: 3349 - 3356.

Cracknell, A. P. (1998). 'Synergy in remote sensing - what's in a pixel?' *International Journal of Remote Sensing* **19**(11): 2025-2047.

Cretaux, J.F. and Birkett, C. (2006) 'Lake studies from satellite radar altimetry.' *C.R. Geoscience* 338 (2006) 1098-1112

Curran, P.J., Steele, C.M. (2005) 'MERIS: the re-banding of an ocean sensor.' *International Journal of Remote Sensing* **26**(9): 1781-1798

Daly, J. (2001). 'TOPEX-Poseidon radar altimetry: averaging the averages.' http://www.john-daly.com/altimetry/topex.htm.

Dash, J. and Curran P. J., (2004). 'The MERIS terrestrial chlorophyll index.' *International Journal of Remote Sensing* **25**(23): 5403-5413.

Dash, J., Mathur, A., Foody, G.M., Curran, P.J., Chipman, J.W. and Lillesand, T.M. (2007). 'Land cover classification using multi-temporal MERIS vegetation indices.' *International Journal of Remote Sensing* **28**(6): 1137-1159.

Dennison, P. E. and Roberts D. A. (2003). 'Endmember selection for multiple endmember Spectral Mixture Analysis using endmember average RMSE.' *Remote Sensing of Environment* **87**(2003) 123-135.

Dieleman, P. J. and De Ridder N. A. (1963). 'Studies of salt and water movement in the Bol Guini Polder, Chad Republic.' *Journal of Hydrology* **1**(4): 311 - 343.

Drake, N. and Bristow C. (2006). 'Shorelines in the Sahara: geomorphological evidence for an enhanced monsoon from palaeolake Mega Chad.' *The Holocene* **16**(6): 901-911.

Drake, N. A., Mackin, S., and Settle, J.J. (1998). 'Mapping vegetation, soils and geology in semiarid shrublands using spectral matching and mixture modelling of SWIR AVIRIS imagery.' *Remote Sensing of Environment* **68** (1998) 12-25.

ESA (2006). 'The MERIS hand book, European Space Agency.' Issue 2, 14th April, 2006.

Evans, T. E. (1974). 'Water balance of Lake Chad." *South Chad Irrigation Project Eastern Area Feasibility Study*. Federal Ministry of Agriculture and Natural Resources Nigeria/MRT. Consulting Engineers/Mott MacDonald.

Evans, S. Y., Bradbrook, K. Braund, R and. Bergkamp, G. (2003). 'Assessment of the

restoration potential of the Logone flood plain (Cameroon)." *Water and Environment Journal* **17**(2): 123-28.

FEWSNET (1997) 'Lake Chad untapped potential." *Famine Early Warning System Special Report* 97- 4, May 27

Fisher, P. (1997). 'The pixel: a snare and a delusion.' *International Journal of Remote Sensing* **18**(31): 679-685.

Franke-Sharfe, I (2000) 'Integration of land use and related information with in the Geographic Information System of the Chad Basin in NE Nigeria." *BERICHTE DES SONDERFORSCHUNGSBEREICHS* 268 Kulturentwicklung und Sprachgeschchte imNaturraum Westafrikanische Savanne. BAND 14 Frankfurt am Main 2000.

Franke-Sharfe, I., Krings, M., Plate, E.and Thiemeyer, H (2000) 'Uncharted territory on Chad - sustainable use of potentials?' *Geographical Review* **52**(11): 28-34

Franke-Sharfe, I., (2001) 'Dry season farming area in the Nigerian Chad basin mapped from aerial photographs.' *BERICHTE DES SONDERFORSCHUNGSBEREICHS* **268** 'Kulturentwicklung und Sprachgeschchte imNaturraum Westafrikanische Savanne. BAND 17 Frankfurt am Main 2001.

Franke-Sharfe, I. and Skoropinsky, T., (2000) 'Mapping of desertification areas by satellite image interpretation and soil survey." *BERICHTE DES SONDERFORSCHUNGSBEREICHS* **268** 'Kulturentwicklung und Sprachgeschchte imNaturraum Westafrikanische Savanne. BAND 14 Frankfurt am Main 2000.

Gilabert, M.A., Garcia-Haro, F.J. and Melia, J. (2000) 'A mixture modeling approach to estimate vegetation parameters for heterogeneous canopies in remote sensing.' *Remote Sensing of Environment* **72** (2000) 328 - 345

Glenn, N. F., Mundt, J. T., Weber, K.T., Prather, T.S., Lass, L. W., and Pettingill, J. (2005). 'Hyperspectral data processing for repeat detection of small intestations of leafy spurge.' *Remote Sensing of Environment* **95**(2005) 399-412.

Gonzalez Alonso, F., Merino-De-Miguel, S., Roldan-Zamarron, A. Garcia-Gigorro, S., and Cuevas, J.M (2007). 'MERIS Full Resolution data for mapping level of damage caused by forest fires; the Valencia de Alcantara event in August 2003.' *International Journal of Remote Sensing* **28**(3-4): 797-809.

Govaerts, Y., Verstraete, M., Michel, M., Pinty, B., and Gobron, N. (1999). 'Designing optimal spectral indices: a feasibility and proof of concept study.' *International Journal of Remote Sensing* **20**(9): 1853-1873.

Grandell, J., Pullianen, J., and Hallikainen, M. (1998). 'Subpixel land use classification and retrieval of forest stem volume in the boreal forest zone by employing SSM/I data.' *Remote Sensing of Environment* **63** (1998)140-154.

Guganeshrajah, K. (1974). 'Statistical modelling of water levels of Lake Chad.' *South Chad Irrigation Project Eastern Area Feasibility Study*. Federal Ministry of Agriculture and Natural Resources Nigeria/MRT. Consulting Engineers/Mott MacDonald/Hunting Technical Services Ltd, Dec 1974.

Gumnior, M. and Thiemeyer H. (2003). 'Holocene fluvial dynamics in the NE Nigerian Savanna: some preliminary interpretations.' *Quaternary International* **111**: 51 - 28.

Hostert, P., Roder, A., and Hill, J. (2003). 'Coupling spectral unmixing and trend analysis for monitoring of long term vegetation dynamics in Mediterranean rangelands.' *Remote Sensing of Environment* **87** (2003) 183-197.

Huang, S. and Sigert, F. (2004). 'ENVISAT multisensor data for fire monitoring and impact assessment.' *International Journal of Remote Sensing* **25**(20): 4411-4416.

Huete, A. R. (2004). 'Remote sensing of soils and soil processes.' *Remote Sensing for Natural Resources Management and Environmental Monitoring: Manual of Remote Sensing*,. S. L. Ustin, John Wiley & Sons. **Chapter 1:** 1-48.

Hung, M. and Ridd M.K. (2002). 'A subpixel classifier for urban landcover mapping based on a maximum-likelihood approach and expert system rules.' *Photogrammetric Engineering & Remote Sensing*, **68**: 1173–1180.

Jensen, J. R. (1996). 'Introductory digital image processing: a remote sensing approach' Prentiss Hall, 1996.

Jones, K. Sambo, G. H. Adamu, S.A., and Schouten, L., (2006). *'GlobWetland - Africa: The case of Lake Chad.'* TIGER 2006 Workshop. Cape Town, South Africa.

Isiorho, S. A. and Matisoff G. (1990). 'Ground water recharge from Lake Chad.' *Limnology and Oceanography* **35**: 931-938.

Isiorho, S. A., Matisoff, G.Wehn, K.S (1996). 'Seepage relationships between Lake Chad and the Chad aquifers.' *Ground Water* **34**(5): 819 - 826.

Kameyama, S., Yamagata, Y., Nakamura, F., and Kaneko, M. (2001). 'Development of WTI and turbidity estimation model using SMA- application to Kushiro Mire, eastern Hokkaido, Japan.' *Remote Sensing of Environment* **77** (2001) 1-9.

Kindler, J. O., Warshall, P., Arnaud, E.J. Hutchinson, C.F., and Varady, R., (1990). 'The Lake Chad Conventional Basin - a diagnostic study of the environmental degradation.' UNEP and UNSO.

Koblinsky, C.J., Clark, R.T., Brenner, A.C., and Frey, H. (1993) 'Measurement of river level variations with satellite altimetry.' *Wat. Resour. Res*. **29**(6), 1839-1848.

L.C.B.C. (1998). 'Integrated and sustainable management of international waters of Lake Chad Basin.' N'Djamena, Lake Chad Basin Commission, 1998.

Leblanc, M. J., Leduc, C. Razack, M., Lemoalle, J., Dagorne, D., and Mofor, L., (2003). 'Application of remote sensing and GlS for ground water modelling of large semi arid areas: example of the Lake Chad basin, Africa.' *Hydrology of Mediterranean and semiarid regions.* Servant E, Najem W, Leduc C and S. A. (eds). Wallingford, UK, IAHS**:** 186-192.

Leblanc, M. J., Leduc, C. Stagnitti, F., van Oevelen, P. J., Jones, C., Mofor, L.A., Razack, L.A., and Favereau, G. (2006). 'Evidence for Mega Lake Chad, north-central Africa, during the late quaternary from satellite data.' *Palaeogeography, palaeoclimatology, Palaeoecology* **230**: 230 - 242.

Lemoalle, J. (1978). 'LANDSAT images for the bathymetric curve of Lake Chad.' *Hydrobiol* **12**(1): 83-87.

Lemoalle, J. (1991). 'The hydrology of Lake Chad during the drought period (1973 - 1989).' *F.A.O. Fisheries Report* **445 :** 54-61 Rome, F.A.O.

L'Hote, T., Mahe, G., Some, B. and Triboulet, J.P. (2002) 'Analysis of a Sahelian annual rainfall index from 1896 to 2000; the drought continues' *Hydrological Sciences Journal*, **47**: pp563 - 572

Lobell, D. B. and Asner G. P. (2006). 'Cropland distributions from temporal unmixing of MODIS data.' *Remote Sensing of Environment* **93**: 412-422.

Lu, D., Moran, E. and Batistella, M. (2003). 'Linear Mixture Modelling applied to Amazonian vegetation classification.' *Remote Sensing of Environment* **87**(2006) 456-469.

Lu, D., Mausel, P., Brondizios, E., and Moran, E. (2004). 'Change detection techniques.' *International Journal of Remote Sensing* **25**(12): 2365-2407.

Luque, S. S. (2000). 'Evaluating temporal changes using multi-spectral scanner and Thematic Mapper data on the landscape of a natural reserve: the New Jersey Pine barrens; a case study.' *International Journal of Remote Sensing*, **21**: 2589–2611

Macleod, R. D. and Congalton R. G. (1998). 'A quantitative comparison of change detection algorithms for monitoring eelgrass from remotely sensed data.' *Photogrammetric Engineering and Remote Sensing* **64**: 207–216.

MacMillan, D., Bock, Y., Fang, P., Beckley, B., and Ma, C. (2006) 'Calibration of the TOPEX and Jason-1 altimeter microwave radiometers using VLBI and GPS derived tropospheric delays.' NASA, 2006

Mather, P. M. (2004). 'Computer processing of remotely sensed images: an introduction.' John Wiley and Sons.

McGwire, K., Minor, T., and Fenstermaker, L. (2000). 'Hyperspectral Mixture Modelling for quantifying sparse vegetation cover in arid environments.' *Remote Sensing of Environment* **72**(2000) 360-374.

Merheim-Kealy, P., Huot, J. P., and Delwart, S. (1999). 'The MERIS ground segment.' *International Journal of Remote Sensing* **20**(9): 1703-1712.

Metternicht, G. I. and Fermont A., (1998). 'Estimating erosion surface features by Linear Mixture Modeling.' *Remote Sensing of Environment* **64**(1998) 254-269.

Mundt, J. T., Glenn, N. F., Weber, K.T., Prather, T.S., Lass, L. W., and Pettingil, J., (2005). 'Discrimination of hoary cress and determination of its detection limits via hyperspectral image processing and accuracy assessment techniques.' *Remote Sensing of Environment* **96**(2005) 509-517.

National Population Commission, (1999) 'The 1991 Census.' National Population Commission of Nigeria.

NASA/USDA (2008). 'Global reservoir and lake monitor." http://www.pecad.fas.usda.gov/cropexplorer/global_reservoir/.

Nichol, J. and Wong, M. S., (2007) 'Remote sensing of urban vegetation life form by spectral mixture analysis of high resolution IKONOS satellite images.' *International Journal of Remote Sensing*_28 (5): 985-1000.

Nicholson, S. E., Some, B. and Kone, B. (2005). 'On the question of the recovery of the rains in the West African Sahel.' *Journal of Arid Environments* **63**: 615-641.

Novo, E.M. and Shimabukuro, Y. E. (1997) 'Identification and mapping of the Amazon habitats using a mixing model.' *International Journal of Remote Sensing* **18**:663-670

Odada, E., Oyebande, L., and Oguntola J. (2003) 'The agro-climatic and water balance situation of the Chad Basin.' *Evaluation of the Proposed Management Schemes to Improve the Water Balance of the Lake Chad.* UNEP MISSION REPORT; Nairobi.

Oki, K., Hiroyuki, O., and Mikio, S. (2002). 'Subpixel classification of alder trees using multi temporal LANDSAT Thematic Mapper imagery.' *Photogrammetric Engineering and Remote Sensing* **68**(1): 77-82.

Olivry, J. C., Chouret, G., Vuillaume, G., Lemoalle, J., and Bricquet, J.P. (1996). 'Hydrologie du Lac Tchad.' Paris, ORSTOM.

Papa, F., Legresy, B., and Remy, F. (2003). 'Use of TOPEX/POSEDON dual frequency rada altimeter over land surfaces.' *Remote sensing of Environment* **87**: 136-147.

Petit, C., Scudder, T. and Lambin, E. (2001). 'Quantifying processes of land-cover change by remote sensing: resettlement and rapid land-cover change in southeastern Zambia' *International Journal of Remote Sensing*_ **22**: 3435–3456.

Phinn, S. M., Sanford, P., Scarth, A.T., Murray A.T., and Shy, P.T. (2002). "Monitoring the composition of urban environments based on the vegetation - impervious surface soil (VIS) model by sub pixel analysis techniques.' *International Journal of Remote Sensing* **23**(4131-4153).

Pietroniro, A., Soulis, E. D., and Solomon, S.I. (1990). 'Hydrometreorological data extension for the Sudan - Sahel Zone of West Africa using satellite remote sensing.' *IEEE Transaction on GeoScience and Remote Sensing* **28**(5): 955 -962.

Pontius, J., Hallet, R., Martin, M. (2005). 'Using AVIRIS to assess hemlock abundance and early decline in the Catskills, New York." *Remote Sensing of Environment* **97**(2005) 163-173.

Powell, R., Roberts, D. A., Dennison, P.E., and Hess, L.L. (2007). 'Subpixel mapping of urban land cover using Multiple Endmember Spectral Mixture Analysis: Manaus, Brazil.' *Remote Sensing of Environment* **106**(2007) 253-267.

Pu, R., Gong, P., Michishita, R., and Sasagawa, T. (2008). 'Spectral Mixture Analysis for mapping abundance of urban surface components from the Terra/ASTER data." *Remote Sensing of Environment* **112**: 939-954.

R.S.I. (2005). 'Spectral analysis with ENVI.' Research Systems Inc. Boulder, Colorado,

Radeloff, V.C., Mladenoff, D. J., and Boyce, M.S. (1999). 'Detecting and forecasting Jack Pine budworm defoliation using spectral mixture analysis.' *Remote Sensing of Environment* **69**(1999) 56-169.

Rahman, H. and G. Dedieu (1994). 'SMAC: a simplified method for the atmospheric correction of satellite measurements in the solar spectrum.' *International Journal of Remote Sensing* **15**(1): 123-143.

Rashed, T., Weeks, J. R., Roberts, D.A., Rogan, J., and Powell, R. (2003). 'Measuring the physical composition of urban morphology using Multiple Endmember Spectral Mixture Modeling.' *Photogrammetric Engineering and Remote Sensing* **69**(9).

Rast, M., J. Bezy, L., and Bruzzi,S. (1999). 'The ESA Medium Resolution Imaging Spectrometer MERIS- a review of the instrument and its mission.' *International Journal of Remote Sensing* **20**(9): 1681-1702.

Rees, W.G., (2001) 'Physical principles of remote sensing.' Cambridge University Press, (2001).

Ridd, M. K. (1995). 'Exploring a V–I–S (vegetation–impervious surface–soil) model for urban ecosystem analysis through remote sensing: comparative anatomy for cities' *International Journal of Remote Sensing* **16**: 2165-2185.

Roberts D. A., Gardner, M., Church, R., Ustin, S. and Green, R.O. (1998). 'Mapping chaparral in the Santa Monica Mountains using multiple endmember spectral mixture models.' *Remote Sensing of Environment* **65**: 267 - 279.

Robichaud, P. R., Lewis, S. A., Laes, D.Y.M., Hudak, A.T., Kokaly, R.F., and Zamudio, J.A. (2007). 'Post fire soil burn severity mapping with hyperspectral image unmixing.' *Remote Sensing of Environment* **108**(1998) 467-480.

Rogan, J., Franklin, J., and Roberts, D.A. (2002). 'A comparison of methods for monitoring multitemporal vegetation change using Thematic Mapper imagery.' *Remote Sensing of Environment* **80**(2002) 143-156.

Rosema, A. and J. L. Fiselier (1990). 'METEOSAT-based evapotranspiration and thermal inertia mapping for monitoring transgression in the Lake Chad region and Niger Delta.' *International Journal of Remote Sensing* **11**: 741-752.

Rosmorduc, V., Benveniste, J., Lauret, O., Milagro, M. and Picot, N. (2006) 'Radar altimetry tutorial.' Benveniste, J. and Picot, N. (Eds)., http://www.altimetry.info, 2006

Rosso, P. H., Ustin, S. L., and Hastings, A. (2005). 'Mapping marshland vegetation of San Francisco Bay, California, using hyperspectral data' *International Journal of Remote Sensing* **26**(23): 5169-5191.

Sarch, M. T. and Birkett, C. (2000). 'Fishing and farming at Lake Chad: responses to lake level fluctuations.' *Geographical Journal* **166**: 156-172.

Sato, H. P. and Tateishi, R., (2004). 'Land cover classification in SE Asia using near and short wave infrared bands.' *International Journal of Remote Sensing* **20**: 2821-2832.

Schneider S.R., Mc Ginnis Jr, D. F., and Stephens, G. (1985.). 'Monitoring Africa's Lake Chad basin with LANDSAT and NOAA satellite data.' *International Journal of Remote Sensing* **6** 59-73.

Scholte K., Garcia- Haro, K. and Kemper, T. (2006). 'Variable Multiple Endmember Spectral Mixture Analysis for geology applications.' *Remote Sensing Image Analysis* De Jong S. M. and van der Meer, F.D.(eds). SpringerLink Netherlands. **5**: 181-200.

Seiler, R. and Csaplovics E. (2004). 'Monitoring land cover changes in the Niger inland delta (Mali) by means of ENVISAT MERIS data.' *Proceedings of MERIS User Workshop*. Frascatti, Italy.

Servant, M. and Servant S. (1983). 'The Lacustrine environment and its evolution: paleolimnology of an upper quaternary endorheic lake in Chad basin.' *Lake Chad: Ecology and Productivity of a Shallow Tropical System Monographiae Biologica* 53 Carmouze, J. P., J. R. Durand, and C. Leveque, (eds.). Dr. W. Junk Publishers.

Small, C. (2002). 'Multitemporal analysis of urban reflectance.' *Remote Sensing of*

Environment **81**(2002) 427-442.

Small, C, (2003). 'High spatial resolution spectral mixture analysis of urban reflectance.' *Remote sensing of Environment* **88**(2003) 170-186.

Smith, M. O., Johnson, P. E., and Adams, J.B.,(1985). 'Quantitative determination of mineral types and abundances from reflectance spectra using principal components analysis.' Proceedings of the 5th Lunar and Planetary Science Conference, Part 2, *Journal of Geophysical Research*, **Vol. 90** (Supplement): 797-804.

Sohn, Y. and McCoy R.M.(1997). 'Mapping desert shrub rangeland using spectral unmixing and modeling spectral mixtures with LANDSAT TM data.' *Photogrammetric Engineering and Remote Sensing* **63**(6): 707-716.

Song, C. (2005). 'Spectral Mixture Analysis for subpixel vegetation fractions in the urban environment: how to incorporate endmember variability?' *Remote Sensing of Environment* **95**(2005) 248-263.

Sonnetag, O., Chen, J.M., Roberts, D.A., Talbot, J., Hallingan, K.Q., and Govind, A. (2007). 'Mapping tree and shrub leaf area indices in an ombrotrophic peatland through multiple endmember spectral unmixing.' *Remote Sensing of Environment* **109**(2007) 342-360.

Souza, C. J. and P. Barreto (2000,). 'An alternative approach for detecting and monitoring selectively logged forests in the Amazon.' *International Journal of Remote Sensing* **21**:173–179.

Stehman, S. V. and Czaplewski R. L., (1998). 'Design and analysis for thematic map accuracy assessment: fundamental principles.' *Remote Sensing of Environment* **64**(1998) 331-344.

Tang, J., Wang, L., and Myint, S.W. (2007). 'Improving urban classification through fuzzy supervised classification and spectral mixture analysis.' *International Journal of Remote Sensing* **28**(2007) 4047-4063.

Thiemeyer, H. (2000). 'From Mega Chad to Micro Chad - environmental changes during the Holocene.' *BERICHTE DES SONDERFORSCHUNGSBEREICHS*, Frankfurt a.M **14**: 11-19. 'Kulturentwicklung und Sprachgeschchte imNaturraum Westafrikanische Savanne. BAND 14 Frankfurt am Main 2000.

Townshend, J. R. G., Huang, C., Kalluri, S.N.V., Defries, R.S., Liang, S., and Yang, K. (2000). 'Beware of per-pixel characterization of land cover.' *International Journal of Remote Sensing* **21**: 839-843.

.

UNDTCD/UNEP/LCBC (1993). 'Mathematical model of the hydrological behavior of Lake Chad and its feeder rivers.' Mott MacDonald 1993.

UNEP, Fortnam M. P., and Oguntola J.A. Eds. (2004). 'Lake Chad Basin.' *GIWA Regional Assessment* **43.** Kalmar, University of Kalmar.

USGS (2001) Earthshots: 'Satellite images of environmental change, Lake Chad, West Africa.' http://edc.usgs.gov/earthshots/slow/LakeChad/LakeChad.

Vanderbilt, V. C., Shruti, K., and Ustin, S.L. (2007). 'Impact of pixel size on mapping surface water in subsolar imagery.' *Remote Sensing of Environment* **109**(2007)1-9.

Van der Meer, F. D., (1999). 'Iterative Spectral Unmixing (ISU).' *International Journal of Remote Sensing* **20**(17): 3431-3436.

Van der Meer, F. D., Bakker, W. H., Scholte, K., Skidmore, A.K., and De Jong, S.M. (2001). 'Spatial scale variations in vegetation indices and above - ground biomass estimates : implications for MERIS.' *International journal of remote sensing* **22** (17): 3381-3396.

Verhoeye, J. and R. De Wulf (2002). 'Land cover mapping at subpixel scales using linear optimization techniques.' *Remote Sensing of Environment* **79**(2002) 96-104.

Verstraete, M. M., Pinty, B., and Curran P.J. (1999). 'MERIS potential for land applications.' *International Journal of Remote Sensing* **20**(1999)1747-1756.

Viera, A. J. and Garrett J. M., (2005). 'Understanding inter-observer agreement: the Kappa statistic.' *Family Medicine* **37**(5): 360-363.

WWF (2003) 'Water use for agricultural in priority river basins.' http://www.panda.org/

Wang, C., Menenti, M., Stoll, M., Belluco, E., and Marani, M. (2007). 'Mapping mixed vegetation communities in salt marshes using airborne spectral data.' remote sensing of environment **107**(2007) 559-570.

Wang, Y. and Zhang X., (2004). 'A SPLIT model extraction of subpixel impervious surface information.' *Photogrammetric Engineering and Remote Sensing* **70** (7).

Wickens, G. E. (1974). 'Report on the Krenowa intake channel vegetation study, Lake Chad.' *South Chad Irrigation Project Eastern Area Feasibility Study*. Federal Ministry of Agriculture and Natural Resources Nigeria/MRT. Consulting Engineers/Mott MacDonald/Hunting Technical Services Ltd.

World Bank (2002). 'GEF Reversal of Land and Water Degradation trends in the Lake Chad Basin ecosystem.' *Project Appraisal Document*, World Bank, 2002.

Wu, C. (2004). 'Normalized spectral mixture analysis for monitoring urban composition using ETM+ imagery.' *Remote Sensing of Environment* **93**(2004) 480-492.

Wu, C. and Murray A.T., (2003). 'Estimating impervious surface distribution by Spectral Mixture Analysis.' *Remote Sensing of Environment* **84**(2003) 493-505.